INFORMATION TO USERS

This material was produced from a microfilm copy of the original document. While the most advanced technological means to photograph and reproduce this document have been used, the quality is heavily dependent upon the quality of the original submitted.

The following explanation of techniques is provided to help you understand markings or patterns which may appear on this reproduction.

1. The sign or "target" for pages apparently lacking from the document photographed is "Missing Page(s)". If it was possible to obtain the missing page(s) or section, they are spliced into the film along with adjacent pages. This may have necessitated cutting thru an image and duplicating adjacent pages to insure you complete continuity.

2. When an image on the film is obliterated with a large round black mark, it is an indication that the photographer suspected that the copy may have moved during exposure and thus cause a blurred image. You will find a good image of the page in the adjacent frame.

3. When a map, drawing or chart, etc., was part of the material being photographed the photographer followed a definite method in "sectioning" the material. It is customary to begin photoing at the upper left hand corner of a large sheet and to continue photoing from left to right in equal sections with a small overlap. If necessary, sectioning is continued again — beginning below the first row and continuing on until complete.

4. The majority of users indicate that the textual content is of greatest value, however, a somewhat higher quality reproduction could be made from "photographs" if essential to the understanding of the dissertation. Silver prints of "photographs" may be ordered at additional charge by writing the Order Department, giving the catalog number, title, author and specific pages you wish reproduced.

5. PLEASE NOTE: Some pages may have indistinct print. Filmed as received.

University Microfilms International
300 North Zeeb Road
Ann Arbor, Michigan 48106 USA
St. John's Road, Tyler's Green
High Wycombe, Bucks, England HP10 8HR

PRESSURE DEPENDENCE OF THE ELASTIC MODULI OF BODY-CENTERED-CUBIC TRANSITION METALS

A DISSERTATION SUBMITTED TO THE GRADUATE DIVISION OF THE UNIVERSITY OF HAWAII IN PARTIAL FULFILLMENT OF THE REQUIREMENTS FOR THE DEGREE OF

DOCTOR OF PHILOSOPHY

IN GEOLOGY AND GEOPHYSICS

AUGUST 1977

By

Keith W. Katahara

Dissertation Committee:

Murli H. Manghnani, Chairman
Edward S. Fisher
Augustine S. Furumoto
William Pong
George H. Sutton

ACKNOWLEDGEMENTS

I would like first of all to thank my advisor, M. H. Manghnani for his constant support and encouragement. E. S. Fisher initially suggested the idea for this project and provided invaluable guidance in every phase of the work. I am deeply indebted to J. Balogh for expert maintenance of the equipment and for help with experimental techniques. C. S. Rai, T. Matsui, and L. C. Ming deserve thanks for many fruitful discussions. I am also grateful for the samples and unpublished data provided by G. W. Shannette and L. J. Graham. This research was supported by the U.S. Energy Research and Development Administration (Contracts E(04-3)-235 and EY-76-S-03-0235).

ABSTRACT

The single-crystal elastic moduli, C_{ij}, and their pressure derivatives, dC_{ij}/dP, have been measured ultrasonically at 25°C for body-centered-cubic Ti-V-Cr, Nb-Mo, and Ta-W solid solutions. The rigid-band model for the alloy electronic structure is known to work fairly well for these metals in predicting the density of states at the Fermi energy and related properties. The results of this study show that changes in the composition dependence of the C_{ij} and, particularly, the dC_{ij}/dP appear to be related to topological changes in the Fermi surface which occur as the electron population varies in the rigid-band model. The relationship between the band structure and the C_{ij} is discussed and a qualitative explanation is given for the correlations between the moduli and the Fermi surface.

Sources of error in the ultrasonic measurements are considered in detail. It is found that compression of the pressure medium can cause significant errors in the dC_{ij}/dP values under certain experimental conditions, and methods for minimizing these errors are suggested.

The results are also compared to other ultrasonic measurements and to X-ray and shock-wave compression experiments. Possible sources of disagreement, where it exists, are discussed.

TABLE OF CONTENTS

TABLE OF CONTENTS (Continued)

LIST OF TABLES

LIST OF ILLUSTRATIONS

I. INTRODUCTION

The electronic band structures of transition metals are characterized by the presence of narrow d-electron conduction bands which cross and hybridize with a broader nearly-free-electron (NFE) band. The d-electron states may be thought of as arising from a scattering resonance in the conduction band or, equivalently, from a "virtual" bound state which is not entirely destroyed by the overlap of atomic potentials when the atoms are brought together to form the solid [Ziman, 1971]. The d-electron states are intermediate in nature between NFE and tightly-bound states. Because of this and because of the hybridization, it is difficult in practice, if not in principle, to calculate transition metal properties such as elastic shear moduli and phonon dispersion relations. Calculations of such properties using rigorous "first-principles" techniques such as the augmented-plane-wave method [Ziman, 1971], would be laborious and expensive and would not necessarily yield a great deal of physical insight into the problem. What is needed is a simpler approximate method like the pseudopotential approach which has proved to be successful and efficient in calculating a wide variety of properties in the simple metals [Cohen and Heine, 1970; Heine and Weaire, 1970].

This study is an experimental approach to the problem of how transition metal elastic properties are related to

the band structure. As such it may be regarded as complementary to recent theoretical efforts along these lines [Peter et al., 1974; Oli and Animalu, 1976].

The elastic moduli, C_{ij}, and their pressure derivatives, dC_{ij}/dP, have been measured at 25°C for a total of 21 single crystals in the Ti-V, V-Cr, Nb-Mo, and Ta-W alloy systems. The compositions of these metals will be characterized here by the average number of conduction electrons per atom, e/a (e.g., e/a = 5 for Nb and 6 for Mo), and by the type of d-electrons in the unfilled atomic shells, i.e., 3d, 4d and 5d for the three long periods of the periodic table. The transition metals of Groups IVB-VIIB (and VIII to some extent) form randomly disordered solid solutions with each other which are stable or metastable in the body-centered-cubic (bcc) structure over a very wide range of compositions: $4.2 < e/a < 6.3$ at room temperature. These metals are particularly suitable for evaluating band structure effects because the rigid band model works fairly well for them (this point is discussed in Chapter V). Thus by changing the alloy composition the electron population can be varied over a wide range within a slowly varying band structure. In other words, differences in behavior of different electronic energy levels can be examined experimentally over a wide energy range. The results of this study should thus provide a good test for any theoretical models devised to calculate the C_{ij} or dC_{ij}/dP: such a model should be able to at least qualitatively reproduce the experimental

results merely by varying the Fermi energy.

It has already been established that many of the elastic properties of these metals are dominated by the d-electrons [Fisher, 1975]. In the present work this conclusion is extended to include the dC_{ij}/dP where the influence of the band structure is found to be even more pronounced. These points will be discussed in Chapter V which is devoted to the relationship between the electronic band structure and the elastic properties.

It is rather well known to workers in this field that there is often substantial disagreement between ultrasonic measurements made on the same material by different investigators using different methods. Differences of several percent in dC_{ij}/dP values are not uncommon [Davies and O'Connell, 1977, Table 1]. Several instances of this sort of discrepancy were encountered for the metals studied here. This situation is far from satisfactory because modern ultrasonic techniques are capable of much better precision. An attempt was therefore made in this study to identify possible sources of errors. Chapters II and III and the appendices accordingly present a detailed description of the experimental procedure, the reduction of the data, and the error analysis used in this work. Then in Chapter IV the results are compared to previous work and causes for disagreement are discussed.

One aspect of ultrasonic measurements under pressure that has previously been ignored is that the compression of

the pressure medium can have significant effects on the dC_{ij}/dP values. These effects arise in various ways which are considered in Chapter IV and in Appendices A and C. The discussion presented in Appendix A does not have much direct bearing on the ultrasonic measurements made in this study, but it is of potential practical importance because it suggests a method of eliminating one of the most troublesome sources of error in experiments of this kind.

A few remarks concerning the geophysical relevance of this research are in order. The portions of the present work which are directed toward identifying and eliminating experimental errors have a direct bearing on geophysics because ultrasonic techniques are in widespread use in geophysical studies. On a more fundamental level, this study may be regarded as a preliminary effort toward understanding the influence of d-electrons and alloying on the shear moduli of transition metals. In this respect it may ultimately be useful in understanding the properties of the earth's inner core which is generally believed to be composed mainly of solid iron--a transition metal.

II. MATERIALS AND METHODS

A. General Considerations

The second-order adiabatic elastic moduli of a crystal are directly related to its density and to its ultrasonic velocities [e.g., see Truell et al., 1969]. The purpose of this chapter is to describe the single crystal specimens and the experimental procedures by which their densities and velocities were determined.

In this study, velocities were measured for elastic wave propagation along the [110] and [001] crystallographic directions for which there are, respectively, three and two distinct modes of propagation. These modes are shown in Table 1 together with the relationships between the adiabatic moduli and the quantities ρv_i^2, for cubic crystals where ρ is the density and v_i is the velocity for the ith mode. For some of the samples to be described, measurements were carried out only on modes 3, 4 and 5 for propagation along [110]. However, a crystal with cubic symmetry has only three independent elastic moduli, which are here taken to be C_{11}, C_{12} and C_{44} in the usual contracted matrix notation (see Truell et al. [1969], p. 5). The three modes for [110] propagation are thus sufficient by themselves for the determination of all three moduli.

B. Samples

The single crystal specimens used in this study are listed in Table 2. These crystals were obtained from a

Table 1.--Elastic wave propagation modes. Modes 1 and 5 are longitudinal modes and the others are shear modes. Mode 2 is degenerate because of the fourfold rotation symmetry about [001] for cubic crystals.

Mode number i	Direction of wave propagation	Direction of particle motion	
1	[001]	[001]	$\rho v_1^2 = C_{11}$
2	[001]	[001]	$\rho v_2^2 = C_{44}$
3	[110]	[001]	$\rho v_3^3 = C_{44}$
4	[110]	$[1\bar{1}0]$	$\rho v_4^2 = C' \equiv (C_{11} - C_{12})/2$
5	[110]	[110]	$\rho v_5^2 = C_L \equiv (C_{11} + C_{12} + 2\ C_{44})/2$

Table 2.--Composition, e/a, density, and lengths of the specimens. Where two densities are listed for one crystal, the second value was used in subsequent calculations.

		Density		Lengths (mm)	
Composition	e/a	value (g/cm^3)	error (%)	[110]	[001]
Ti-29.4%V	4.294	4.910	0.6		4.9001
		4.929[a]	0.1		
Ti-38.5%V	4.385	5.044	0.2		9.4113
Ti-53%V	4.53	5.328	0.3	6.9984	6.0056
Ti-73%V	4.73	5.640	0.5	5.2755	5.1795
V	5.000	6.102	0.18	7.7845	7.4938
V-17.5%Cr	5.175	6.35[b]	1.4	3.5155	4.0949
		6.32[b]			
Nb	5.000	8.575	0.4	4.9175	5.0671
		8.578[c]			
Nb-25%Mo	5.25	8.981	0.09	6.8031	7.4659
Nb-31%Mo	5.31	9.081	0.08	8.6927	7.8506
Nb-37%Mo	5.37	9.187	0.10	7.6519	6.8773
Nb-44%Mo	5.44	9.294	0.09	7.0518	7.4356
Nb-53%Mo	5.53	9.452	0.09	5.0412	5.0263
Nb-72%Mo	5.72	9.759	0.10	7.3632	8.5518
Mo	6.000	10.216	0.10	8.6815	7.8991
Ta	5.000	16.675	0.05	7.4148	8.5381
Ta-9.6%W	5.096	16.983[d]			20.2388
Ta-21.5%W	5.215	17.311[d]			9.7154
Ta-40.0%W	5.400	17.883[d]		10.6839	4.4578
Ta-64%W	5.64	18.452	0.2	6.3094	6.9476
Ta-90.4%W	5.904	19.023[d]			12.2943
W	6.000	19.253	0.11	8.3678	9.1854

[a] L. J. Graham, personal communication.

[b] E. S. Fisher, personal communication.

[c] Ming and Manghnani [1977].

[d] G. W. Shannette, personal communication.

number of different sources. The pure elements V, Nb, Ta and Mo were acquired from Materials Research Corp. of Orangeburg, New York. The Nb-Mo alloys and the Ta-64% W alloy were purchased from Aremco Products, Inc., Ossining, New York. The remaining Ta-W alloy crystals were borrowed from G.W. Shannette of Michigan Technological University and will be described in a future publication by M. L. Carpenter and G. W. Shannette, who have investigated the temperature dependence of the elastic moduli of these alloys. L. J. Graham of Rockwell International Science Center, Thousand Oaks, California, supplied the Ti-29.4% V and Ti-38.5% V crystals. The Ti-53% V, Ti-73% V, V-17.5% Cr and pure W samples were provided by E. S. Fisher of Argonne National Laboratory.

The purity of some of the samples is shown in Table 3. The purity of the Nb-35% Mo sample is probably typical of all the Nb-Mo alloys since the same starting materials and growth methods were used for all of these crystals.

The particular Nb-Mo sample listed in Table 3 was unfortunately found to be polycrystalline and was not used in this study. Some of the other samples obtained from Aremco Products, Inc. were also polycrystalline as was indicated by the observation of grain boundaries after the sample surfaces were etched. In these cases, suitably large grains were selected and the other grains were removed by cutting or grinding.

In the course of this work sample surfaces were pre-

Table 3.--Purity of samples

Sample	Purity (wt%)	Major Impurities
V [a]	99.95	C - 120 ppm Si - 150 ppm
Nb [a,b]	99.96	Ta - 200 ppm
Ta [a]	99.996	
Mo [a]	99.98	W - 50 ppm
Nb - 35% Mo [c]	99.93	Ta - 280 ppm Hf - 70 ppm W - 60 ppm

[a]Analysis by Materials Research Corp. includes mass spectrographic, vacuum fusion, and conductometric techniques.

[b]Nominal purity for "typical" crystal grown by Materials Research Corp.

[c]Mass spectrographic analysis only, by Aremco Products, Inc.

pared for ultrasonic measurements for the pure elements and for the alloys obtained from Aremco Products, Inc. The other crystals were already prepared as received except for the Ta-40% W specimen which required the preparation of (110) surfaces. Laue X-ray diffraction was used to orient pairs of sample faces to within 1^{o} of the desired crystallographic planes. The faces were ground and polished by standard metallographic techniques. The final polishing step was carried out with 1 μm diamond abrasive which produced a finish suitable for optical observation of the flatness. Some of the faces on the previously prepared samples were also fine-polished in order to improve flatness or to remove tarnish. Over the areas covered by the ultrasonic transducers, the final surfaces were flat and parallel to within about 1/2 μm. Lengths and parallelism were measured by means of a dial gage comparator and precision gage blocks from Scherr-Tumico, St. James, Minn. Lengths are shown in Table 2.

In the case of vanadium, interstitially dissolved hydrogen was removed by heating the sample in a high vacuum. This was generously done by E. S. Fisher at Argonne National Laboratory.

The sample densities, which are shown in Table 2, were measured by the buoyancy (Archimedes') method. The sample weights were measured in air and in freshly boiled distilled water and the density was calculated according to

$$\rho = \frac{W_A \rho_W - W_W \rho_A}{W_A - W_W} \qquad (1)$$

where W_A and W_W, and ρ_A and ρ_W are the sample weights in air and water, and the densities of air and water respectively. W_W was measured by submersing the sample while holding it in a basket or a loop suspended from the balance by means of a thin nickel-chromium alloy wire 0.14 mm in diameter. The procedure may be thought of as a greatly simplified version of the very high precision technique of Bowman and Schoonover [1967], who give an exhaustive discussion of error sources. In the present case, most of the uncertainty arose from the smallness of the samples and the limited accuracy, $\sim \pm 0.25$ mg, of the balance (Mettler model H10). Some aspects of the method of Bowman and Schoonover were thus superfluous and were not followed. In particular, the suspension wire was not specially prepared, and dissolved air was not as effectively kept out of the water because a much smaller volume of water was used. However, their technique of boiling the samples to minimize surface grease and bubbles was followed. For some samples, more accurate density values were available from other sources. These are also listed in Table 2 and were used in subsequent calculations.

Following Hubbell and Brotzen [1972], the compositions of the Nb-Mo alloys were calculated by assuming the density to be a linear function of e/a within a given period. X-ray diffraction data [Pearson, 1958, 1966] show this to be a

fairly good assumption--the compositions are probably accurate to within 3 atomic percent. The composition of the Ta-64% W crystal was obtained by interpolating between the density-composition points of Carpenter and Shannette [to be published]. It should be pointed out here that the densities of the Ta-W alloys shown in Table 2, except for the Ta-64% W crystal, were measured by Carpenter and Shannette.

With the exception of the Ti-53% V, Ti-73% V, and V-17.5% Cr samples, all of the alloy crystals used in this study were grown by the electron-beam-zone refining technique, which produces cylindrical rod-shaped specimens. Alloy crystals grown in this way tend to be somewhat inhomogeneous with composition varying along the rod axis. This inhomogeneity produces effects which will be discussed in Chapter III.

C. Ultrasonic Measurements

Virtually all of the ultrasonic measurements both at atmospheric pressure and at high pressures were carried out by the pulse superposition (PSP) technique of McSkimin [1961]. In this method a single, thin, disc-like piezoelectric transducer is attached by a thin bonding layer to one of two accurately parallel faces of the specimen. When an electrical pulse, in the form of a short RF sine-burst, is applied to the transducer, an ultrasonic wave train is generated in the specimen and bounces back and forth between the two faces. The diameter of the transducer is generally

much larger than the ultrasonic wavelength so that plane-wave conditions are closely approximated. If a series of pulses is applied such that the time interval between pulses, T, is a multiple, p, of the ultrasonic delay time, δ, then the echoes of each pulse will interfere constructively with the echoes of the other pulses. This "in-phase" condition is attained experimentally by adjusting T to achieve a maximum amplitude of the summed echoes. Maxima are observed not only when $T = p\delta$, but also when T differs from $p\delta$ by one or more periods of the carrier frequency. More generally, the "in-phase" delay time is given by

$$T = p\left(\delta - \frac{\phi}{2\pi f}\right) + \frac{n}{f}, \qquad (2)$$

where f is the carrier frequency of the pulses, n is an integer equal to the number of cycles of mismatch, and ϕ is a small phase shift resulting from diffraction effects and from reflection of waves from the transducer and bond. ϕ is discussed further in Chapter III and Appendix A. For the moment it is sufficient to point out that ϕ is usually very small provided that f is equal to the transducer resonance frequency or a harmonic. The objective of the measurement is, of course, to determine δ from which the velocity, $v = 2\ell/\delta$, follows directly.

Measurements are usually carried out at the "in-phase" condition for which $n = 0$. This can be determined by a method described by McSkimin [1961] and McSkimin and Andreatch [1962]. (A brief summary is also given in Appen-

dix A.) This method can be ambiguous in certain cases and it was usually checked by using other interferometric methods. One such method was the phase comparison technique using a buffer rod between sample and transducer as developed by McSkimin [1953, 1957]. The pulse-echo overlap (PEO) method of May [1958] and Papadakis [1967] can easily be adapted for use with a buffer rod and in this way was also used to obtain unambiguous delay time measurements. In addition, measurements with either the PSP or PEO methods can be carried out with different transducers, i.e., at different values of f in equation (2), in order to obtain the n=0 condition. All of these techniques were used at one time or another to determine n.

A schematic diagram of the PSP system is shown in Figure 1. The heart of the system is a PM Custom Electronics Model 5B sine-burst generator (SBG). The SBG produces both rf and trigger pulses at a repetition rate, $F' = 1/T$, determined by a stable oscillator. F' can be adjusted either manually or by an external controlling voltage. In addition, by applying an external gating pulse the sine-bursts (but not the trigger signal) can be suppressed so that the decay pattern of the echoes can be observed without being swamped by the pulses. The RF pulses from the SBG are attenuated in order to avoid excessive amplifier overload, and then applied to the transducer through an impedance matching device. The echoes are picked up by the same transducer and amplified and displayed on an oscilloscope. Adjustment of

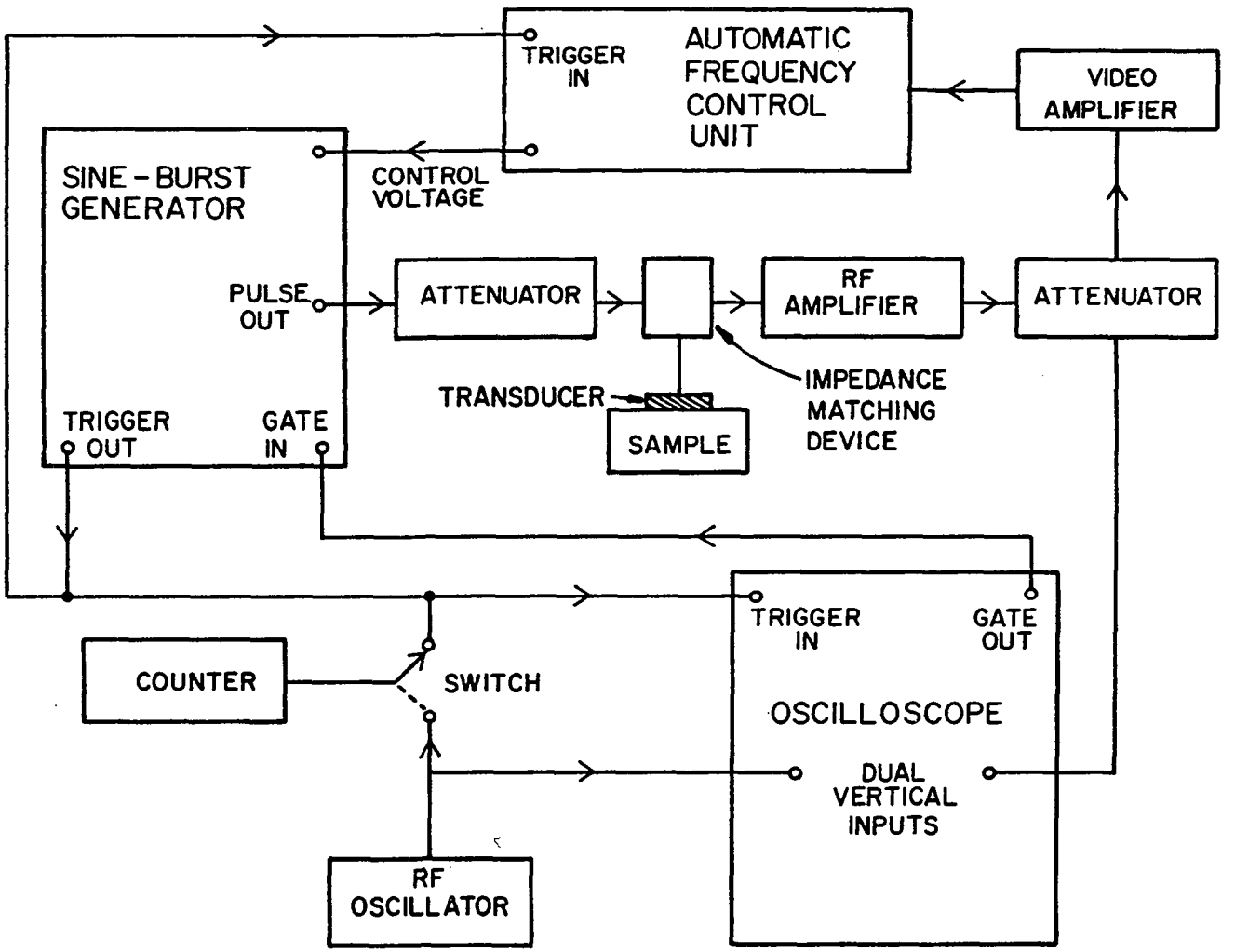

Figure 1. Schematic diagram of the PSP system.

F' for maximum echo amplitude is accomplished either manually while watching the oscilloscope, or by feeding the rectified signal (in the p=0 mode of operation with no gating) into an automatic frequency control (AFC) unit (also from PM Custom Electronics) which monitors the echoes and generates a control voltage for the SBG. The AFC unit has been described by Mattaboni [1970] and is similar in principle to that of McSkimin [1965]. When the AFC unit was used, F' could be determined with a precision of better than 1 ppm as opposed to about 10 ppm by manual adjustment. The trigger signal from the SBG is used to synchronize the AFC unit and the oscilloscope, and it is also connected to a counter which measures the repetition rate, F'. The carrier frequency of the sine-bursts is determined by beating the output of an RF oscillator with the unrectified signal from the SBG by using a dual input oscilloscope in its adding mode. Although the rf oscillator and the sine-bursts are not coherent, it is possible to make out envelopes of the mixed signals with the oscilloscope intensity turned up.

The configuration shown in Figure 1 was used in the work on the 3d metals. Earlier measurements on the 4d and 5d metals and were carried out differently. No attempt was made to accurately set the RF as described above and the AFC unit was used only in a few cases. Readings were instead taken manually with p=1 and with the oscilloscope gate used to suppress the pulses during the sweeptime of the oscilloscope. The observed echoes resulted from a series of from

about 10 to over 100 pulses depending on the sample and the propagation mode. The sine-bursts included from 20 to 50 RF cycles as opposed to 50 to 100 cycles in the later work on the Ti-V-Cr metals. As will be discussed in Chapter III, these differences make the earlier results perhaps less reliable than the later measurements.

The PEO technique in the form developed by Papadakis [1967] was also employed in a few experiments. In this method the time between sine-bursts is adjusted to be a large multiple (1000 in the present case) of the specimen travel time, δ, so that the echoes of one pulse have died out before the next pulse is applied. Any two echoes in the echo train can be selected and the delay time between them can be measured. This method was found in practice to be somewhat less precise than the PSP method. It was found to work better for samples with high attenuation--mainly because higher voltage pulses could be used. The PEO method was particularly useful in cases where the later echoes were of poor quality because of beam-spreading and reflection off of the lateral sides of the sample. In these cases it is possible to use the first few echoes whereas the PSP method superposes a large number of echoes including those far out in the echo train. The details of the present PEO system are very similar to those of Papadakis [1967] and will not be described here.

X-cut and Y-cut quartz discs were used as transducers for longitudinal and shear waves respectively. The trans-

ducer diameters were either 3.1 or 4.7 mm. The fundamental resonance frequencies were chosen to be in the range of 20 to 60 MHz. Shear mode measurements were usually carried out at 20 or 30 MHz and longitudinal measurements were generally done at 40 or 60 MHz. Higher frequencies for the higher longitudinal velocities and lower frequencies for the lower shear velocities were used in order to make the ultrasonic wavelengths similar.

The transducers were bonded to the samples with Nonaq stopcock grease (Fisher Scientific Co.). In a few cases the bonding material was a poly-α-methyl-styrene resin (Dow Chemical resin 276-V9). The latter is a better coupling agent for shear waves but it hardens rapidly with increasing pressure causing the thinner transducers to crack because of differential compression.

All measurements were carried out at 25°C with the sample in a pressure vessel which was immersed in a temperature-regulated oil bath. Temperatures were monitored by means of a chromel-alumel thermocouple placed within a few mm of the specimen. The thermocouple cold junctions were kept at 0°C in an ice bath or in an ice-point cell (Omega Engineering, Model TRC). The thermocouple emf was measured with a Leeds and Northrup K-3 potentiometer. The measured temperatures were probably accurate to within 1%. More importantly, the temperature was kept constant within a range of 0.1°C or better during a given pressure run.

High pressures were generated by a two-stage intensifi-

cation system employing 1:1 and 16:1 intensifiers purchased from Harwood Engineering Co. Pressures were measured to within 0.2% by means of a manganin coil whose resistance, which is a virtually linear function of pressure, was obtained from a Carey-Foster bridge. The coil and bridge, both from Harwood Engineering, were calibrated periodically against a controlled-clearance piston gage (Harwood DWT-300). High-purity nitrogen was used as the pressure medium.

Ultrasonic measurements under pressure were made at intervals of about 0.28 kbar up to about 5 kbar. Occasionally the maximum pressure was limited to 3 or 4 kbar because of leaks in the pressure apparatus, or in order to avoid fracturing of the transducer when the Dow resin 276-V9 was used. Most of the readings were taken with increasing pressure but a few were made with decreasing pressure to check for hysteresis which, in fact, was never observed. Usually two or three such pressure runs were carried out for each mode with a newly prepared bond, and often with a different transducer, for each run.

Measurements on the 3d metals were carried out with the carrier frequency adjusted to be equal to the resonance frequency, f_r, of the transducer, or to an odd harmonic. The variation of f_r with pressure was calculated from the results of McSkimin et al. [1965] for quartz. The term "resonance frequency" is taken here to denote the frequency at which the transducer thickness is 1/2 the ultrasonic wavelength. In practice f could be set to the desired frequency to

within a few parts in 10^4, i.e., to within a few percent of the total change in f_r over the 5 kbar pressure range. The resonance frequency was not followed during pressure runs on the 4d and 5d metals. The carrier frequency was instead kept constant at a value only approximately equal to f_r.

III. DISCUSSION OF ERRORS, DATA ANALYSIS AND RESULTS

This chapter describes the computation of the elastic moduli and their pressure derivatives and discusses the uncertainties in these quantities. Consideration of one source of error--namely, guided wave effects-- is postponed to the next chapter.

A. Uncertainty in the Density

As mentioned previously, the major source of error in the density is due to the limited accuracy of the balance. This uncertainty is shown in Table 2 and is discussed in Appendix B. There are, in addition, other possible sources of error which are difficult to evaluate such as surface oxide layers and grease and bubbles adhering to the sample during the weighings. These would tend to give systematically low density values. The magnitude of these errors appears to be rather small, however, as shown by a comparison in Table 4 between the buoyancy measurements and densities obtained by Ming and Manghnani [1977] from X-ray diffraction determinations of the lattice parameters of the pure element samples. With the exception of Mo, the hydrostatic-weighing densities are in each case lower than the X-ray densities as expected. However, the differences are within the standard deviations in the x-ray values which are also shown in Table 4. Furthermore, the disagreement is worse for Mo where the X-ray density is lower. The system-

Table 4.--Comparison of hydrostatic-weighing densities of the present study, X-ray diffraction densities of Ming and Manghnani [1977] and the "typical" densities of Westlake [1977] for the pure elements (in g/cm^3)

Element	Hydrostatic ρ	X-ray ρ	"Typical" ρ
V	6.102	6.111 ± .010	6.098
Nb	8.575	8.578 ± .022	8.575
Ta	16.675	16.683 ± .022	16.677
Mo	10.216	10.202 ± .010	
W	19.253	19.256 ± .026	

atic errors mentioned above are therefore not serious and are probably on the order of 0.1% or less.

Westlake [1977] has recently reviewed the literature on the densities of the Group VB elements. The last column of Table 4 shows the density values he considers to be typical of commercially-available high-purity single crystals. The agreement among the three sets of values is very good. It may therefore be concluded that the present density measurements are essentially accurate although the values for some of the smaller crystals are rather imprecise.

B. Velocities and Moduli

The primary data from the ultrasonic experiments are the pulse repetition frequencies $F' = 1/T$ at the "in-phase" conditions. The desired quantity is the reciprocal of the sample delay time, $F = 1/\delta$, in terms of which the velocity

is

$$v = 2\ell F \tag{3}$$

In this notation, equation (2) can be written as

$$F = \frac{pF'}{1 + p\frac{F'}{f}\frac{\phi}{2\pi} - \frac{nF'}{f}} \tag{4}$$

The velocities were calculated by assuming ϕ to be negligible and by using only values of F' corresponding to n=0. Ignoring ϕ results in errors of a few parts in 10^4.

Because up to 5 independent propagation modes were studied for a given sample, the three independent elastic moduli were in general overdetermined. This was handled by using a least-squares procedure [e.g., see Mathews and Walker, 1965]. The "best-fit" C_{ij} were determined by minimizing the sum

$$\chi^2 = \sum_{n=1}^{N} \left(\frac{(\rho v_n^2)_{\text{observed}} - (\rho v_n^2)_{\text{calculated}}}{\sigma_n} \right)^2, \tag{5}$$

where $(\rho v_n^2)_{\text{calculated}}$ is computed from the "best-fit" moduli according to the expressions in Table 1, and σ_n is the estimated uncertainty in $(\rho v_n^2)_{\text{observed}}$. Strictly speaking, it would be more correct to minimize χ^2 with the directly observed velocities replacing the derived ρv^2 in equation (5) as was done by McSkimin et al. [1965]. However, it has been pointed out by E. R. Cohen [personal communication] that there is no significant difference in the results,

and, furthermore, it is computationally much simpler to use the ρv^2 since they are linear functions of the C_{ij} for the propagation modes used here.

Another simplification introduced for computational convenience was that the sum in equation (5) was taken over each individual velocity measurement rather than over the number of independent propagation modes. This was done even in cases where only three modes were studied. The disadvantage of this is that the measurements carried out on a single mode are not independent but instead have in common the effects of length, crystal orientation, bond, and diffraction errors. Modes for which a greater number of velocity determinations have been made are thus given too large a weight in the fitting procedure. Here again, since a roughly equal number of measurements were generally made for each mode, the "best-fit" values are not seriously affected.

The above simplifications can be seen to be even less important when it is recognized that the estimates of σ_n are rather crude and somewhat subjective. Appendix C describes the estimation of σ_n in detail. In summary, rough approximations were made for bond and diffraction contributions to ϕ in equation (4). These two types of errors tend to cancel, thus justifying in part the neglect of ϕ in computing the velocity. The bond and diffraction errors tend to be generally large for small samples and small for large samples. These errors were then combined with the uncertainty in length to obtain σ_n. The uncertainty in the density was

deliberately excluded since it is the same for all modes.

The results of the fitting procedure are shown in Table 5. In this table C' and C_L are shear and longitudinal effective moduli for waves propagating along [110] as defined in Table 1; $K_s = (C_{11} + 2\ C_{12})/3 = (\partial P/\partial \ell n \rho)$ is the adiabatic bulk modulus; and $A = C_{44}/C'$ is the elastic shear anisotropy ratio. Also shown in Table 5 is the ratio of error measures, r, which is here defined by

$$r^2 = \chi^2/(N - 3) \quad . \tag{6}$$

For large N, and for normally distributed errors, there is a 50% probability that $\chi^2 < N - 3$. Thus r can be thought of as a crude measure of the goodness of the fit in terms of the input σ_n. A value of r in the neighborhood of 1 indicates that the σ_n are reasonable. When r is much smaller or much larger than 1, then the internal consistency of the data is much better or much worse, respectively, than is indicated by the σ_n. In the cases where r was greater than 1, each σ_n was multiplied by r in order to make $\chi^2 = N - 3$. The resulting "renormalized" uncertainties in the "best-fit" moduli are shown in Table 5. The original uncertainties can be recovered simply by dividing by r. This applies only to the samples for which $r > 1$. Where r is less than 1, the uncertainties shown are those obtained from the original fit. In these cases, it would be unwise to scale down the σ_n since they represent systematic errors to some extent. Since the uncertainties in the velocities are approximately repre-

Table 5.--Adiabatic elastic moduli. Values and uncertainties are from least-squares fits as described in the text. $A = C_{44}/C'$, and r are dimensionless. All other quantities are in units of Mbar.

Sample	C_{11}	C_{12}	C_{44}	C'	C_1	K_s	A	r
3d Metals								
Ti-29.4%V	1.4002 ±.0009	0.9949 ±.0009	0.3966 ±.0003	0.20263 ±.00010	1.5941 ±.0005	1.1300 ±.0009	1.957 +.002	1.6
Ti-38.5%V	1.4896 ±.0006	1.0053 ±.0006	0.40945 ±.00017	0.24213 ±.00009	1.6569 ±.0006	1.1668 ±.0006	1.9610 ±.0010	
Ti-53%V	1.6760 ±.0009	1.0509 ±.0011	0.4129 ±.0004	0.3125 ±.0003	1.7763 ±.0010	1.2593 ±.0010	1.321 ±.002	3.5
Ti-73%V	1.9227 ±.0004	1.1106 ±.0005	0.41476 ±.00009	0.40602 ±.00016	1.9314 ±.0004	1.3813 ±.0004	1.0215 ±.0005	0.7
V	2.3092 ±.0005	1.2001 ±.0005	0.43360 ±.00011	0.55454 ±.00020	2.1882 ±.0005	1.5698 ±.0005	0.7819 ±.0004	1.6
V-17.5%Cr	2.5507 ±.0008	1.2036 ±.0009	0.43968 ±.00013	0.6735 ±.0003	2.3168 ±.0009	1.6526 ±.0009	0.6528 ±.0004	0.7

Table 5.--(Continued) Adiabatic elastic moduli. Values and uncertainties are from least-squares fits as described in the text. $A = C_{44}/C'$, and r are dimensionless. All other quantities are in units of Mbar.

Sample	C_{11}	C_{12}	C_{44}	C'	C_1	K_s	A	r
4d Metals								
Nb	2.4619 ±.0003	1.3294 ±.0004	0.28688 ±.00006	0.56627 ±.00017	2.1825 ±.0003	1.7069 ±.0003	0.5066 ±.0002	0.9
Nb-25%Mo	2.8433 ±.0003	1.4108 ±.0004	0.31935 ±.00006	0.71624 ±.00020	2.4464 ±.0003	1.8883 ±.0003	0.4459 ±.0002	0.3
Nb-31%Mo	2.9569 ±.0011	1.4388 ±.0013	0.34612 ±.00019	0.7591 ±.0005	2.5439 ±.0011	1.9448 ±.0012	0.4560 ±.0004	2.7
Nb-37%Mo	3.1316 ±.0007	1.4288 ±.0008	0.41078 ±.00016	0.8514 ±.0004	2.6910 ±.0007	1.9964 ±.0007	0.4825 ±.0003	1.8
Nb-44%Mo	3.3630 ±.0010	1.4178 ±.0011	0.5125 ±.0002	0.9726 ±.0005	2.9030 ±.0009	2.0662 ±.0009	0.5260 ±.0004	2.0
Nb-53%Mo	3.6751 ±.0007	1.4188 ±.0008	0.65468 ±.00018	1.1281 ±.0004	3.0438 ±.0007	2.1709 ±.0007	0.5803 ±.0003	0.4
Nb-72%Mo	4.1437 +.0017	1.4657 ±.0022	0.8663 ±.004	1.3390 ±.0010	3.6710 ±.0016	2.3583 ±.0018	0.6470 ±.0006	2.6
Mo	4.6479 ±.0009	1.6157 ±.0019	1.0894 ±.0005	1.5161 ±.0010	4.2212 ±.0011	2.6264 ±.0013	0.7186 ±.0005	1.6

Table 5.--(Continued) Adiabatic elastic moduli. Values and uncertainties are from least-squares fits as described in the text. $A = C_{44}/C'$, and r are dimensionless. All other quantities are in units of Mbar.

Sample	C_{11}	C_{12}	C_{44}	C'	C_1	K_s	A	r
5d Metals								
Ta	2.6600 ±.0004	1.6094 ±.0004	0.82473 ±.00012	0.52528 ±.00012	2.9594 ±.0004	1.9596 ±.0004	1.5701 ±.0002	0.4
Ta-9.6%W	2.8579 ±.0006	1.6482 ±.0006	0.84269 ±.00014	0.60486 ±.00009	3.0957 ±.0006	2.0514 ±.0006	1.3932 ±.0003	0.5
Ta-21.5%W	3.1018 ±.0005	1.7001 ±.0005	0.85269 ±.00017	0.70086 ±.00012	3.2537 ±.0004	2.1673 ±.0005	1.2166 ±.0003	0.8
Ta-40.0%W	3.5267 ±.0017	1.8053 ±.0024	0.86316 ±.00024	0.8607 ±.0019	3.5292 ±.0009	2.3791 ±.0013	1.003 ±.002	1.9
Ta-64%W	4.240 ±.007	1.871 ±.007	1.0645 ±.0015	1.1846 ±.0022	4.120 ±.007	2.661 ±.007	0.899 ±.002	10.4
Ta-90.4%W	4.9812 ±.0012	1.9745 ±.0012	1.4614 ±.0003	1.5033 ±.0003	4.9392 ±.0011	2.9767 ±.0012	0.9721 ±.0003	0.3
W	5.2269 ±.0009	2.0456 ±.0011	1.6060 ±.0003	1.5907 ±.0004	5.2422 ±.0009	3.1060 ±.0010	1.0096 ±.0003	0.2

sented by σ_n, a large value of r in Table 5 indicates the presence of additional errors due to the nature of the sample. These errors include misorientation of specimen faces and inhomogeneity in the crystal. It should also be emphasized that only three propagation modes were used for those alloy samples that have only one length listed in Table 2. The uncertainties listed in Table 5 for those samples are therefore underestimates since they do not allow for misorientation or inhomogeneity.

At this point it is appropriate to recall that, except for the Ti-53%V, Ti-73%V, and V-17.5%Cr compositions, all the alloy crystals were grown by the floating-melt-zone technique. In this method a narrow cross-sectional zone is melted in a rod of the desired composition. The molten zone is gradually moved through the rod, and favorably oriented crystal grains will grow and predominate behind the zone at the expense of other grains. By repeatedly passing the zone through the rod (or by starting with a seed crystal at one end) a single crystal can be obtained. When an alloy crystal is grown it is difficult in general to obtain homogeneity because the melting point is a function of composition and because the vapor pressures of the components are different. The result is that the chemical composition tends to vary along the rod axis. When velocities are measured in a direction close to the rod axis, the ultrasonic delay times will correspond to those expected of a homogeneous sample with the average composition of the inhomogeneous crystal. On the other hand, velocities along

directions more nearly perpendicular to the rod axis will depend on where the transducer is placed. This was actually observed in velocity measurements on the Ta-40%W crystal in the [110] direction which was perpendicular to the growth axis. The velocities for mode 4, which shows the strongest composition dependence of all the modes, varied by about 0.3% across the crystal, which corresponds to a difference in composition of perhaps 0.5 atomic % from end to end. In this case and for other crystals as well, velocities were measured with the transducer near the center of the specimen, and the internal consistency was surprisingly good.

Inhomogeneity as described above was probably present to some degree in all of the alloy samples. Aside from the question of the composition of the volume sampled by the ultrasonic wave, there is also the problem caused by wedging of the elastic properties. If the velocity varies across the area of the transducer, the wave-fronts will distort and the situation is equivalent to one in which a homogeneous sample has nonparallel faces. This produces recognizable effects in the echo train--i.e., there are oscillations superposed on the exponential decay pattern as discussed by Truell et al. [1969]. This was observed on all the samples, but it was difficult to decide how much of it was due to inhomogeneity and how much was due to actual nonparallelism and consequently no attempt was made to allow for this in estimating the σ_n. This effect was particularly noticeable for the Ta-W alloys.

Inhomogeneity was probably the cause of the very poor

internal consistency for the Ta-64%W crystal. In this case reproducibility in the velocities was poor even though an attempt was made to place the transducers in the same position for each measurement. Another possible source of error was that this sample was not a perfect crystal. The Laue patterns showed a mosaic structure with subgrains spread in orientation by 2^{o} or 3^{o}. However, this sample was fairly close to being elastically isotropic (i.e., $A \underset{\sim}{} 1$) so this sort of problem should not have a large effect on the velocities.

In summary, the uncertainties in Table 5 crudely reflect 1) bond, diffraction and length errors, 2) reproducibility of the ultrasonic measurements, and 3) internal consistency in cases where more than 3 modes were studied.

For purposes of comparison to other measurements, maximum errors excluding density errors are perhaps 2 or 3 times larger than shown in Table 5 for the pure elements. The maximum errors for the alloys may be considerably greater because of inhomogeneity.

C. Pressure Derivatives of the Moduli

A very useful review paper on the relation of ultrasonic data to the pressure or strain derivatives of the moduli has been written by Thurston [1965]. The following derivation has been abstracted from Thurston's work. The treatment for crystals of cubic symmetry is particularly simple since they compress isotropically under hydrostatic pressure.

For a given propagation mode, the elastic wave velocity is given by equation (3), and it follows that

$$\frac{\rho v^2}{\rho_o v_o^2} = \left(\frac{\ell_o}{\ell}\right)^3 \left(\frac{F\ell}{F_o \ell_o}\right)^2 = \left(\frac{F}{F_o}\right)^2 \frac{\ell_o}{\ell} \tag{7}$$

where the zero subscript denotes evaluation at zero pressure. Differentiation of (7) yields

$$(\rho v^2)' = \left(\frac{\partial(\rho v^2)}{\partial P}\right)_T = \rho_o v_o^2 \left(\frac{1}{F_o^2}\left(\frac{\partial F^2}{\partial P}\right)_T + \frac{1}{3K_T}\right) \tag{8}$$

where the derivatives are evaluated at P = 0, and

$$K_T = \left(\frac{\partial P}{\partial \ell n \rho}\right)_T \tag{9}$$

is the isothermal bulk modulus. In equation (8), $\rho_o v_o^2$ and F(P) are obtained as described in Chapter II. K_T can be obtained from the adiabatic bulk modulus by means of the formula

$$K_T = \frac{K_s}{1+\alpha\gamma T} \tag{10}$$

where α is the volume coefficient of thermal expansion. The Gruneisen parameter, γ, is defined by

$$\gamma = \frac{\alpha K_s}{\rho C_p} \tag{11}$$

where C_p is the specific heat per unit mass at constant pressure.

Once the derivatives of ρv^2 are calculated from equation (8), the quantities $(\partial C_{ij}/\partial P)_T$ follow directly by differentiating the relations in the last column of Table 1. The $(\partial C_{ij}/\partial P)_T$ are derivatives of the effective adiabatic elastic coefficients as defined by Thurston and Brugger [1964]

and are the quantities usually reported in the ultrasonic literature. They should not be confused with derivatives of other types of moduli such as the derivatives of the thermodynamic elastic constants as defined by Brugger [1964]. Note also that the derivatives are "mixed" in that the C_{ij} are isentropic strain derivatives of the elastic energy while the pressure derivatives are measured along an isotherm. For the purposes of the discussion in Chapter V, the differences between adiabatic and isothermal derivatives is negligible.

The difference should not be ignored, however, when the ultrasonic data are extrapolated to very high pressures for comparison with isothermal equations of state determined by X-ray or shock compression experiments. For this purpose, it is necessary to compute [Thurston, 1965]

$$K_T' = \left(\frac{\partial K_T}{\partial P}\right)_T = \left(\left(\frac{\partial K_S}{\partial P}\right)_T - \alpha\gamma T g \right) \Big/ (1+\alpha\gamma T)^2 \qquad (12)$$

where

$$g = 2\left(\frac{1}{\alpha K_S}\left(\frac{\partial K_S}{\partial T}\right)_P - \gamma\right) - 1 - 3\gamma\,\frac{T}{\alpha}\left(\frac{\partial \alpha}{\partial T}\right)_P - 2\,\alpha\gamma T\left(1 - \frac{1}{\alpha C_p}\left(\frac{\partial C_p}{\partial T}\right)_p\right) \qquad (13)$$

Consider now the more practical aspects of the calculations. As in the previous section, "best-fit" values of $(\partial C_{ij}/\partial P)_T$ were obtained by minimizing

$$\chi^2 = \sum_{n=1}^{N} \left(\frac{(\rho v_n^2)'_{\text{observed}} - (\rho v_n^2)'_{\text{calculated}}}{\sigma_n} \right)^2 \qquad (14)$$

where N is the number of experimental frequency-pressure runs, and the prime denotes the isothermal pressure derivative. The $(\rho v_n^2)'_{observed}$ are determined through equation (8) from the ultrasonic data and the $(\rho v_n^2)'_{calculated}$ are obtained from the "best-fit" C'_{ij} through the equations in Table 1.

The primary ultrasonic data from a pressure run are the frequencies F'(P), and it is necessary to determine the derivative of F(P) for use in equation (8). Differentation of equation (4) followed by evaluation at zero pressure gives

$$\left(\frac{\partial \ell nF}{\partial P}\right)_T = \frac{F_o}{pF_o'}\left(\frac{\partial \ell nF'}{\partial P}\right)_T - \frac{F_o}{f_o}\left(\frac{\partial(\phi/2\pi)}{\partial P}\right)_T + \frac{F_o}{f_o}\left(\frac{\phi}{2\pi} - \frac{n}{p}\right)\left(\frac{\partial \ell nf}{\partial P}\right)_T \tag{15}$$

Now $\phi/2\pi$ and F_o/f_o are much less than one and are of the same order of magnitude. To first order in these quantities, and with n=0, equation (15) becomes

$$\frac{1}{F_o}\left(\frac{\partial F}{\partial P}\right)_T = \frac{1}{F'}\left(\frac{\partial F'}{\partial P}\right)_T - \frac{F_o}{f_o}\left(\frac{\partial(\frac{\phi}{2\pi})}{\partial P}\right)_T \tag{16}$$

or

$$\frac{1}{F_o^2}\left(\frac{\partial F^2}{\partial P}\right)_T = \frac{1}{(F_o')^2}\left(\frac{\partial F'^2}{\partial P}\right)_T - \frac{2F_o}{f_o}\left(\frac{\partial(\frac{\phi}{2\pi})}{\partial P}\right)_T \tag{17}$$

Note that the change in F' over the 5 kbar pressure range was very small--on the order of a few tenths of a percent. In all cases, both F' and F'^2 could be considered linear and

the difference between

$$\frac{2}{F'_o}\left(\frac{\partial F'}{\partial P}\right)_T$$

and

$$\frac{1}{F'^2_o}\left(\frac{\partial F'^2}{\partial P}\right)_T$$

was negligible. In this study a linear least squares fit was made to the F'^2 versus P data and the resulting slopes were used in the calculations. Now the contribution of the diffraction phase shift to the second term in (16) is negligible because the sample and transducer dimensions change very slowly under pressure. When the transducer resonance frequency is followed carefully, as was the case for the 3d metals, the transducer-bond phase shifts are also virtually independent of pressure as shown by McSkimin and Andreatch [1962] and Davies and O'Connell [1977] (see also Appendix A). Thus the second term is equation (16) was ignored for the Ti-V-Cr solid solutions. The correction term is, at any rate, difficult to estimate. For the purpose of the least-squares analysis, the uncertainty in $(\partial \ell n F^2/\partial P)_T$ arising from ϕ was assumed to be 0.01 Mb^{-1} for the 3d metals. This corresponds over the 5 kbar range to an uncertainty in Φ of $\sim 1^o$, which is probably a reasonable figure (see Appendix A). For the 3d metals, the above estimate was combined with the uncertainty in the pressure scale (0.2%) and the standard error in the least-squares-fit slope (usually a few tenths

of a percent) to obtain σ_n for use in equation (14).

The earlier measurements on the 4d and 5d metals were treated differently because the ultrasonic carrier frequency was kept constant under pressure. McSkimin and Andreatch [1962] have pointed out that this leads to errors in the frequency slopes if no correction is applied. More recently, Davies and O'Connell [1977] have pointed out that the errors can be substantial if the carrier frequency is not fixed at a value close to the resonance frequency at zero pressure. The latter authors have, in addition, derived an approximate correction term for the case in which f is fixed at a zero pressure value f_o. In the present notation this is

$$\left(\frac{\partial(\frac{\phi}{2\pi})}{\partial P}\right)_T = \left(\frac{Z_1}{Z_3}\right) \left(\frac{f_o}{f_{ro}}\right) \left(\frac{\partial \ell n\, f_r}{\partial P}\right)_T \qquad (18)$$

Here Z_1 and Z_3 are the acoustical impedance (ρv) of the transducer and sample respectively and f_{ro} is f_r at $P = 0$. Equation (17) can now be written as

$$\frac{1}{F_o^2}\left(\frac{\partial F^2}{\partial P}\right)_T = \frac{1}{F_o'^2}\left(\frac{\partial F'^2}{\partial P}\right)_T + \Delta \qquad (19)$$

where

$$\Delta = -2\left(\frac{Z_1}{Z_3}\right)\left(\frac{F_o}{f_{ro}}\right)\left(\frac{\partial \ell n\, f_r}{\partial P}\right)_T \qquad (20)$$

In order to test the validity of this correction, a number of observations were made on the 3d metals in which slopes obtained by keeping f constant at $f = f_{ro}$ were sub-

tracted from slopes obtained with $f = f_r$. The results are compared in Table 6 to values of Δ from equation (20). The variation of f_r with pressure was obtained from the work of McSkimin et al. [1965]. The observed values of Δ are probably good to only 20%. It is still significant, however, that the observed values of Δ tend to be lower than the calculated values. This is to be expected since bond effects, which are neglected in equation (20), will give a negative contribution to Δ. The magnitude of the bond contribution should also be greater for shear waves than for longitudinal waves because the ratio of the bond thickness to the wavelength is greater for shear waves than for longitudinal waves at the frequencies used here. This is generally borne out in Table 6. Thus if the correction is applied, its magnitude will be too large for shear waves and too small for longitudinal waves. Nevertheless, the evidence in Table 6 indicates that more accurate values result from applying the approximate correction than from ignoring it entirely.

The conditions under which the 4d and 5d metals were studied are not strictly comparable to the later measurements because no effort was made either to measure the transducer frequency accurately or to set f close to f_r. This could result in errors comparable to the magnitude of the correction itself as pointed out by Davies and O'Connell [1977], chiefly through amplification of bond effects. Furthermore, shorter pulse widths were used for the earlier measurements. The wider frequency band-widths could affect

Table 6.--Calculated and observed corrections to frequency slopes

Sample	Mode	Z_1/Z_3	F/f_r	Δ ($Mbar^{-1}$) calculated	Δ ($Mbar^{-1}$) observed
Ti-29%V	3	0.74	0.0096	0.052	0.036
	5	0.54	0.0096	-0.016	-0.010
					-.014
Ti-39%V	3	0.72	0.0051	0.027	0.021
	4	0.93	0.0039	0.027	0.021
	5	0.53	0.0049	-0.008	-0.011
Ti-53%	4	0.80	0.0068	0.040	0.036
V	3	0.63	0.0057	0.027	0.016
					-0.018
	4	0.56	0.0067	0.028	0.024
	5	0.42	0.0066	-0.017	-0.012
V-18%Cr	2	0.62	0.0125	0.057	0.051
					0.056
	3	0.62	0.0107	0.049	0.037
	4	0.50	0.0133	0.049	0.046
	5	0.40	0.0122	-0.015	-0.022
Ti-73%V	1	0.46	0.028	-0.039	-0.03
	5	0.46	0.028	-0.039	-0.06

the measurements because both the diffraction and transducer-bond reflection phase shifts are frequency dependent, and because the transducer-bond assembly acts to some extent as a filter [Truell et al., 1969] whose response characteristics change drastically as a function of pressure [Davies and O'Connell, 1977].

It is possible to roughly evaluate these effects because a number of pressure runs were carried out for vanadium using the earlier technique. Table 7 shows values of $(\partial(\rho v^2)/\partial P)_T$ as measured by the earlier method with and without the correction of equation (20). Also shown for comparison are values obtained by the later technique which is presumably more accurate. The results are rather mixed. For the shear modes 3 and 4 the corrections are clearly of the correct sign but are overestimates as they were in Table 6.

It is clearly impossible to draw any unequivocal conclusions from these results. Nevertheless, the corrections of equation (20) were applied to the data on the 4d and 5d metals for two reasons. First, in a negative sense, the corrections do not seem to produce significant errors. Second, the errors produced by the corrections appear for the most part to be directly or indirectly related to bond effects which should be smaller in the 4d and 5d metals because of their relatively high acoustical impedances. In other words, the corrections probably hold better for the heavier metals than for vanadium. In view of the possible

Table 7.--Comparison of early values of $(\partial(\rho v^2)/\partial P)_T$ for vanadium obtained from uncorrected and corrected slopes with later "accurate" values obtained by following the transducer resonance.

Mode	f_r (MHz)	$(\partial(\rho v^2)/\partial P)_T$ Resonance not followed uncorrected	Resonance not followed corrected	resonance followed "best-fit" value
1	60	5.63	5.61	5.65
3	20	0.184	0.202	
	20	0.181	0.199	
	30	0.166	0.178	0.185
	30	0.179	0.191	
4	20	1.029	1.052	
	30	1.016	1.031	1.042
5	60	4.77	4.75	4.51
	60	4.79	4.77	
$(\frac{\partial K_S}{\partial P})_T$		4.27	4.23	4.26

errors in the corrections, the corrections themselves were used as uncertainties to obtain the σ_n in equation (14) for the fitting procedure.

Table 8 shows the "best-fit" derivatives of the moduli and the resulting uncertainties. Here again, as in Table 5, r indicates the suitability of the input uncertainties and the degree of internal consistency, and the uncertainties have been scaled upwards whenever $r > 1$. To varying degrees for different samples the uncertainties in Table 8 reflect 1) transducer-bond phase shift errors, 2) the reproducibility of the F' versus P slopes, and 3) internal inconsistencies resulting from misorientation and inhomogeneity.

Table 9 exhibits K_T and the thermal parameters used in equation (10). For the 4d and 5d metals, α and the molar heat capacity were assumed to be linear functions of e/a. The thermal expansion and the molar heat capacity were assumed to be constant and equal to the values for V for the 3d alloys. These approximations may result in errors of a few tenths of a percent in K_T.

K_T' and the additional parameters used to compute it from equations (12) and (13) are shown in Table 10 for the pure elements. All things considered, these K_T' values are probably good to within 2 or 3 percent although maximum errors of 5 or 6% are conceivable for the 4d and 5d metals. Note that the bottom row of Table 7 also compares uncorrected, corrected and "accurate" K_S' values. The spread is within 1% which indicates that transducer and bond effects

Table 8.--Isothermal pressure derivatives of the adiabatic moduli. $\partial A/\partial P$ is in units of $Mbar^{-1}$. All other quantities are dimensionless.

Sample	$\partial C_{11}/\partial P$	$\partial C_{12}/\partial P$	$\partial C_{44}/\partial P$	$\partial C'/\partial P$	$\partial C_L/\partial P$	$\partial K_s/\partial P$	$\partial A/\partial P$	r
3d Metals								
Ti-29.4%V	4.49 ±.07	3.56 ±.07	0.466 ±.011	0.467 ±.009	4.49 ±.07	3.87 ±.07	-2.21 ±.11	2.8
Ti-28.5%V	4.63 ±.03	3.56 ±.03	0.431 ±.005	0.533 ±.004	4.52 ±.03	3.92 ±.03	-1.94 ±.04	
Ti-53%V	4.89 ±.02	3.56 ±.02	0.350 ±.004	0.668 ±.004	4.58 ±.02	4.00 ±.02	-1.70 ±.02	1.1
Ti-73%V	5.34 ±.06	3.62 ±.06	0.238 ±.007	0.858 ±.014	4.72 ±.06	4.19 ±.06	-1.57 ±.04	2.0
V	5.65 ±.03	3.56 ±.02	0.185 ±.003	1.042 ±.006	4.79 ±.03	4.26 ±.03	-1.14 ±.01	0.2
V-17.5%Cr	6.09 ±.03	3.76 ±.03	0.238 ±.003	1.165 ±.008	5.16 ±.03	4.54 ±.03	-0.776 ±.009	0.7

Table 8.--(continued) Isothermal pressure derivatives of the adiabatic moduli. $\partial A/\partial P$ is in units of $Mbar^{-1}$. All other quantities are dimensionless.

Sample	$\partial C_{11}/\partial P$	$\partial C_{12}/\partial P$	$\partial C_{44}/\partial P$	$\partial C'/\partial P$	$\partial C_L/\partial P$	$\partial K_S/\partial P$	$\partial A/\partial P$	r
4d Metals								
Nb	5.22 ±.03	3.37 ±.03	0.281 ±.006	0.925 ±.013	4.57 ±.03	3.98 ±.03	-0.332 ±.016	0.6
Nb-25%Mo	5.35 ±.02	3.24 ±.02	0.580 ±.005	1.053 ±.011	4.87 ±.02	3.94 ±.02	0.155 ±.010	0.8
Nb-31%Mo	5.58 ±.02	3.25 ±.02	0.724 ±.004	1.166 ±.009	5.14 ±.02	4.03 ±.02	0.254 ±.008	0.7
Nb-37%Mo	6.17 ±.02	3.29 ±.02	1.035 ±.006	1.442 ±.013	5.77 ±.02	4.25 ±.02	0.398 ±.010	1.1
Nb-44%Mo	6.43 ±.02	3.15 ±.03	1.266 ±.007	1.641 ±.012	6.06 ±.02	4.25 ±.02	0.413 ±.010	0.9
Nb-53%Mo	6.50 ±.05	3.37 ±.05	1.299 ±.012	1.564 ±.021	6.24 ±.05	4.42 ±.05	0.347 ±.015	0.6
Nb-72%Mo	6.39 ±.04	3.32 ±.04	1.333 ±.010	1.538 ±.018	6.19 ±.04	4.34 ±.04	0.252 ±.011	1.3
Mo	6.41 ±.03	3.45 ±.05	1.396 ±.012	1.478 ±.023	6.33 ±.03	4.44 ±.04	0.220 ±.013	1.0

Table 8.--(continued) Isothermal pressure derivatives of the adiabatic moduli. $\partial A/\partial P$ is in units of $Mbar^{-1}$. All other quantities are dimensionless.

Sample	$\partial C_{11}/\partial P$	$\partial C_{12}/\partial P$	$\partial C_{44}/\partial P$	$\partial C'/\partial P$	$\partial C_L/\partial P$	$\partial K_s/\partial P$	$\partial A/\partial P$	r
5d Metals								
Ta	5.079 ±.014	3.110 ±.016	1.004 ±.007	0.984 ±.007	5.099 ±.012	3.767 ±.014	-1.03 ±.03	1.6
Ta-9.6%W	5.126 ±.007	3.120 ±.007	1.051 ±.003	1.003 ±.002	5.174 ±.006	3.789 ±.007	-0.572 ±.006	1.2
Ta-21.5%W	5.38 ±.05	3.34 ±.05	1.075 ±.021	1.022 ±.017	5.43 ±.04	4.02 ±.04	-0.24 ±.04	4.5
Ta-40.0%W	5.468 ±.010	3.38 ±.06	1.139 ±.005	1.05 ±.03	5.56 ±.03	4.07 ±.04	0.11 ±.03	1.4
Ta-64%W	6.25 ±.02	3.40 ±.04	1.514 ±.018	1.425 ±.021	6.340 ±.014	4.35 ±.03	0.20 ±.02	2.1
Ta-90.4%W	6.207 ±.014	3.302 ±.014	1.635 ±.006	1.435 ±.006	6.390 ±.011	4.270 ±.013	0.149 ±.005	0.4
W	6.169 ±.009	3.357 ±.015	1.609 ±.008	1.406 ±.008	6.439 ±.008	4.294 ±.011	0.119 ±.007	0.8

Table 9.--Volume coefficients of thermal expansion, specific heats at constant pressure, Grüneisen parameters, and isothermal bulk moduli of the samples.

Sample	$\alpha(10^{-6}{}^{o}C^{-1})$	C_p(j/g-^{o}C)	γ	K_T(Mbar)
Ti-29.4%V	23.4	0.512	1.05	1.122
Ti-38.5%V	23.4	0.509	1.06	1.158
Ti-53%V	23.4	0.505	1.10	1.250
Ti-73%V	23.4	0.499	1.15	1.370
V	23.4[a]	0.490[a]	1.23	1.556
V-17.5%Cr	23.4	0.489	1.25	1.638
Nb	21.3[a]	0.266[a]	1.59	1.690
Nb-25%Mo	19.8	0.261	1.60	1.871
Nb-31%Mo	19.4	0.260	1.60	1.927
Nb-37%Mo	19.0	0.259	1.59	1.979
Nb-44%Mo	18.6	0.258	1.60	2.048
Nb-53%Mo	18.0	0.256	1.61	2.152
Nb-72%Mo	16.8	0.253	1.60	2.339
No	15.0[a]	0.248[a]	1.55	2.608
Ta	19.5[a]	0.140[a]	1.64	1.941
Ta- 9.6%W	18.9	0.139	1.64	2.033
Ta-21.5%W	18.2	0.138	1.65	2.148
Ta-40.0%W	17.1	0.137	1.66	2.359
Ta-64%W	15.7	0.135	1.68	2.661
Ta-90.4%	14.1	0.133	1.66	2.956
W	13.5[a]	0.132[a]	1.65	3.086

[a]American Institute of Physics Handbook.

Table 10.--Temperature derivatives of α, C_p, and K_s, and pressure derivatives of K_s and K_T. All quantities are dimensionless.

Element	$\frac{T}{\alpha}\left(\frac{\partial\alpha}{\partial T}\right)_P$ [a]	$\frac{1}{\alpha C_p}\left(\frac{\partial C_p}{\partial T}\right)_P$ [a]	$\frac{1}{\alpha K_s}\left(\frac{\partial K_s}{\partial T}\right)_p$	$\left(\frac{\partial K_s}{\partial P}\right)_T$	$\left(\frac{\partial K_T}{\partial P}\right)_T$
V	0.0[b]	33	-3.2[c]	4.26	4.27
Nb	0.21	18	-3.2[d]	3.98	4.02
Ta	0.08	16	-3.4[e]	3.77	3.80
Mo	0.12	45	-3.9[f]	4.44	4.46
W	0.13	49	-4.2[g]	4.29	4.32

[a]American Institute of Physics Handbook, 3rd ed., edited by D. E. Gray, McGraw-Hill, 1972.

[b]Estimated from the data of Bolef et al. [1971], and references therein.

[c]Bolef et al. [1971].

[d]Jones et al. [1969].

[e]Leisure et al. [1973].

[f]Davidson and Brotzen [1968].

[g]Lowrie and Gonas [1967].

are not large on the average. However, there is a 5% difference for mode 5 which demonstrates that these errors can be larger on occasion. It should be emphasized once again, however, that such errors should be smaller for the 4d and, particularly, 5d metals than they are for V.

IV. COMPARISON WITH PREVIOUS WORK

A. Elastic Moduli of the Pure Elements

The results of some recent ultrasonic measurements of the elastic moduli of high-purity V, Nb, Ta, Mo and W are listed in Table 11 together with the present results. Experimental uncertainties in the present measurements arising from misorientation and errors in densities, lengths, and ultrasonic delay times have been discussed in Chapter III. These uncertainties amount to 0.2-0.3% in the C_{ij} and are generally similar to the uncertainties in previous studies. In Table 11 there are many instances of disagreement outside this range. The following discussion presents possible explanations for some of the differences in terms of impurities and in terms of inaccurate densities assumed by some investigators.

Vanadium. Alers [1960] originally used a rather low X-ray density value of 6.022 g/cm^3. The C_{ij} values attributed to Alers in Table 11 were recalculated using the more likely value of 6.098 g/cm^3 suggested by Westlake [1977]. Similarly, the density value of Magerl et al. [1976] was high (6.117 g/cm^3) and their C_{ij} were also recalculated, although in this case the recalculation increased the disagreement of their data with the other results. Le Huy [1972] did not mention a density value. The results of Le Huy were, however, very similar to those of Alers [1960], and a recalculation was done here on the assumption that

Table 11.--Densities (in g/cm^3) and elastic moduli (in Mbar) of the pure elements at room temperature.

ρ	C_{11}	C_{44}	C'	C_L	K_s	Reference
			Vanadium			
6.098[a]	2.309	0.4311	0.5530	2.186	1.571	Algers [1960]
6.092	2.310	0.4378	0.5542	2.194	1.571	Bolef et al. [1971]
6.098[a]	2.308	0.4320	0.5523	2.187	1.569	Le Huy [1972]
6.094	2.307	0.430	0.553	2.184	1.569	Fisher et al. [1975b]
6.098[a]	2.303	0.4277	0.5512	2.179	1.568	Magerl et al. [1976]
6.102	2.309	0.4336	0.5545	2.188	1.570	This work
			Niobium			
8.578	2.465	0.2840	0.5661	2.183	1.710	Graham et al. [1968]
8.578[a]	2.470	0.2811	0.5682	2.183	1.711	Jones et al. [1969]
8.569	2.472	0.2823	0.5705	2.183	1.711	Hubbell and Brotzen [1972]
	2.453	0.2807	0.5636	2.170	1.701	Le Huy [1972]
8.579	2.474	0.280	0.569	2.185	1.715	Fisher et al. [1975b]
8.576	2.460	0.2792	0.5672	2.172	1.704	Magerl et al. [1976]
8.578	2.462	0.2869	0.5662	2.183	1.707	This work

Table 11.--(Continued) Densities (in g/cm^3) and elastic moduli (in Mbar) of the pure elements at room temperature.

ρ	C_{11}	C_{44}	C'	C_L	K_s	Reference
			Tantalum			
16.682[a]	2.660	0.8227	0.5253	2.958	1.960	Magerl et al. [1976]
16.682[a]	2.659	0.8226	0.5253	2.956	1.958	Stewart et al. [1977]
16.682	2.660	0.8241	0.5236	2.960	1.961	Fisher [1977]
16.682[a]	2.661	0.8251	0.5255	2.961	1.960	This work
16.675	2.660	0.8247	0.5253	2.959	1.960	This work
			Molybdenum			
10.219	4.697	1.068	1.511	4.255	2.683	Bolef and de Klerk [1962]
10.225	4.409	1.217	1.342	4.283	2.619	Featherston and Neighbours [1963]
	4.63	1.09	1.51	4.21	2.62	Dickinson and Armstrong [1967]
	4.661	1.095	1.518	4.239	2.638	Davidson and Brotzen [1968]
	4.657	1.089	1.527	4.219	2.621	Le Huy [1972]
10.216	4.648	1.089	1.516	4.221	2.626	This work

Table 11.--(Continued) Densities (in g/cm^3) and elastic moduli (in Mbar) of the pure elements at room temperature

ρ	C_{11}	C_{44}	C'	C_L	K_s	Reference
			Tungsten			
19.266	5.225	1.605	1.603	5.227	3.088	Bolef and de Klerk [1962]
19.257	5.234	1.607	1.594	5.247	3.108	Featherston and Neighbours [1963]
19.257 19.250	5.223	1.606	1.590	5.239	3.104	Lowrie and Gonas [1967]
19.3615	5.290	1.619	1.602	5.310	3.158	Ayres et al. [1975]
19.253	5.227	1.606	1.591	5.242	3.106	This work

[a]Densities of Westlake [1977] have been used to recalculate the moduli.

they used the same density.

Note that the results of Alers [1960] and Fisher et al. [1975b] are in very good agreement with each other (and with the original, but not the recalculated, values of Magerl et al. [1976]), particularly when the density difference is taken into account. If these are taken, tentatively, as the best values for high purity vanadium, then it is possible to account for some of the other values. The C_{44} and C' of Le Huy are respectively higher and lower than the "best" values. This can be explained by assuming that a small amount of interstitial hydrogen was dissolved in LeHuy's sample. Westlake [1967] has pointed out that vanadium crystals usually contain some hydrogen unless it is removed by vacuum annealing, and Fisher et al. [1975b] and Magerl et al. [1976] have demonstrated that dissolved hydrogen increases C_{44} and decreases C'. The present sample probably did not contain significant amounts of hydrogen, but it did have relatively high concentrations of C and Si which might account for the high values of the shear modulus. Bolef et al. have reported a moderate amount of Si and a large amount of oxygen in their crystal. The oxygen would tend to raise the moduli [Fisher et al., 1975b] in accord with the trends in Table 11. However, Bolef et al. also found large amounts of hydrogen which should produce a low value of C'. Discussion of the effects of impurities is complicated by the fact that the impurities pin lattice dislocations. This leads in general to an increase in the moduli. The magnitude of the

increase depends on a number of factors including the concentration and nature of the impurity. The generally high moduli of this study and of Bolef et al. may be related to this phenomenon.

Niobium. The samples of Jones et al. [1969], Fisher et al. [1975b] and Magerl et al. [1976] were annealed in vacuum to remove interstitial impurities, although Fisher et al. used lower temperatures and vacuums. These three sets of elastic moduli are in fairly good agreement and should be taken as the "best" values for high purity Nb. The values of Magerl et al. are slightly low as was the case for their V measurements. The present sample and that of Graham et al. were obtained from the same source and were prepared by similar procedures with no attempt being made to remove interstitials. Not surprisingly, the C_{ij} values measured on these two samples are comparable. Note that C' is low and C_{44} is high relative to the work on purer crystals. Fisher [see Katahara et al., 1976] has pointed out that this is probably due to $\sim$ 1 atomic % hydrogen which could easily have been introduced during the preparation of the specimens. As is the case for the other Group VB elements, the presence of dissolved hydrogen raises C_{44} and lowers C' [Fisher et al., 1975b; Magerl et al., 1976]. The values of Hubbell and Brotzen are in fair agreement with the "best" values. The results of Le Huy [1972] are generally low--probably due again to a different density. No recalculation

was done, but note that Le Huy's C_{44} is relatively high which implies that some hydrogen was present in this case also.

Tantalum. Fisher [1977] has recently reviewed the ultrasonic literature on the elastic moduli of tantalum in view of Westlake's [1977] evaluation of the density data. Fisher recalculated the C_{ij} of previous workers using ρ = 16.682 g/cm^3 for ultra-high purity Ta as suggested by Westlake. A similar recalculation shown in Table 11, has been done here for some of the most recent data. A slight departure from Fisher's procedure was made in that data from all four of the crystals of Stewart et al. was used. This does not affect Fisher's observation that the agreement is good.

Molybdenum. The values of Featherston and Neighbours [1963] are clearly unreasonable when compared with the other data listed in Table 11 for Mo. The reason for this is unknown. Their crystal did have rather large amounts of interstitial impurities (930 ppm O_2, 140 ppm N_2, and 10 ppm H_2), but it is unlikely that these could cause such large changes in the moduli. The last 4 sets of values are in generally good agreement. The differences are small enough that impurities and different assumed densities can probably account for the differences. Unfortunately, chemical analyses and density values are available only for the present sample and that of Bolef and de Klerk [1962].

Tungsten. The results of this study are in excellent agreement with Lowrie and Gonas [1967] who used two crystals from the same source (Union Carbide). The values of Bolef and de Klerk [1962] and Featherston and Neighbours [1963] are also in fairly good agreement. The moduli of Ayres et al., on the other hand, are uniformly high. This can be attributed in part to their density value which is about half a percent higher than the others. A recalculation with ρ = 19.25 g/cm^3 would eliminate most of the discrepancy in the shear moduli, but the longitudinal moduli would still be high by about 0.5%. Here again the differences are probably due to impurities and lattice dislocations.

B. Elastic Moduli of the Alloys

Figures 2, 3 and 4 show the elastic moduli of the 3d, 4d, and 5d alloys obtained in this work and in other studies. Many of the alloy crystals have been studied both here and in other laboratories. In these cases, the differences are not large enough to be noticeable on these figures. It is clear, however, that there is considerable scatter when smooth curves are drawn through the data. The scatter is not particularly disturbing for the 3d and 5d metals because it is not systematic. It was pointed out in Chapter III that substantial errors are possible because of inhomogeneity in the alloy crystals. The points of Carpenter and Shannette [unpublished], shown in Figure 4, are from crystals with particularly large amounts of chemical segrega-

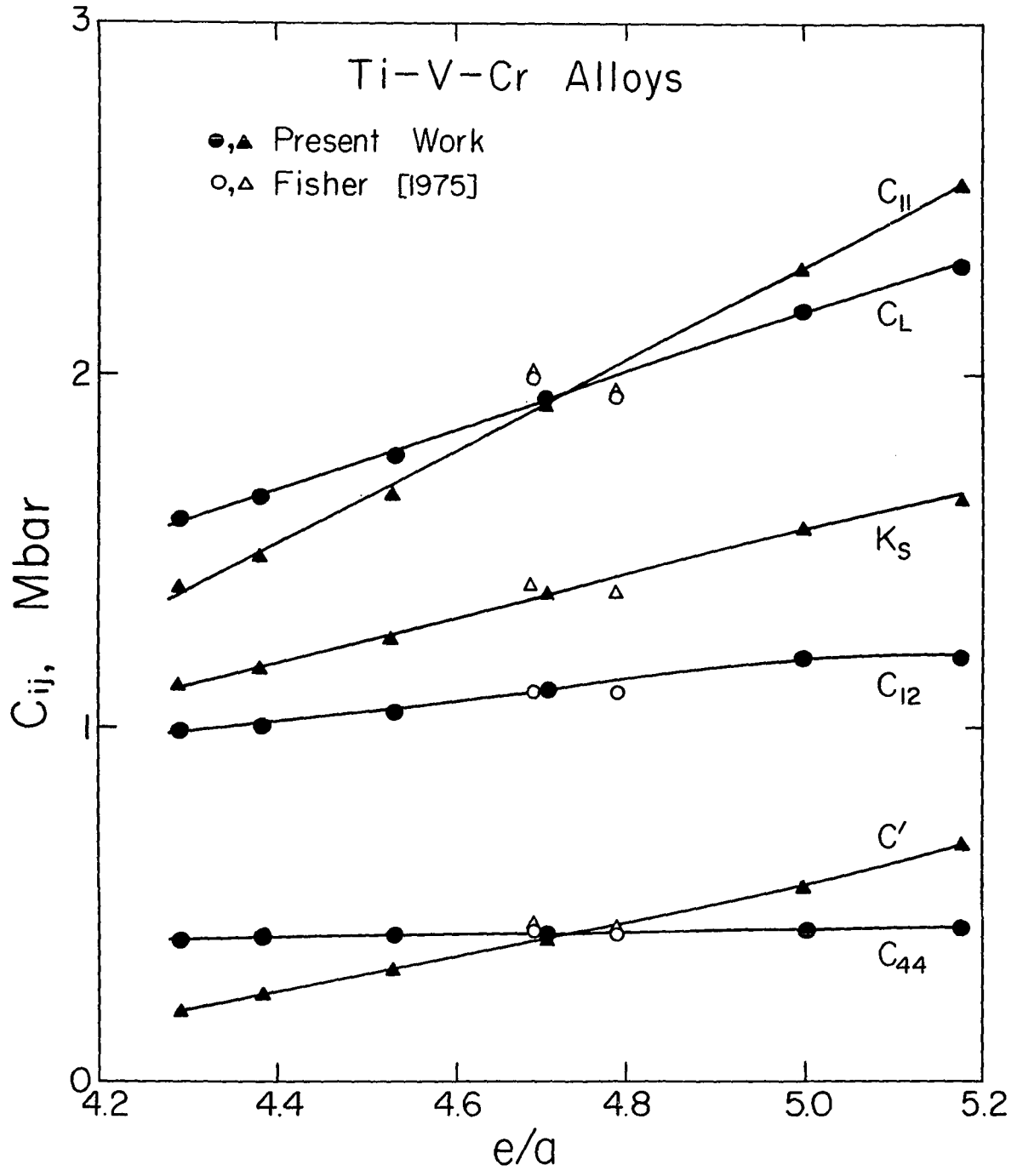

Figure 2. C_{ij} of Ti-V-Cr alloys.

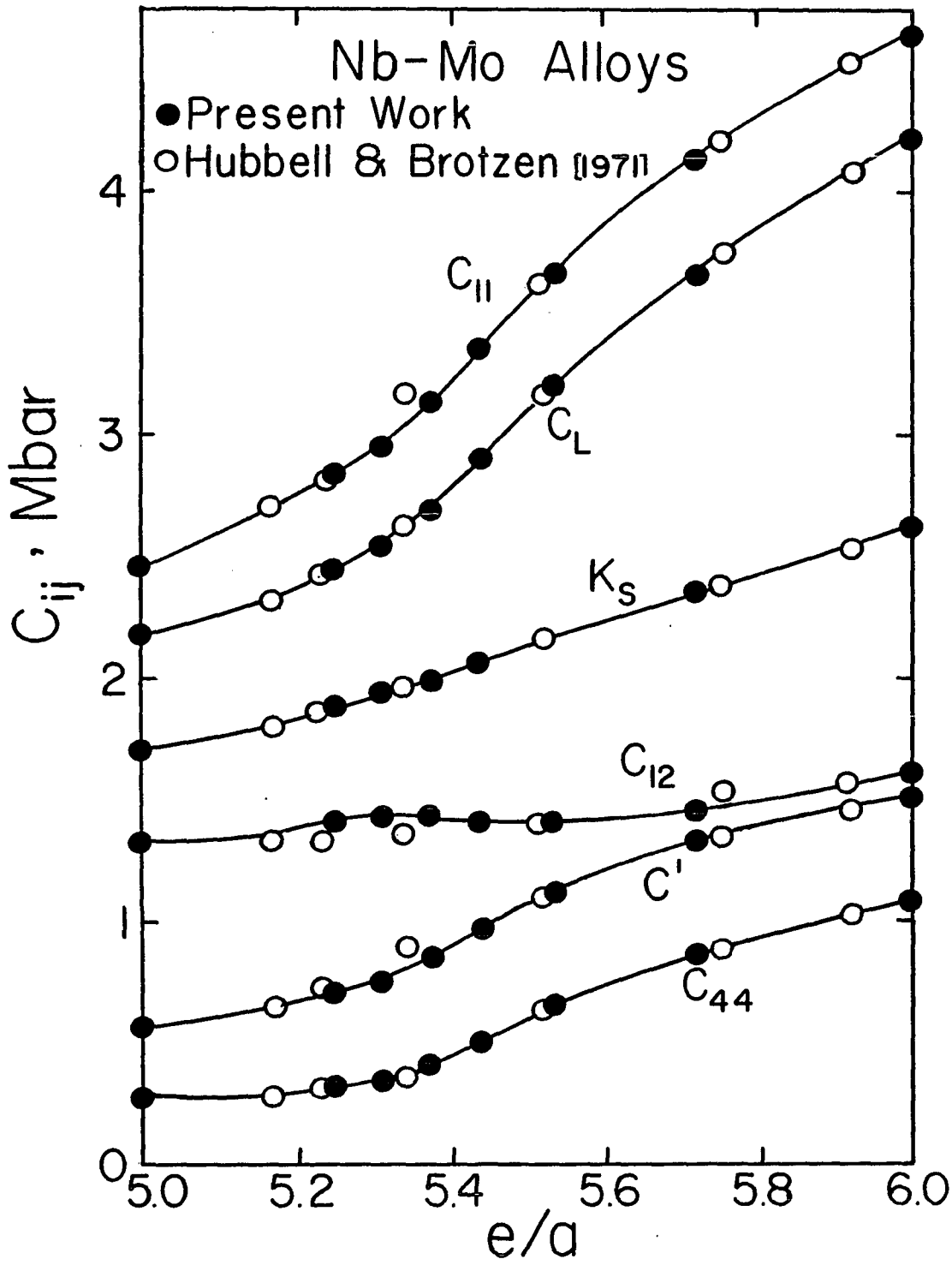

Figure 3. C_{ij} of Nb-Mo alloys.

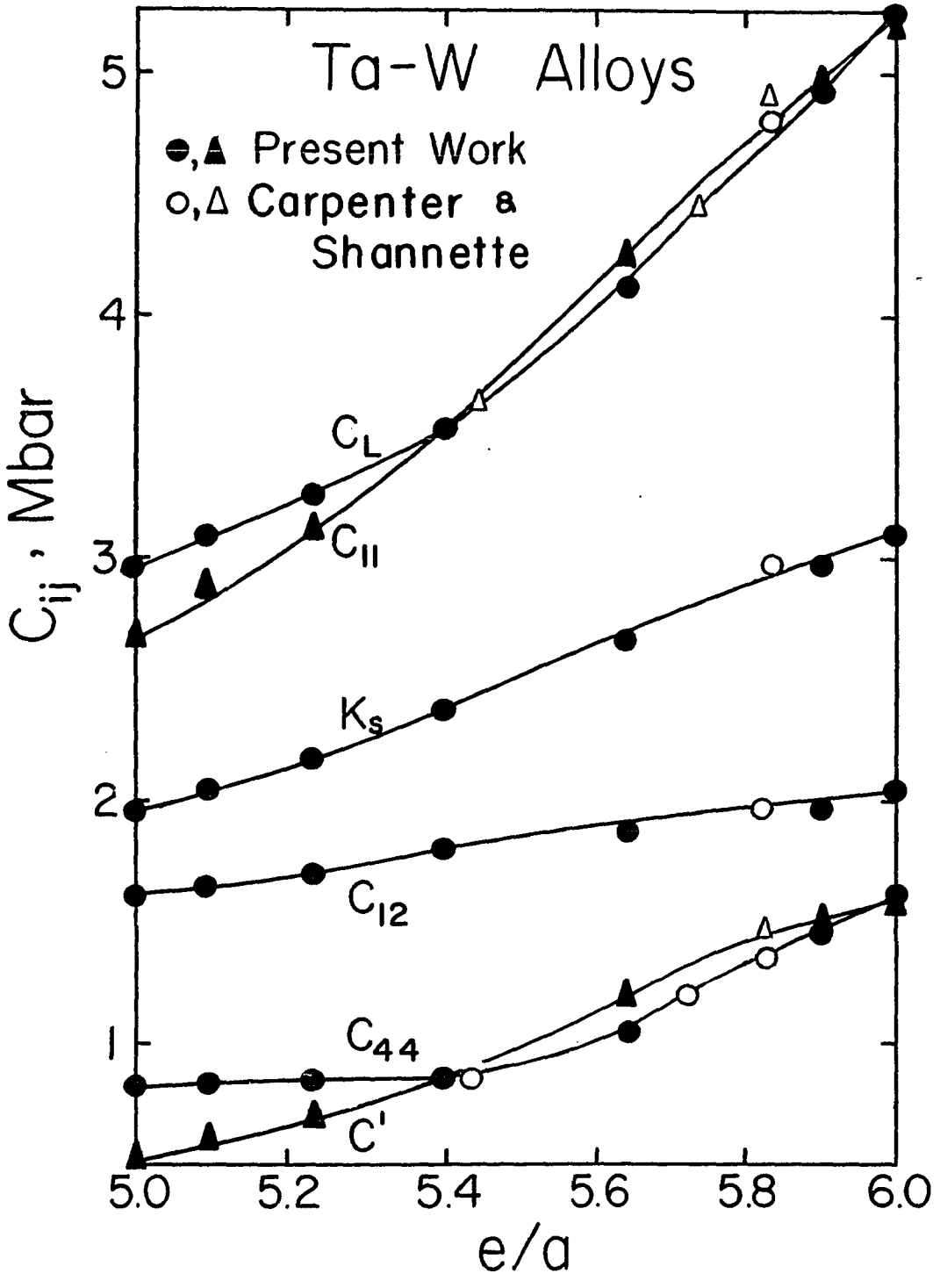

Figure 4. C_{ij} of Ta-W alloys.

tion--up to 5% composition differences from end to end [G.W. Shannette, personal communication]. Large errors are also possible in some of the density and composition determinations. The most troublesome differences occur for the Nb-Mo alloys near e/a $\sim$ 5.3 where the C_{11} and C' values of Hubbell and Brotzen are significantly higher than the results of this study. This is difficult to explain because the C_L and C_{44} moduli agree very well. It was thought at first that the discrepancy might be due to hydrogen contamination as discussed in the previous section. (Hydrogen solubility is known to decrease rapidly with e/a in these alloys [Jones et al., 1960; Jones and McQuillan, 1962]. However, E.S. Fisher of Argonne National Laboratory extracted the hydrogen by heating the present Nb-rich alloys in a vacuum and found that insignificant amounts of hydrogen were present. The cause of the discrepancy is therefore not known at this time.

C. $(\partial C_{ij}/\partial P)_T$ for the Pure Elements

Table 12 presents the data currently available on the pressure derivatives of the C_{ij} of the Group VB and VIB elements. Isbell et al. [1972], Voronov and Vereschagin [1961], and Smith et al. [1966] studied polycrystalline specimens so only $\partial K_s/\partial P$ values are shown. In the following discussion it should be kept in mind that the present $\partial C_{ij}/\partial P$ values are probably good to 2 or 3%, but that maximum errors of up to

Table 12.--$(\partial C_{ij}/\partial P)_T$ for the pure elements.

$\partial C_{11}/\partial P$	$\partial C_{44}/\partial P$	$\partial C'/\partial P$	$\partial C_L/\partial P$	$\partial K_S/\partial P$	Reference
			Vanadium		
5.3	0.15	0.96	4.5	4.0	Le Huy [1972]
5.65	0.185	1.042	4.79	4.26	This work
			Niobium		
8.05	0.279	0.952	7.38	6.78	Graham et al. [1968]
4.9	0.28	0.75	4.4	3.9	Le Huy [1972]
5.22	0.281	0.925	4.57	3.98	This work
			Tantalum		
				3.79	Isbell et al. [1972]
4.54	1.03	1.01	4.56	3.19	Chechille [1967]
5.08	1.004	0.984	5.10	3.77	This work
			Molybdenum		
				4.4	Voronov and Vereshchagin [1961]
				3.1	Smith et al. [1966]
7.2	1.1	1.4	6.9	5.3	Le Huy [1972]
6.41	1.40	1.48	6.33	4.44	This work

about 5% are possible. The exceptions to this are the derivatives of C_{44} for V and Nb--these quantities are so small that the percentage of errors in them are a little larger.

Le Huy [1972] has measured the $\partial C_{ij}/\partial P$ of V, Nb and Mo. (This work is available only as an unpublished thesis although the results were also presented at a conference [Le Huy et al., 1973].) The data were presented only in graphical form and the derivatives shown in Table 12 were obtained by reading slopes directly off the C_{ij} versus P plots. These values are thus uncertain by a few percent for this reason alone. Le Huy's results are consistently lower than those of the present study for V and Nb. In the case of V the differences are a little too large and too consistent to be acceptable. There would appear to be systematic errors in one or both sets of measurements. The agreement between this study and Le Huy's results are satisfactory for Nb except for $\partial C_{44}/\partial P$. Le Huy is probably in error in this case since the derivatives of the shear moduli of Graham et al. [1968] are in good agreement with the present results. There are clearly unacceptable differences between this study and Le Huy [1972] for Mo. In this case, Le Huy's data are in poor agreement with shock compression measurements [McQueen et al., 1970] which are discussed later in this chapter. Thus the present results are probably more reliable for Mo also.

As mentioned above, Graham et al. and this study are in accord for $\partial C_{44}/\partial P$ and $\partial C'/\partial P$ for Nb. There is, however,

gross disagreement for the longitudinal moduli. A possible explanation for this is given in the next section. The very high $\partial K_s/\partial P$ value of Graham et al. leads to very poor agreement with the shock-wave data so the present values of $\partial C_{11}/\partial P$ and $\partial C_L/\partial P$ are to be preferred.

The derivatives of the shear moduli obtained by Chechille [1967] on Ta agree well with the present values, but again the longitudinal mode results differ appreciably. There are three reasons for rejecting Chechille's values. First, the results of this study are in better agreement with shock-wave experiments. Second, there were serious errors in Chechille's delay times. Chechille measured velocities 4% higher than were observed by Featherston and Neighbours [1963] on a similar crystal. Now the C_{ij} values of Featherston and Neighbours were from 0.3 to nearly 2% lower than those shown in Table 11 for Ta. Assuming that Featherston and Neighbours were in error in their velocity measurements, Chechille's velocities are still too high by about 3%. There is therefore the possibility that Chechille's pressure derivatives are also in error. A third reason for preferring the results of this study is that Chechille's sample was of relatively low purity. This might have a small effect on the measured pressure derivatives.

Consider now the work carried out on polycrystalline samples. Isbell et al. [1972] measured $\partial K_s/\partial P = 3.79$ for Ta in good agreement with the value obtained here. However, their value for the derivative of the shear modulus was

about 25% higher than the $\partial C_{44}/\partial P$ and $\partial C'/\partial P$ values shown in Table 12. Their results are thus not entirely reliable. Similarly, Voronov and Vereshchagin [1961] also obtained a K_S' value for Mo close to that measured here, but their K_S value itself was low by about 10%. Smith et al. [1966] measured a very low K_S' on a sintered Mo sample. Such samples are known to yield unreliable K_S' values [Spetzler et al., 1972]. It is not surprising therefore that the K_S' value of Smith et al. does not agree as well with the shock-wave data as does the value measured in this study.

It is possible to draw the following conclusions from the foregoing discussion: (1) there is generally better agreement for the pressure derivatives of the shear moduli than there is for the derivatives of the longitudinal moduli, and (2) with the possible exception of the data of Le Huy [1972] on V and Nb, the results of this study are probably more accurate than the previous work.

D. Densification of the Pressure Medium and Related Errors

It was pointed out in section A of this chapter that the Nb crystal used in this study was obtained from the same source (Materials Research Corp.) as the crystal of Graham et al. [1968]. Furthermore, the moduli measured at room temperature and atmospheric pressure on these samples are in good agreement. It was thus expected that good agreement would also be found for the pressure derivatives. It is obvious from Table 12 that this was not the case for the long-

itudinal modes.

Before attempting to explain the discrepancy, it is useful to note that the present results on Nb were obtained only after an initial period in which the pressure measurements could not be repeated. These early experiments (chronologically the first carried out in this work) were made with carrier frequencies of 20 or 30 MHz. Some of the repetition frequency versus pressure results are shown in Figure 5 for mode 5 of Nb. Also shown for comparison is an extrapolation of the data of Graham et al. obtained at 16 MHz. Similar results were obtained on mode 1, the other longitudinal mode. It can be seen in Figure 5 that the F(P)/F(0) slopes tend to decrease and become more reproducible as the carrier frequency increases. The data of Graham et al. appear to fall in with the trend toward higher slopes at lower carrier frequencies, and it thus seems likely that there is a single cause for all of the discrepancies shown in Figure 5.

The effects seen in Figure 5 could not be caused by variations in transducer and bond phase shifts as discussed by McSkimin and Andreatch [1962], Davies and O'Connell [1977] or in Chapter III and Appendix A. For one thing, transducer and bond effects appear to be much too small. For another, they should cause higher slopes at higher frequencies--which is just the opposite of what is observed. In addition, compression of the bond should produce more noticeable errors in the derivatives of shear moduli than in derivatives of

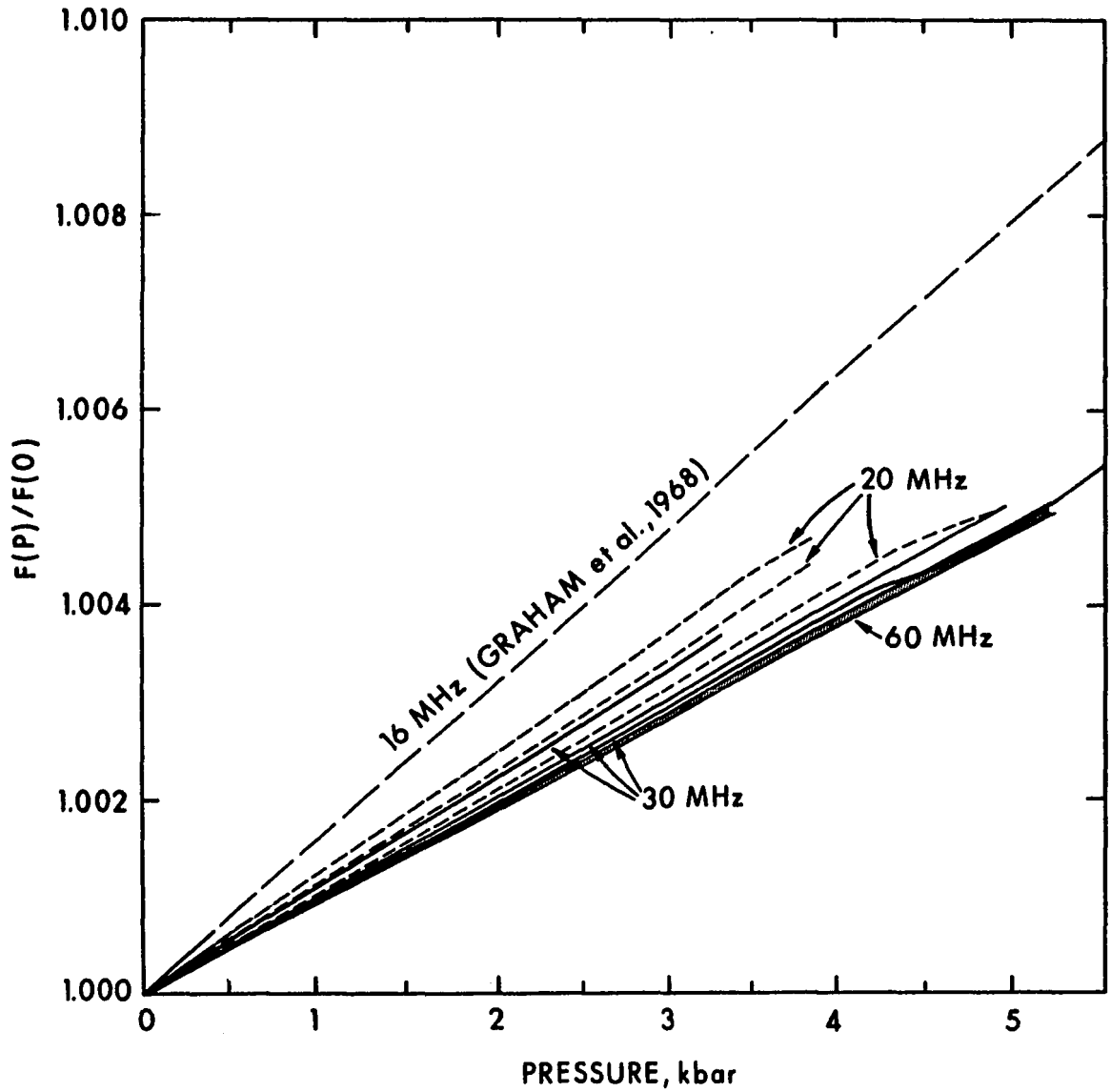

Figure 5. Pulse repetition frequency ratio, F(P)/F(0) vs. pressure for mode 5 for Nb. The shaded area represents three 60 MHz runs, solid lines are 30 MHz runs, short-dashed lines are 20 MHz runs, and long-dashed line is an extrapolation of the 16 MHz results of Graham et al. [1968].

longitudinal moduli because shear wave lengths are shorter.

Another possible cause that can be ruled out is the type of diffraction effect discussed at the end of Appendix C. This kind of error should be present in PSP measurements but not in PEO measurements. However, PEO experiments were also carried out and showed the same kind of behavior seen in Figure 5.

A simple experiment was carried out which indicates that the observed slope differences are caused mainly by compression of the pressure medium and not by compression of the bond. Longitudinal velocities were measured by the PSP method, at atmospheric pressure and 25^{o}C, first in air and then with the sample immersed in a liquid whose acoustical impedance was equivalent to that of nitrogen gas at about 3 kbar. Temperature differences between the air and liquid readings were limited to less than 0.05^{o}C. Measurements were made with different bonds and with variations in the position of the transducer on the sample faces. At 20 MHz, positive increments in the apparent velocity were observed ranging from 14 to 45 parts in 10^5. At 60 MHz, the apparent velocities increased by only 2 or 3 parts in 10^5. The magnitude of these changes is sufficient to explain most of the slope variations, and bond compression effects are thus relatively minor.

It is possible to identify at least one type of effect which might change appreciably with pressure and carrier

frequency. This refers to wave-guide effects arising from the diffraction of the ultrasonic waves and their subsequent interaction with the lateral sides of the sample. Application of pressure alters the boundary conditions on the specimen surfaces and might thus produce spurious F'(P) slopes. The lack of reproducibility at low carrier frequencies might then be attributed to changes in transducer position and perhaps partly to variations in bond thickness and uniformity. Uneven thickness in the bond affects the distribution of acoustic energy into the various wave-guide modes [Redwood and Lamb, 1957], and this should also vary with pressure. An increase in the carrier frequency decreases the wavelength relative to the sample and transducer sizes and thus reduces beam-spreading and waveguide effects.

A theoretical analysis of the subject of wave-guide effects under pressure would be very complex and is beyond the scope of this investigation. It would not be sufficient to study the variation of the phase or group velocities of the appropriate wave-guide modes as a function of the properties of the pressure medium. This would be a formidable problem in itself even if the sample is assumed to be isotropic and to have a simple geometry. But it would also be necessary to study the propagation of the ultrasonic wave train as a time dependent phenomenon since the relevant experiments use pulse techniques rather than continuous waves. Thus the pressure dependent distribution of energy into the different modes (predominantly high order modes with phase

velocities close to the free-space velocities) would have to be considered and it would be necessary to calculate the stress profile over the transducer area for each echo.

In the absence of a theoretical treatment, it is suggested here that the measured apparent velocity increases with pressure faster than the free-space velocity because the rapid increase in velocity and density of the pressure medium changes the wave-guide boundary conditions. There is empirical support for this suggestion. For instance, McSkimin and Andreatch [1964] have observed this kind of phenomenon in ultrasonic measurements where uniaxial stresses were applied perpendicular to the wave propagation direction. In the low stress region they observed anomalously rapid changes in the delay times which they attribute to the changing quality of the contact between the lateral surfaces of the sample and the load platens. They also demonstrated that this effect can be minimized by increasing the ultrasonic frequency.

There is other experimental evidence which is consistent with wave-guide effects being the cause of the observed slope variations. For instance, longitudinal mode measurements were made on Ta at 30, 40, and 60 MHz without significant changes in the F(P) slopes. One difference between the Nb and Ta samples was that the dimensions of the Ta crystal were twice as large, relative to the wavelength at a given frequency, as those of the Nb specimen. Satisfactory results were in general obtained for the present samples when

the specimen lengths exceeded about 50 wavelengths. An additional factor here is that Ta has a higher acoustical impedance than Nb and waves in Ta would thus be affected less by densification of the pressure medium.

The dimensions relative to the wavelength of the Nb crystals of Graham et al. were similar, at 16 MHz, to those of the present sample at 20 MHz. Their samples, however, were in the form of rectangular prisms whereas the specimen used here had only two pairs of flat, polished faces. The presence of more surfaces favorable for guided wave propagation may be the cause of the higher longitudinal mode slopes of Graham et al. Unpublished work by the present author on ruthenium crystals, which had only one pair of flat, polished faces, tends to support this view. The Ru results were qualitatively similar to those shown in Figure 5, but the differences in slope between 20 MHz and 60 MHz runs were much smaller, even though the Ru sample dimension/wavelength ratios were about half of that for Nb. The acoustical impedance of Ru is about twice that of Nb and this would also reduce the pressure dependence of the wave-guide effects.

It is somewhat more difficult to explain the curvature in the F(P) data for some of the 20 and 30 MHz runs shown in Figure 5. A possibly relevant observation is that the longitudinal mode signals grew weaker with pressure because of transmission losses into the pressure medium. At high pressures, these losses may be large enough that other wave-guide modes having different propagation characteristics

begin to be important. In any case, no curvature was seen in the 60 MHz runs.

The preceding discussion of the discrepancy between the present work and that of Graham et al. has a serious flaw in that Graham et al. obtained excellent internal consistency among different modes on two samples. According to the present interpretation this consistency would have to be fortuitous. It is also not clear why the 20 and 30 MHz runs shown in Figure 5 exhibit good linearity up to 3 kbar since the properties of the pressure medium change rapidly and in a very nonlinear fashion in the low pressure region. Irregardless of the source of the discrepancy, the Nb results of this study might be considered more reliable for two reasons. First, the pressure range covered here is 10 times larger than theirs. Second, shock-wave compression data on Nb, as discussed in the next section, tend to support the lower pressure derivatives of the longitudinal moduli found here.

Before this section is concluded, one final point is in order. Measurements of delay times with different external media could prove to be of use in evaluating the possible effects of densification of the pressure medium. This applies not only to wave-guide effects but also to the transducer-bond and diffraction effects discussed in Appendices A and C. It should be kept in mind, however, that wave-guide effects at high pressure cannot easily be precisely simulated in this way because the wave-guide mode velocities depend in general on both the density and veloc-

ity of the surrounding medium and not simply on its impedance.

E. Comparison with Shock-Wave Compression Experiments

It has been established [e.g., see Anderson, 1966] that ultrasonic measurements, carried out to pressures of a few kbar, can be used with fair success to predict compressions at pressures of hundreds of kbar. McQueen et al. [1970] have obtained shock-wave compression results on the Group VB and VIB elements up to pressures comparable to the bulk modulus. Figures 6-10 present comparisons of their $20^{o}C$ isotherms with extrapolations of the ultrasonic results. (The $5^{o}C$ temperature difference is negligible.) The low pressure region, in which the agreement is generally satisfactory, has been omitted from these figures. The pressures have been normalized to the zero-pressure ultrasonic values of K_T shown in Table 9.

The shock-wave results shown in the figures are of two types. The Hugoniot points are the experimentally determined (P, V) loci of the shocked (hot) material. McQueen et al. [1970] have fit these points to a two-parameter equation (the linear shock velocity-particle velocity relation). The isotherms were then derived by making certain assumptions about the specific heat and thermal expansion. McQueen et al. used the Debye theory for the specific heat and assumed that the Grüneisen parameter was a function only of volume such that γ/V is a constant. These assumptions are the ones

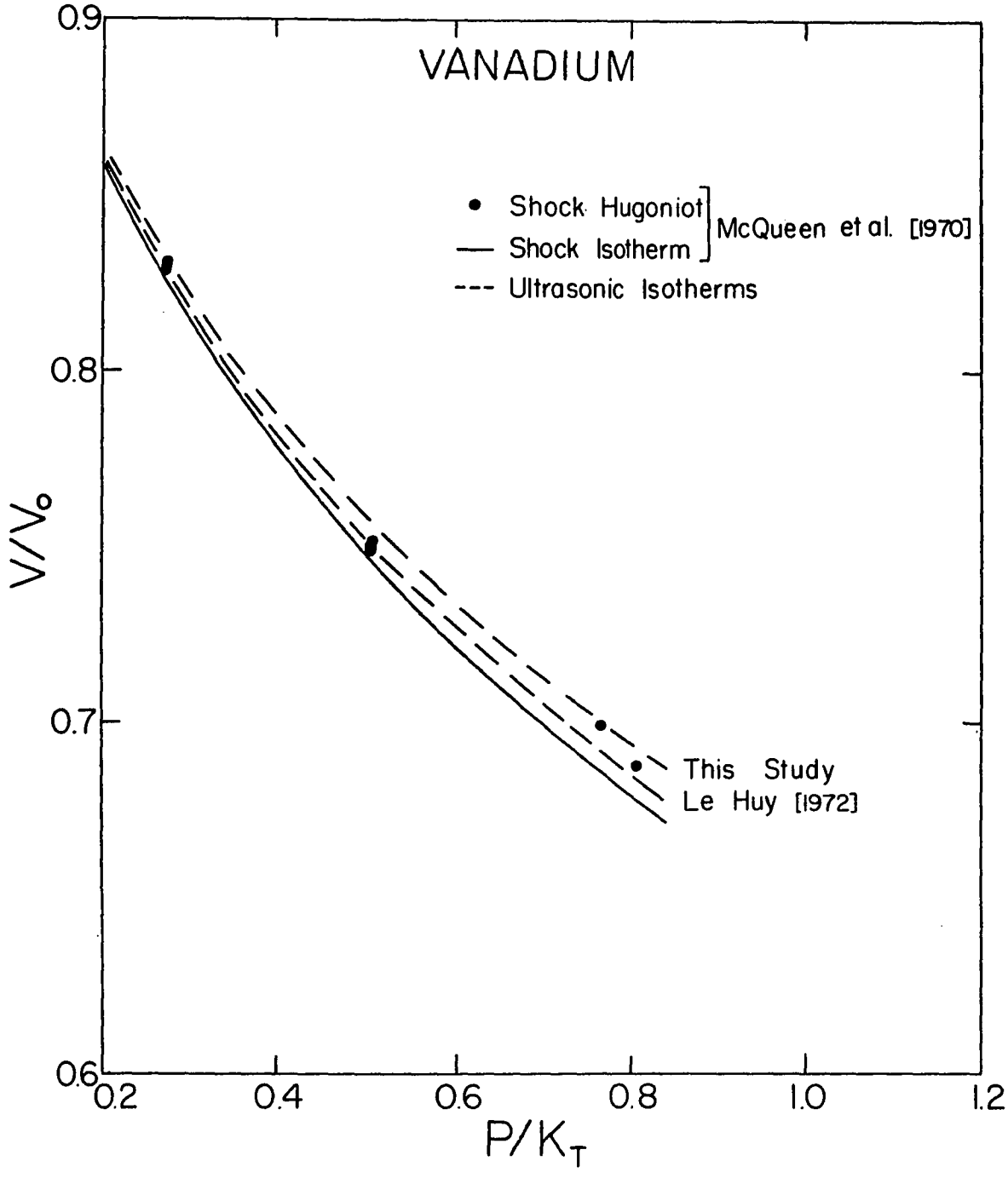

Figure 6. V/V_o vs. P/K_T for vanadium.

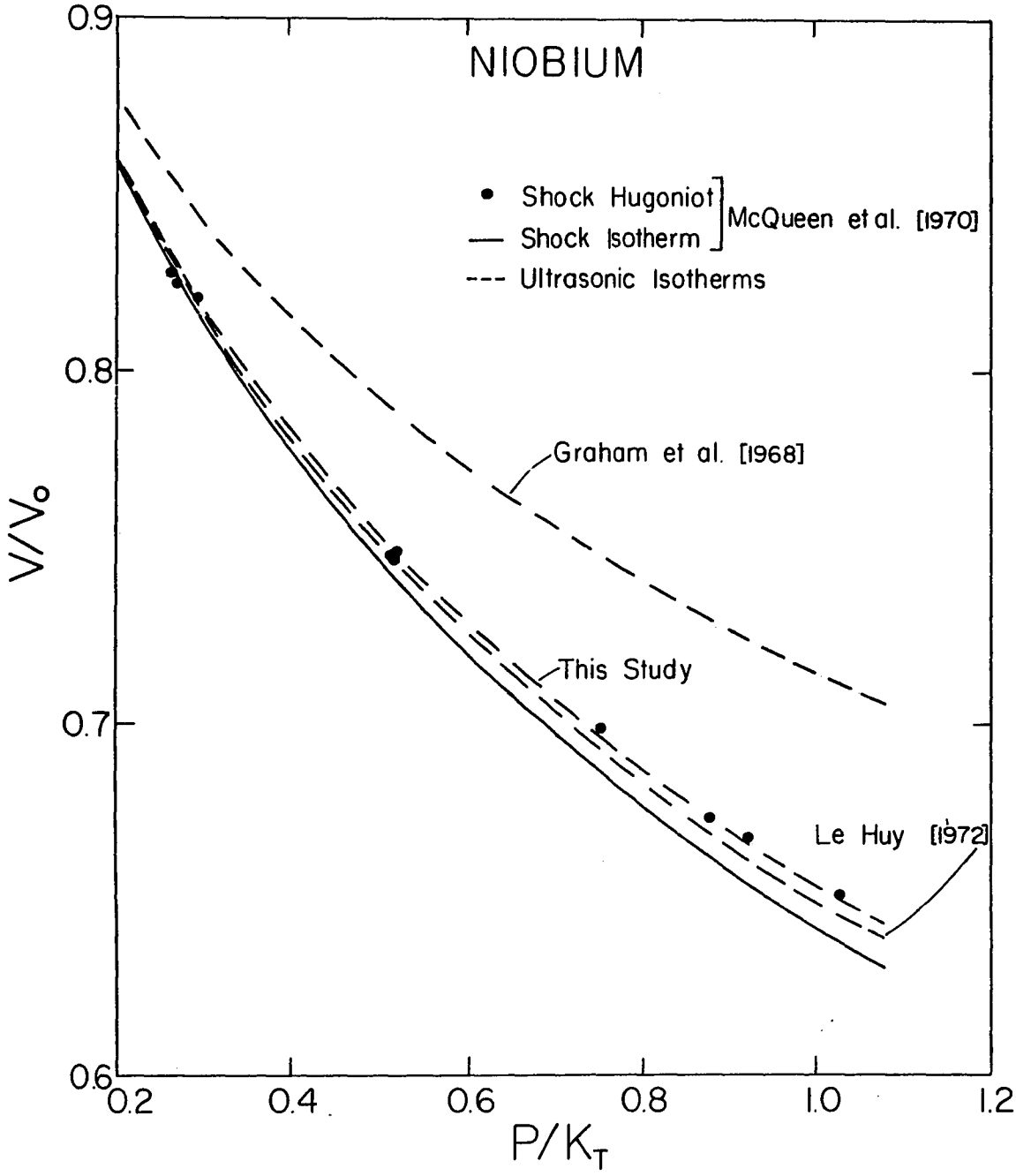

Figure 7. V/V_o vs. P/K_T for niobium.

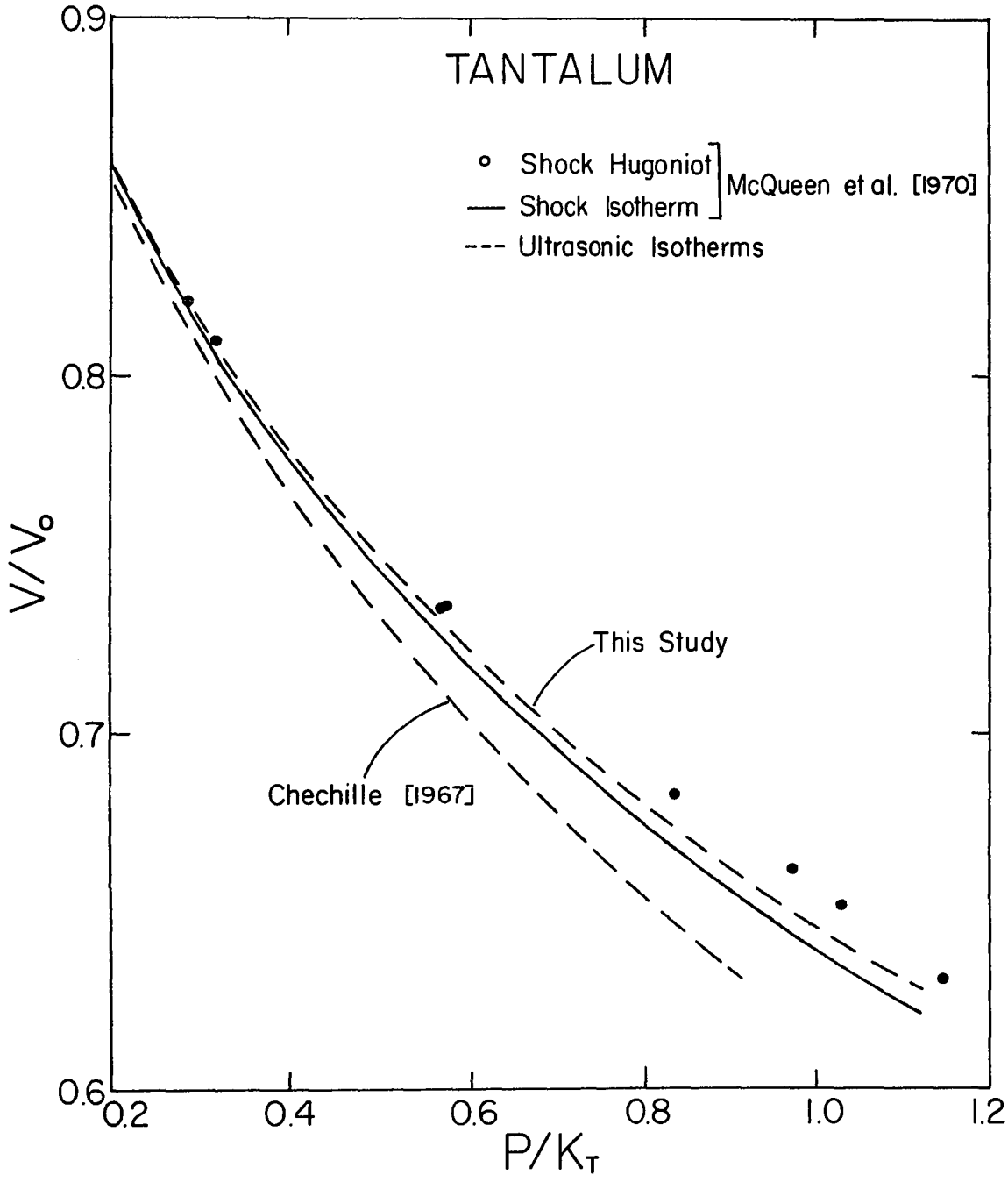

Figure 8. V/V_o vs. P/K_T for tantalum.

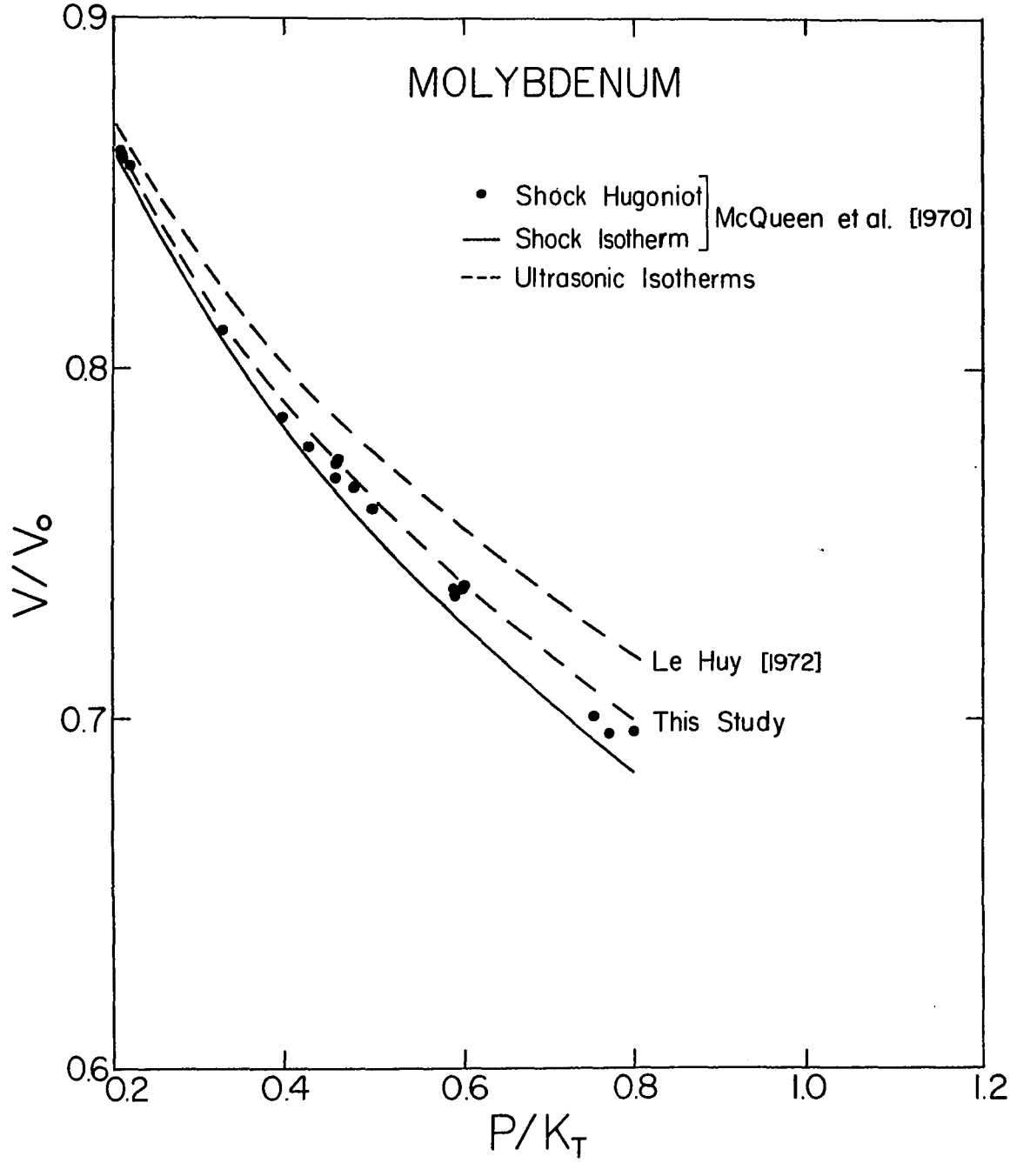

Figure 9. V/V_o vs. P/K_T for molybdenum.

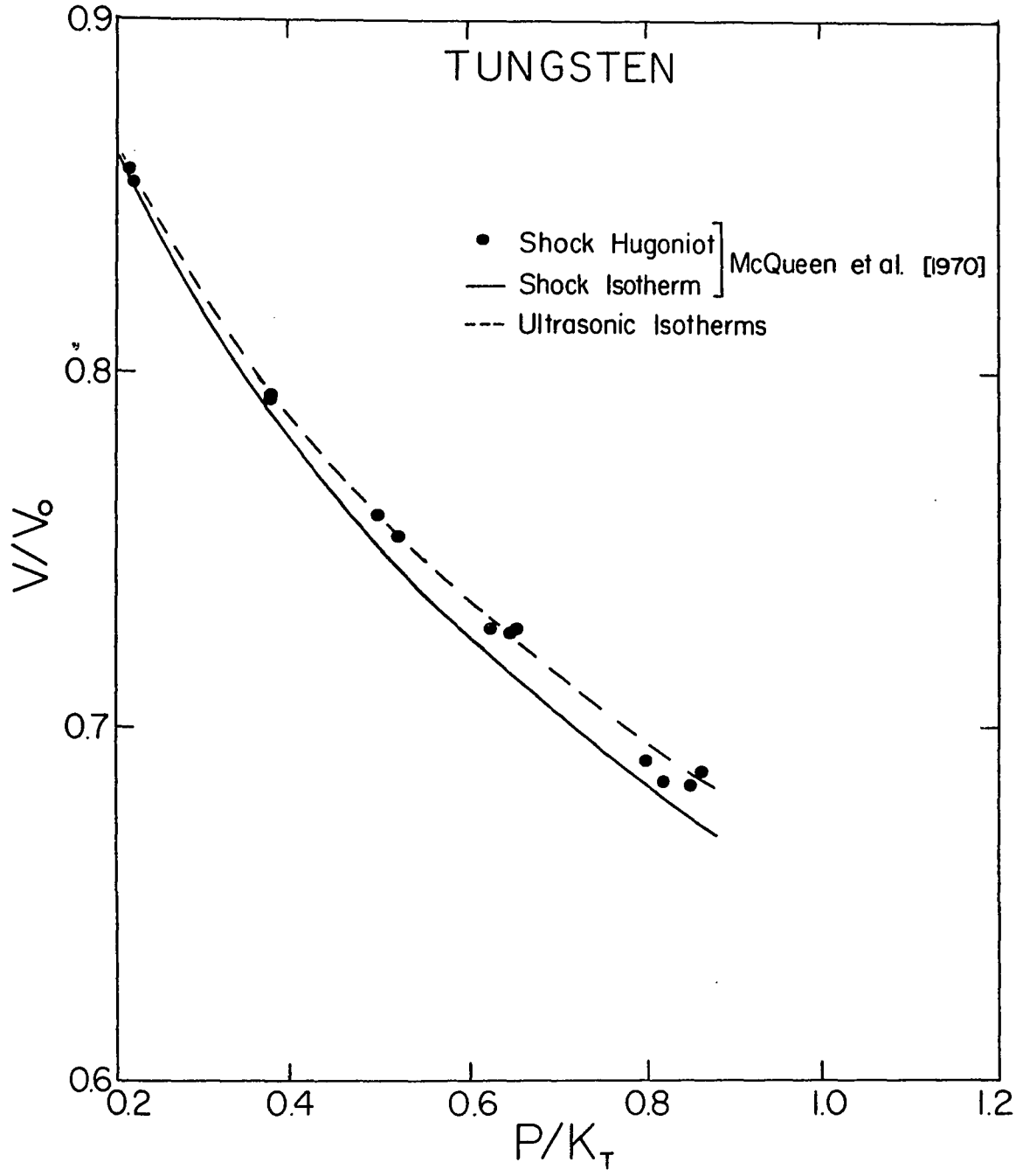

Figure 10. V/V_o vs. P/K_T for tungsten.

usually made in shock-wave studies, and the basis for making them is discussed by, among others, Rice et al. [1958] and McQueen et al. [1970].

The extrapolation of the ultrasonic data has been carried out by means of the Birch-Murnaghan equation [Birch, 1938, 1947] which has proved to be one of the more successful formulas. In essence, the Birch-Murnaghan equation is obtained by writing the free energy as a truncated Taylor series in the Eulerian finite strain as defined by Murnaghan [1937]. The result can be written

$$\frac{P}{K_T} = \frac{3}{2}\left(\frac{V}{V_o}\right)^{-5/3} \sum_{n=1}^{N} b_n \left(\left(\frac{V}{V_o}\right)^{-2/3} - 1\right)^n, \quad (21)$$

where

$$b_1 = 1 \quad (22)$$

$$b_2 = 3/4\ (K_T' - 4) \quad (23)$$

$$b_3 = 1/24\ [143 + 9\ K_T'\ (K_T' - 7) + 9\ K_T\ K_T''], \quad (24)$$

etc. The primes denote isothermal pressure derivatives. All parameters, except P and V of course, are evaluated at P = 0. The number N + 1 will here be called the "order" of equation (21) since this is the order at which the free energy expansion is truncated. The ultrasonic isotherms shown in the figures were calculated with the third order Birch-Murnaghan equation.

In Figure 6, Le Huy's [1972] curve for vanadium agrees well with the shock isotherm, while the extrapolation of the

present results predicts higher volumes and in fact tends to even fall above the Hugoniot points which are at elevated temperatures.

For Nb, Le Huy's extrapolation is again in better agreement with the shock isotherm in Figure 7, but the difference between Le Huy's curve and that of the present study is not very significant. The isotherm calculated from the results of Graham et al. [1968] is clearly in error. In this case significant differences are seen at pressures as low as $P = K_T/10$.

In Figure 8, the present ultrasonic isotherm for Ta is in good agreement with the shock isotherm. Chechille's [1967] curve falls well below the other two curves.

The extrapolation of the present results for Mo, shown in Figure 9, falls above most of the Hugoniot points, and the agreement with the shock isotherm cannot therefore be said to be good. In this case Le Huy's results give worse agreement and appear to be in significant error.

As was the case for Nb, the ultrasonic extrapolation for W (Figure 10) falls on the Hugoniot rather than on the shock isotherm.

It is interesting to note that, except for the Ta results of Chechille [1967], the ultrasonic data uniformly predict higher volumes than are found from the shock data. Furthermore, the present ultrasonic curves tend to fall on or above the Hugoniot in all cases except Ta. The differences can therefore not be ascribed to errors in deducing

the isotherms from the Hugoniot unless the thermal expansion is assumed to rapidly attain very small or negative, values at high pressures.

The differences also cannot be attributed to differences in the samples. Table 13 compares the zero-pressure densities and bulk moduli of this study and of McQueen et al. The densities are in excellent agreement and the K_S values agree satisfactorily. There is no systematic pattern in these quantities which could explain why the ultrasonic curves always predict higher volumes.

There are a number of other possible reasons for the differences. For one, ultrasonic errors arising from densification of the pressure medium as discussed in the previous section tend to give systematically high K' values. Furthermore, errors in setting the carrier frequency, as discussed by Davies and O'Connell [1977] and in Chapter III, will also cause high K' values to be measured. Corrections for the latter effect have been applied for the 4d and 5d metals, but the corrections may have been underestimated somewhat if the carrier frequency was set much higher than the transducer resonance frequency [Davies and O'Connell, 1977].

Another possible explanation for the differences is that the extrapolation formula could be inappropriate for these materials. There is nothing sacred about the third-order Birch-Murnaghan equation, and a number of other equations have been proposed and used [e.g., see Barsch and

Table 13.--Comparison of ultrasonic and shock-wave sample densities and bulk moduli

Element	ρ(g/cm^3)		K_S(Mbar)	
	ultrasonic	shock-wave[a]	ultrasonic	shock-wave[a]
V	6.102	6.100	1.570	1.57
Nb	8.578	8.586	1.707	1.69
Ta	16.675	16.654	1.960	1.94
Mo	10.216	10.206	2.626	2.68
W	19.253	19.224	3.106	3.12

[a]McQueen et al. [1970]

Chang, 1971; Thomsen and Anderson, 1971]. It is at any rate probably unreasonable to expect any two-parameter extrapolation formula to hold at pressures as high as K_T.

It is interesting, however, to explore a little further the nature of the differences between the shock and ultrasonic isotherms. To this end, third- and fourth-order Birch-Murnaghan equations were fit to the shock-wave curves. This was done for the third-order equation by assuming the present value of K_T and adjusting K_T' to obtain a good fit. Similarly, the fourth-order equation was determined by assuming the present ultrasonic values for K_T and K_T', and varying K_T'' in equation (24). This is not the best procedure to use because the isotherms of McQueen et al. [1970] are not based on quite the same assumptions as equation (21) and the functional forms are different. A better procedure would be to construct Hugoniots starting with Birch-

Murnaghan isotherms in the manner prescribed by Davies [1973]. The floating parameter would then be fixed by requiring a good fit to the original Hugoniot points. This procedure is rather laborious and not really necessary in the present case because only approximate agreement is needed. The K_T' and K_T'' values will at any rate depend on the type of equation of state that is used [Davies, 1973]. Only the trends in these parameters and their approximate values are required here. The Birch-Murnaghan equations that were obtained agreed with the shock isotherms to within about 3% in the density over the entire pressure range shown in the figures.

The parameters resulting from the fits are given in Table 14. Note that the difference between the ultrasonic and shock-wave K_T' values decreases with increasing period within a given column of the periodic table and increases in going from Group VB to Group VIB in a given period. It cannot be ruled out that there is some sort of undiscovered ultrasonic experimental error which varies with the sample properties in this way. It is just as likely, however, that these differences are caused by higher order terms in the equation of state. The K_T K_T'' values in Table 14 are not unreasonable. Values for the cesium halides have been measured between -7 and -9 [Barsch and Chang, 1971]. Davies and Dziewonski [1975] have deduced values ranging from -3 to -7 for the earth's lower mantle and outer core (although these values are not well established). It is therefore possible

Table 14.--Values of K_T' and $K_T K_T''$ from the shock compression data of McQueen et al. [1970]

Element	K_T'			$K_T K_T''$
	Ultrasonic	Shock-wave	% Difference	
V	4.27	3.77	12	-8
Nb	4.02	3.72	7	-6
Ta	3.80	3.65	4	-5
Mo	4.46	3.94	12	-8
W	4.32	3.90	10	-7

to speculate that the $K_T K_T''$ values of the bcc transition elements might vary from period to period and from group to group in a manner similar to that shown in Table 14.

F. Comparison with X-ray Data

L. C. Ming [personal communication] has carried out X-ray diffraction measurements of the lattice parameters of the pure elements under hydrostatic pressures up to 100 kbar. The general conclusion that can be drawn is that the X-ray compression data are in satisfactory agreement with the extrapolations of the ultrasonic results using equation (21). The X-ray measurements do not extend to pressures high enough and are not precise enough to allow a judgment to be made as to the accuracy of the ultrasonic K_T' values determined in this study. A detailed comparison will therefore not be made here.

V. THE BAND STRUCTURE AND THE ELASTIC PROPERTIES

A. The Rigid-Band Model

The relationship between the elastic properties and the electronic band structure will be discussed in this chapter in the context of the rigid-band model. This model assumes that the band structure and density of states curve of a metal remain constant when another element is alloyed with it. It is now well known [e.g., see Ehrenreich and Schwartz, 1976, for a discussion and references] that this model is not generally valid. However, it does seem to work for the bcc transition metals considered here. Specifically, there is good agreement between experimentally determined alloy densities of states at the Fermi energy and the corresponding densities of states predicted from theoretical electronic structure calculations by means of the rigid-band assumption [McMillan, 1968; Mattheiss, 1972; Pickett and Allen, 1974]. Furthermore, Powell et al. [1968] have identified Kohn anomalies in the phonon dispersion curves of Nb-Mo alloys. These anomalies occur at wavevectors which change qualitatively with composition as expected from a rigid-band model. Freeman et al. [1975] have also used what is essentially a rigid-band model to predict the instability of the bcc structure in Zr-Nb alloys rich in Zr. It is nevertheless fair to say that the evidence in favor of the rigid-band model is not entirely convincing. It would be desirable to obtain more definitive information such as photo-

emission spectra for the alloys which would provide knowledge of the density of states over the entire conduction band rather than just at the Fermi energy.

It is not expected, of course, that the rigid-band model will work exactly. As e/a increases, the d-bands become wider and tend to move down in energy with respect to the nearly-free-electron band [Friedel, 1969; Evans et al., 1973]. It will be assumed here that, upon alloying, the effects of volume changes and charge transfer between the two types of atomic sites conspire to produce a slowly varying band structure.

It is not assumed that the shape of the bands remains unchanged under a lattice deformation. An assumption very much like this is the basis of Leigh's [1951] model for the shear moduli of simple polyvalent metals, which has also been applied to transition metals by other workers [Rayne, 1960; MacFarlane and Rayne, 1965; Bernstein, 1963]. This model assumes that during shear the unfilled bands move rigidly with the Brillouin zone boundaries, and only the energies and not the band shapes change with strain. This kind of assumption now appears to be in general disfavor because the band structure does change significantly and non-rigidly as the lattice is deformed [Harrison, 1966; p. 195; Suzuki, 1971; Posternak et al., 1975]. In the following it will only be assumed that the bands, and the nature of their variation with strain, do not change very much as an element is alloyed with neighboring elements in the periodic table.

Interperiodic alloys, and alloys between elements not adjacent in the periodic table will be almost entirely excluded from consideration because the rigid-band model is not expected to work as well when elements of widely different atomic size or valence are alloyed.

B. d-Bands Under Strain and the Fermi Surface

The results of this study, together with zero-pressure data from other studies are summarized in Figures 11-15. The general trends for the moduli and the anisotropy have been pointed out and discussed by others [see the review by Fisher, 1975]. The interesting features of the curves in Figures 11 and 14 are as follows: (1) The C' curves, remarkably, fall virtually on top of each other for all three periods (note the Cr points at e/a = 6). C' increases fairly smoothly up to e/a = 6 and then decreases. (2) The C_{44} curves are very similar from period to period even though they do not coincide. For all three periods C_{44} remains virtually independent of composition at low e/a but increases rapidly with e/a in the alloys rich in Group VIB elements. (3) The anisotropy ratio in Figure 14 decreases rapidly with e/a and reaches a minimum in the region $5 < e/a < 6$ after which it again increases.

There is general agreement that these trends are related to the electronic structure and to the d-band electrons in particular. Fisher [1975] has analyzed the data by taking as his point of departure the model of Fuchs [1935,

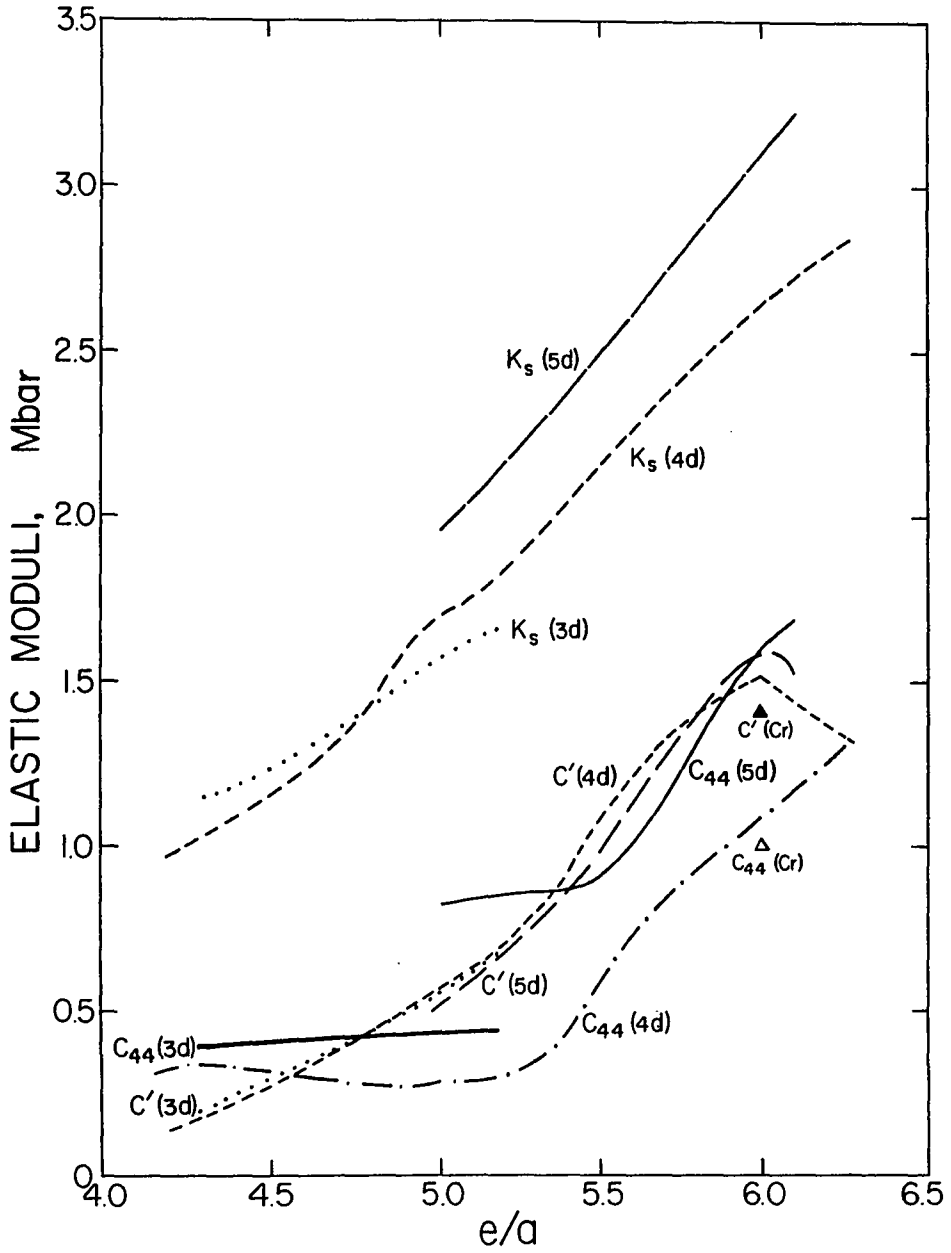

Figure 11. K_T, C_{44}, and C' vs. e/a. The data used to draw these curves were selected from the compilation of Fisher [1975]. In addition more recent results were included from Ayres et al. [1975], Hayes and Brotzen [1974], Carpenter and Shannette [to be published], Walker and Peter [to be published], L. J. Graham [personal communication] and the present study.

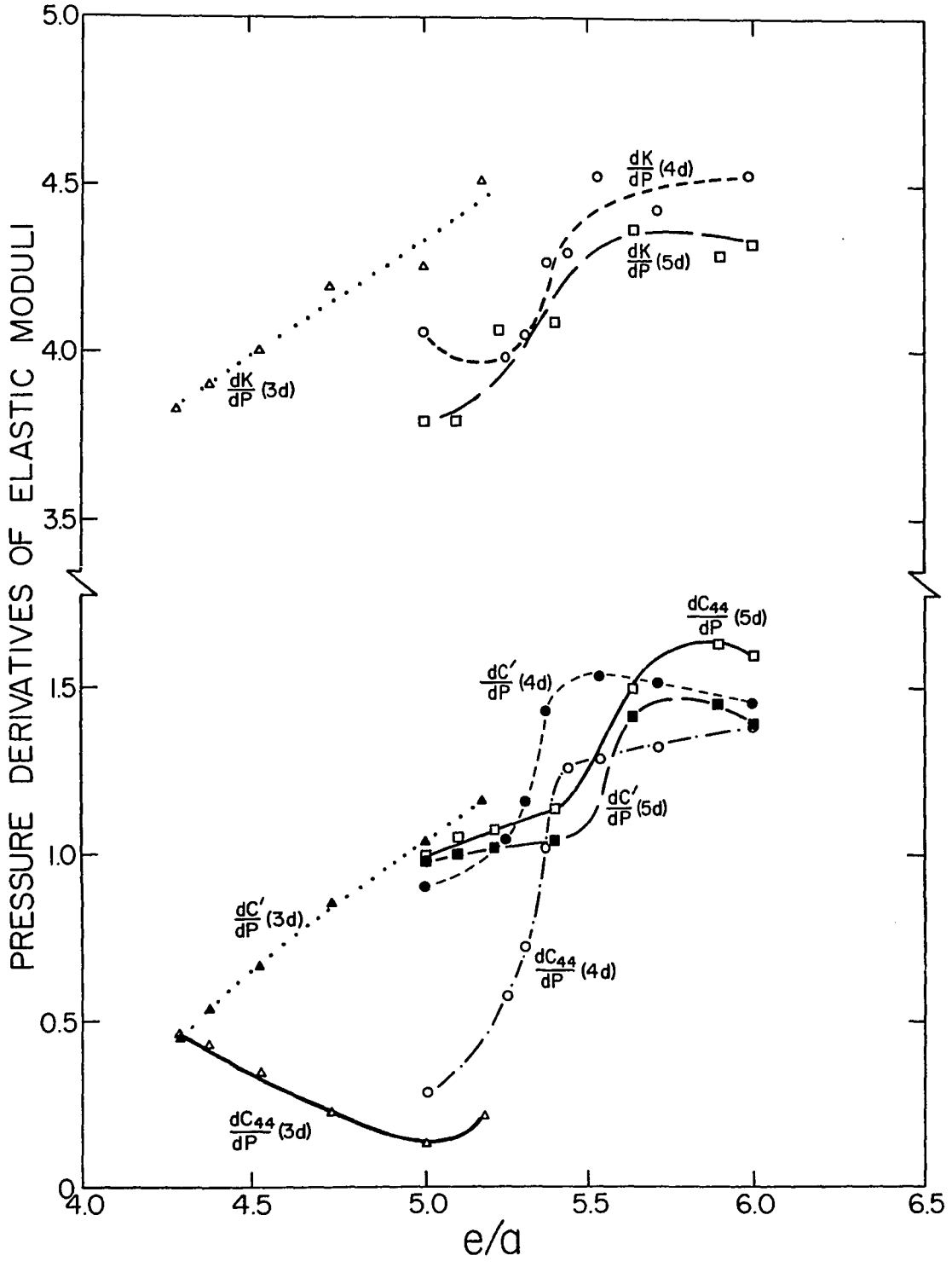

Figure 12. dK/dP, dC_{44}/dP, and dC'/dP vs. e/a.

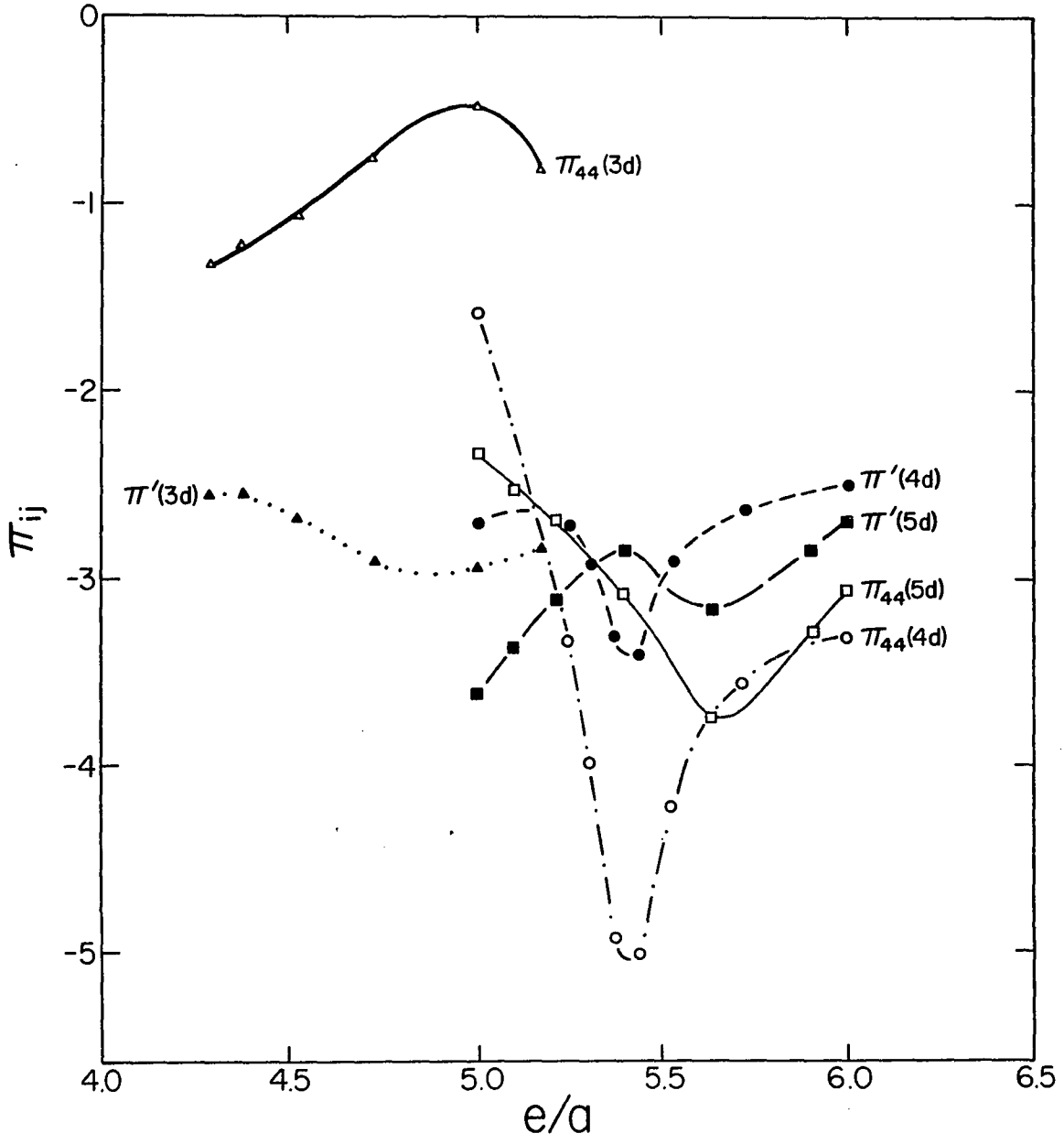

Figure 13. π_{44} and dℓn C_{44}/dℓn V and π' = d n C'/dℓn V vs. e/a

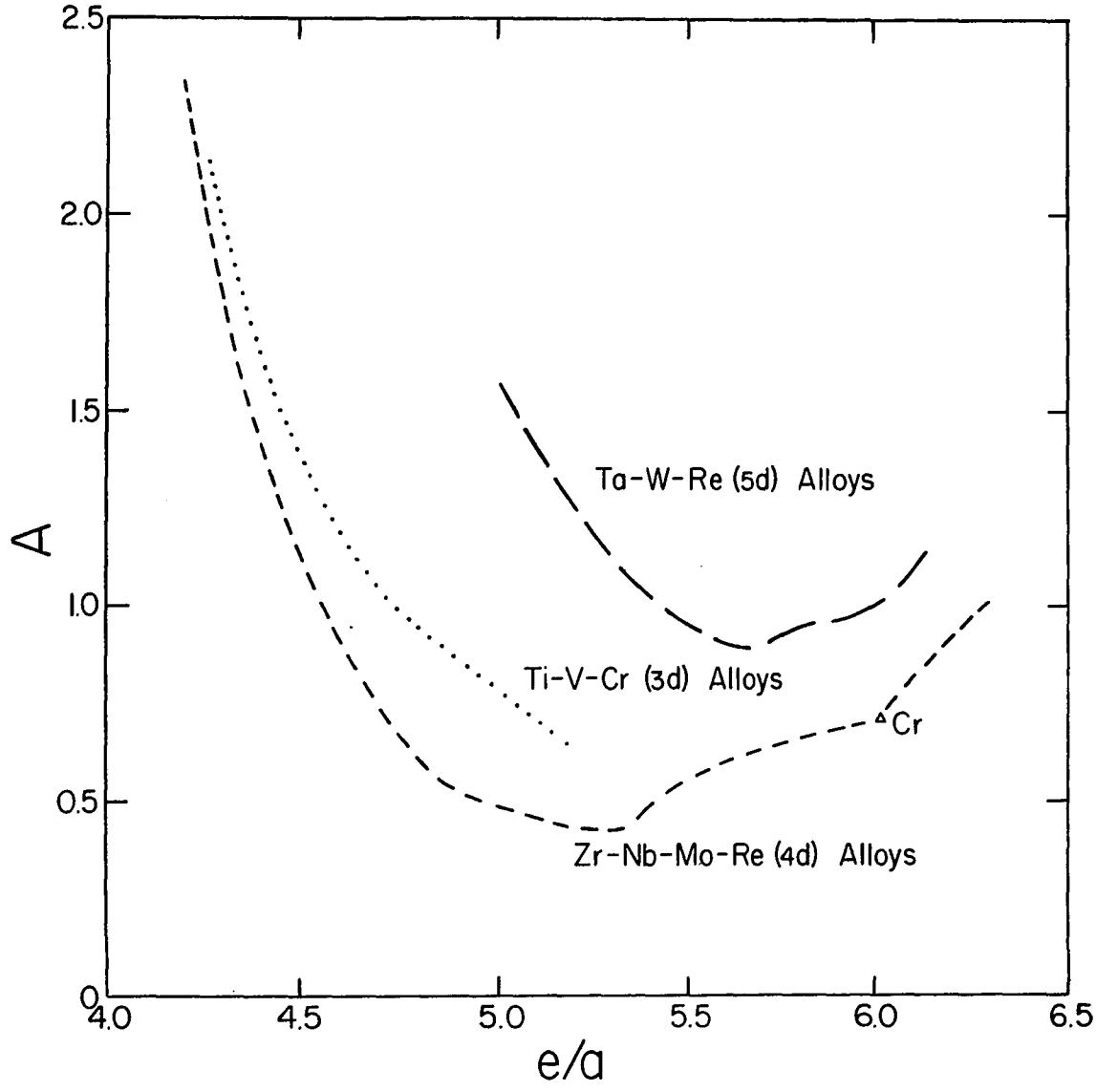

Figure 14. Anisotropy ratio, $A = C_{44}/C'$ vs. e/a. References are the same as for Figure 11. The triangle at e/a = 6 is for the 3*d* element Cr.

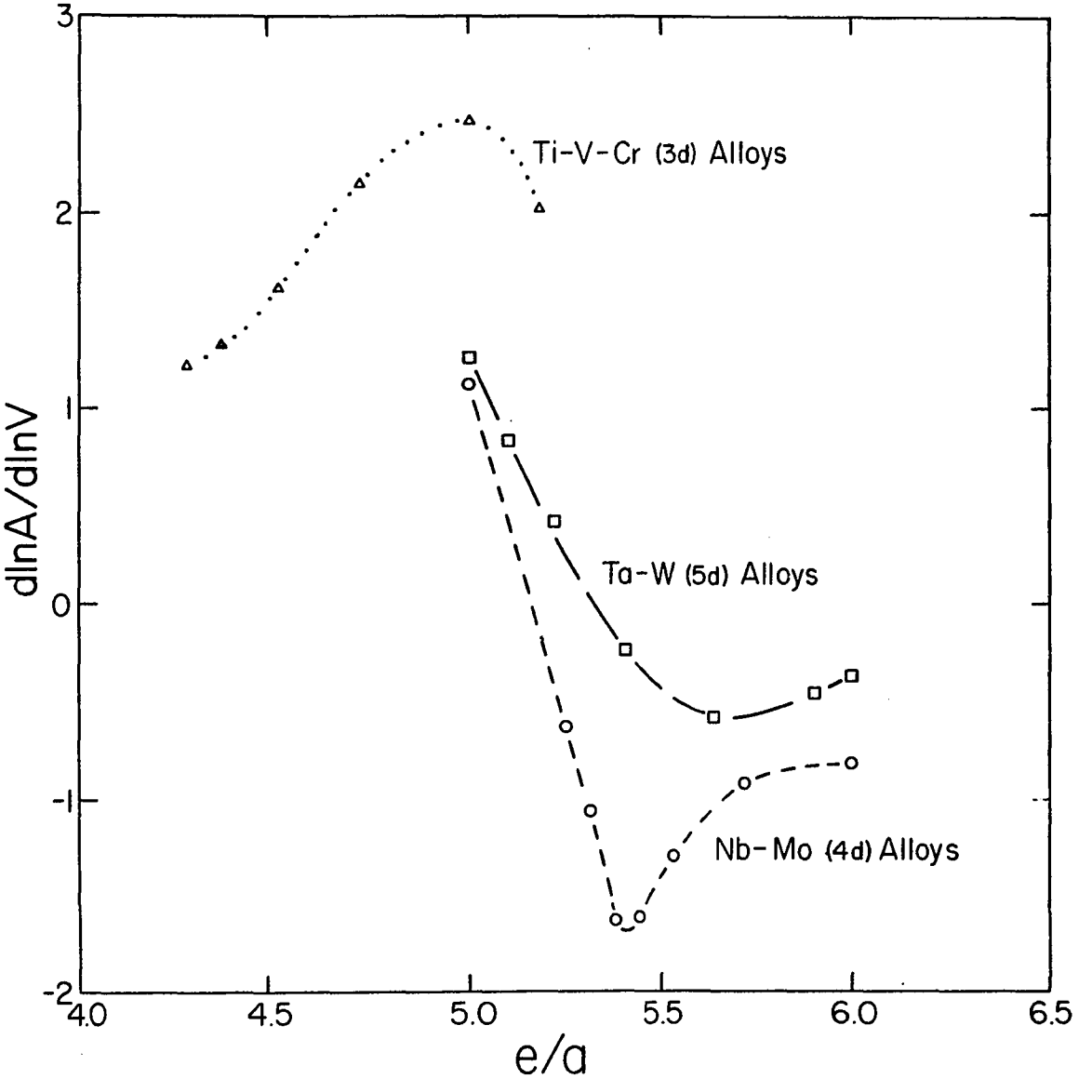

Figure 15. dℓnA/dℓnV vs. e/a.

1936a, 1936b]. In this model the elastic strain energy is composed of three terms: (1) the electrostatic energy of point ions embedded at the lattice sites in a free-electron-gas background, (2) a short-range central potential term arising from the overlap of neighboring ion cores, and (3) the energy of the conduction electrons in a nearly-free-electron (NFE) approximation. (Isenberg [1951] has generalized this model to include transition metals by considering the d-electrons to be part of the ion-cores.) Such models predict values of A much greater than one for bcc metals. Fisher [1975] therefore concluded that the deep minima in A seen in Figure 14 were due to large band-structure effects (i.e., to a departure from NFE conditions) which could not be adequately represented by Fuchs' model. This conclusion is corroborated by the fact that, at about the same e/a values, the d-electron contributions to the cohesive energy reach a maximum [Wigner and Seitz, 1955; Freidel, 1969; Pettifor, 1970].

Very little more than this can be said regarding the composition dependence of the C_{ij} in Fuchs' model. Isenberg [1951] and others [Bolef, 1961; Featherston and Neighbours, 1963] hypothesized that the overlap forces in Fuch's model were different for nearest and next-nearest neighbors. This would account for the small observed A values since overlap forces between nearest-neighbors contribute primarily to C_{44} while C' is influenced more by next-nearest-neighbor forces [e.g., see Fisher, 1975]. But it is now known from neutron-

scattering experiments [Woods, 1972] that the interatomic forces in these metals are of long range and cannot be explained by interactions between near neighbors. Furthermore, it has also been established that the d-electrons are not very well localized and should not be regarded as parts of the ion cores.

Another sort of conjecture was made by Brotzen and his co-workers [Davidson and Brotzen, 1968; Hubbell and Brotzen, 1972; Hayes and Brotzen, 1974]. They tentatively suggested, from a tight-binding viewpoint, that the increase of C' with e/a is due to the filling of a subband of antibonding states directed along [100] (the antibonding subband of e_g symmetry [Goodenough, 1963]). The decrease in C' for e/a > 6 would then indicate that the subband has been filled. This is contrary to the results of actual calculations [Freidel, 1969, pp. 350-355] which indicate that the anti-bonding subband should be filled at much higher values of e/a.

The approach that will be taken here is due to Peter and co-workers [Peter, 1973, 1974; Peter et al., 1974] who have developed a perturbation formalism for the electronic contributions to the shear moduli. A summary of their treatment is given in Appendix D. The result of interest here is their expression for any shear modulus [Peter et al., 1974, equation (52)]:

$$G = \frac{2}{3V} \sum_n \left(f(E_n) \frac{\partial^2 E_n}{\partial \varepsilon^2} + \frac{\partial f(E_n)}{\partial E_n} \left(\frac{\partial E_n}{\partial \varepsilon} \right)^2 \right) \qquad (25)$$

where the summation runs over all eigenstates of the one-electron Hamiltonian, the E_n are the corresponding eigenvalues, ε is a parameter giving the magnitude of the appropriate shear strain, and $f(E_n)$ is the Fermi-Dirac distribution function:

$$f(E_n) = \frac{1}{e^{(E_n-\mu)/kT}+1} \tag{26}$$

with μ = chemical potential. In the limit of vanishing temperature, μ approaches the Fermi energy, E_F, and $f(E_n)$ becomes a unit step function and its derivative becomes a negative delta function. When the sums in (25) are converted to reciprocal-space integrals in the usual way [Ziman, 1972; Kittel, 1971], the shear modulus at $T = 0^o$ K becomes

$$G = \frac{2}{3(2\pi)^3}\int_{E_o}^{E_F} dE \int_{S(E)} \cdot \frac{\partial^2 E}{\partial \varepsilon^2}\frac{dS}{|\nabla E|} - \frac{2}{3(2\pi)^3}\int_{S(E_F)} \left(\frac{\partial E}{\partial \varepsilon}\right)^2 \frac{dS}{|\nabla E|} \tag{27}$$

Here E_o is the bottom of the conduction band and S(E) is the reciprocal-space surface of constant energy E.

The first term on the right in equation (27), or equation (25), is simply the sum over the occupied states of the second strain derivatives of the energies. This term is to be expected from the definition of the elastic moduli as the second derivatives of the crystal energy with respect to

strain. The second term in equation (27) is a surface integral over all sheets of the Fermi surface. It arises because states near the Fermi energy are displaced in energy as the strain is applied. Some initially empty states become occupied and vica versa depending on whether the energies decrease or increase. This term thus gives the contribution of the transfer of electrons between different states. This kind of transfer term was first considered by Leigh [1951] in constructing the model mentioned earlier in this chapter. Leigh's model has recently been generalized and improved by Fischer et al. [1969] who have also derived an equation very similar to (25).

The second term in (27) is of particular interest for reasons that will become apparent. In order to relate this quantity to other physical parameters, it is convenient to define an "average deformation potential," D, at the Fermi energy:

$$D^2 = \frac{\frac{2V}{(2\pi)^3} \int_{S(E_F)} \left(\frac{\partial E}{\partial \varepsilon}\right)^2 \frac{dS}{|\nabla E|}}{\frac{2V}{(2\pi)^3} \int_{S(E_F)} \frac{dS}{|\nabla E|}} \tag{28}$$

The second term in (27) then becomes

$$G_2 = -\frac{1}{3V} D^2 N(E_F) \tag{29}$$

where $N(E_F)$ is the density of states at E_F, and $N(E_F)$ is equal to the denominator in (28) [Kittel, 1971, p. 249].

There are a number of physical quantities that depend

directly on $N(E_F)$ including in particular the paramagnetic susceptibility χ. Although equations (27) - (29) have been evaluated at T = 0 for simplicity, it is possible to start with equation (25) and derive an expression for arbitrary temperatures which relates the shear modulus to the effective density of states and thus to χ [Peter et al., 1974]:

$$G_2 = - \frac{D^2}{3\mu_B{}^2 V} \chi \qquad (30)$$

where μ_B is the Bohr magneton. Correlations between transition metal shear moduli and susceptibilities, and their respective temperature derivatives, have been noted and discussed by Fischer et al. [1969], Weinmann and Steinemann [1974], and Peter [1974] among others. These studies indicate that G_2 can be a large term depending on the particular metal and modulus. In fact dG_2/dT can sometimes be the dominant term in the dC_{ij}/dT. Hubbell and Brotzen [1972] measured dC_{ij}/dT for Nb-Mo alloys, and found anomalous (positive) values of dC_{44}/dT in the Nb-rich alloys. This is similar to the behavior of $d\chi/dT$ found by Jones and McQuillan [1962] for these alloys.

For the purposes of the following discussion the point to be kept in mind is that the electronic contributions to the shear moduli can be large, especially for C_{44}, and are related to the Fermi surface through the second term in equation (27).

Figure 12 shows that dC_{44}/dP and dC'/dP, like C_{44} and

C', vary strongly with composition. Note that there is a very sharp change in behavior at e/a $\sim$ 5.4 for the Nb-Mo alloys. There is a similar break for the 5d metals at e/a $\sim$ 5.7. The 3d data do not extend into this composition region, but note that dC_{44}/dP reaches a minimum at e/a $\sim$ 5.0. These trends are accentuated in Figure 13 which shows $\pi_{44} = d \ln C_{44}/d \ln V$ and $\pi' = d \ln C'/d \ln V$ plotted against e/a, and in Figure 15 where $d \ln A/d \ln V = \pi_{44} - \pi'$ is shown. There are pronounced extrema at e/a $\sim$ 5.0 for the 3d metals, at e/a $\sim$ 5.4 for the 4d metals, and at e/a $\sim$ 5.7 for the 5d metals. A reexamination of Figure 11 shows that there are inflection points in the shear moduli curves at e/a $\sim$ 5.4 and 5.7 for the 4d and 5d alloys respectively. There also appear to be small bumps in the 4d curves for e/a near 4.9 or 5.0. A close examination of the 3d curves (see Fig. 3) reveals that there may also be changes in the composition dependence of C' near e/a $\sim$ 5.0, but this is not certain because of the scatter in the data.

In view of the preceding discussion of the C_{ij} and dC_{ij}/dT, it is clear that the large variations in the dC_{ij}/dP are related to the response of the d-electron bands to strain. It is suggested here that, primarily through the second term in (27), the changes in the e/a dependence of moduli and their pressure derivatives are related to changes in the topology of the Fermi surface as e/a varies within a rigid-band model. These changes could come about not only through changes in the total Fermi surface area over which

the integral in (27) is taken, but also through changes in $dE/d\varepsilon$ and ∇E. The Fermi surface is a surface of constant energy, so a topological change implies $\hat{\nabla} E = 0$ [Lifshitz, 1960]. Thus the second term in (27) should have singularities in the density of states. It is not expected that these will be very visible in the moduli because of broadening due to disorder and temperature effects. However, it may be expected that the pressure derivatives of the moduli would exhibit the singularities to a greater degree.

The Fermi surfaces of Group VB and VIB elements are shown in Figure 16 [e.g., see Halloran et al., 1970; Hoekstra and Stanford, 1973]. The Group VB Fermi surface is composed of three sheets as follows. (1) There is a second-band hole surface (Fig. 16a) shaped approximately like an octahedron which is located at the Brillouin zone center, Γ. This surface will be denoted here by OCT(Γ). (2) There is a multiply-connected third-band hole surface (Fig. 16b) which is known as the "jungle-gym" (JG) surface. (3) Ellipsoidal third-band hole surfaces (ELL) are centered on the zone faces at the (110) points, N (Fig. 16b). As electrons are added according to the rigid-band hypothesis, all of these surfaces shrink since they are hole surfaces. OCT and JG near the center of the zone shrink relatively rapidly with increasing e/a, and eventually OCT disappears and JG pinches off near Γ leaving octahedral surfaces at H. At about the same e/a, a fourth-band electron surface begins to grow at Γ. By the time e/a = 6 is reached, the Fermi surface looks

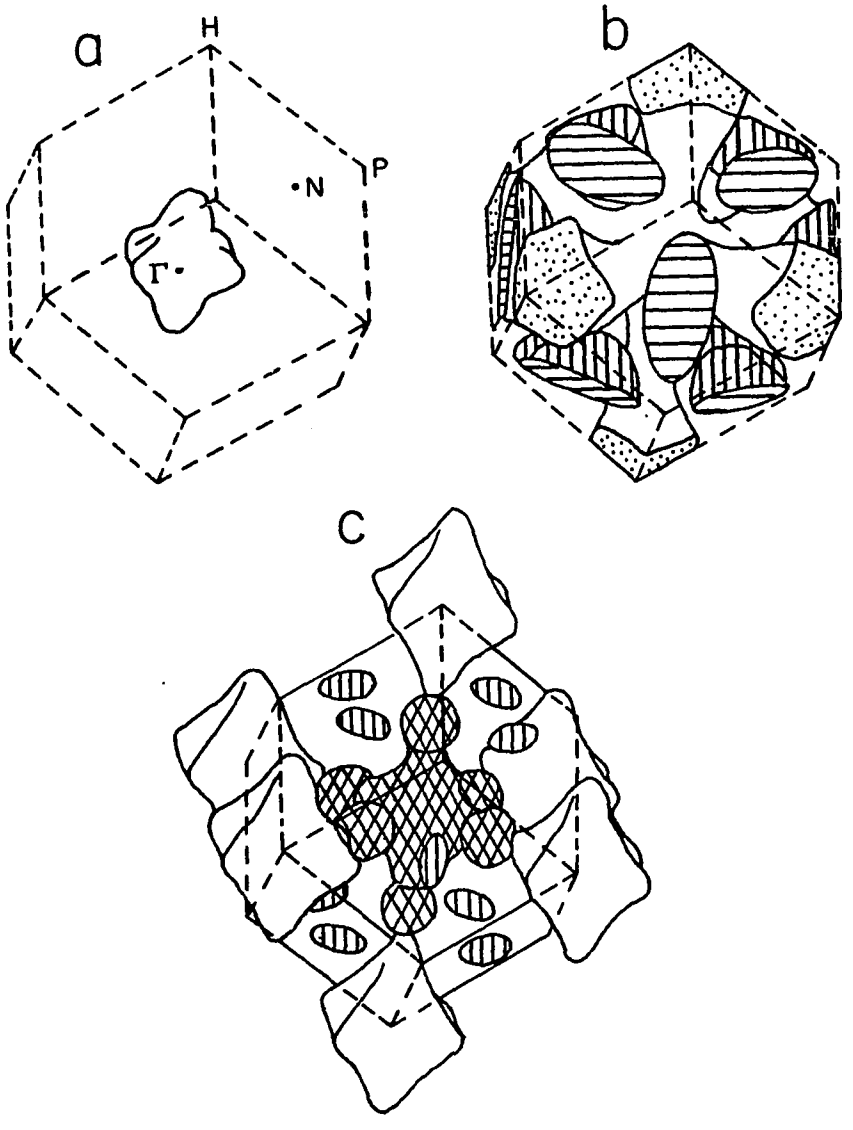

Figure 16. Fermi surfaces of Group VB and VIB elements. (a) Octahedral hole surface at Γ for e/a = 5. (b) Hole ellipsoids and "Jungle-gym" for e/a = 5. (c) Fermi surface for e/a = 6 including ellipsoids at N and octahedra at H which are remnants of (b). There is an electron "jack" at the zone center. For Mo but not for W there are also lens-shaped electron surfaces within the "necks" of the "jack".

like that depicted in Figure 16c. There is now a fourth-band electron "jack" at the zone center. The ELL surfaces are considerably smaller, and the octahedra at the zone corners are the remnants of JG.

The band structure along Γ-H (the [100] direction in reciprocal space) for a typical bcc transition metal is shown in Figure 17. The disappearance of OCT(Γ) and the pinching off of JG occur in the neighborhood of $E_F = \Gamma_{25}'$. The corresponding e/a can be estimated from existing band structure calculations. For instance, e/a values of about 5.5 and 5.8 are found respectively from the Nb and Ta band structures of Mattheiss [1970, Fig. 3]. On the other hand, a Mo band structure [Koelling et al., 1974] yields e/a ∿ 5.2. while a W band structure [Mattheiss, 1965] gives e/a ∿ 5.6. The differences between the Group VB and VIB values are to be expected from the discussion in the previous section. The greater band widths of the Group VIB elements lead to lower densities of states. The lower N(E) together with the relative depression of the d-bands imply that a Group VI band structure will predict $E_F = \Gamma_{25}'$ at a lower e/a. The averages of the above values, 5.4 for the 4d metals and 5.7 for the 5d metals, coincide very nicely with the extrema in Figures 13 and 15 and with the inflection points in Figure 11.

It is interesting to note that for Nb the (111) extremal cross-sectional areas of OCT(Γ) and JG at Γ have negative pressure derivatives while the derivatives of extremal areas

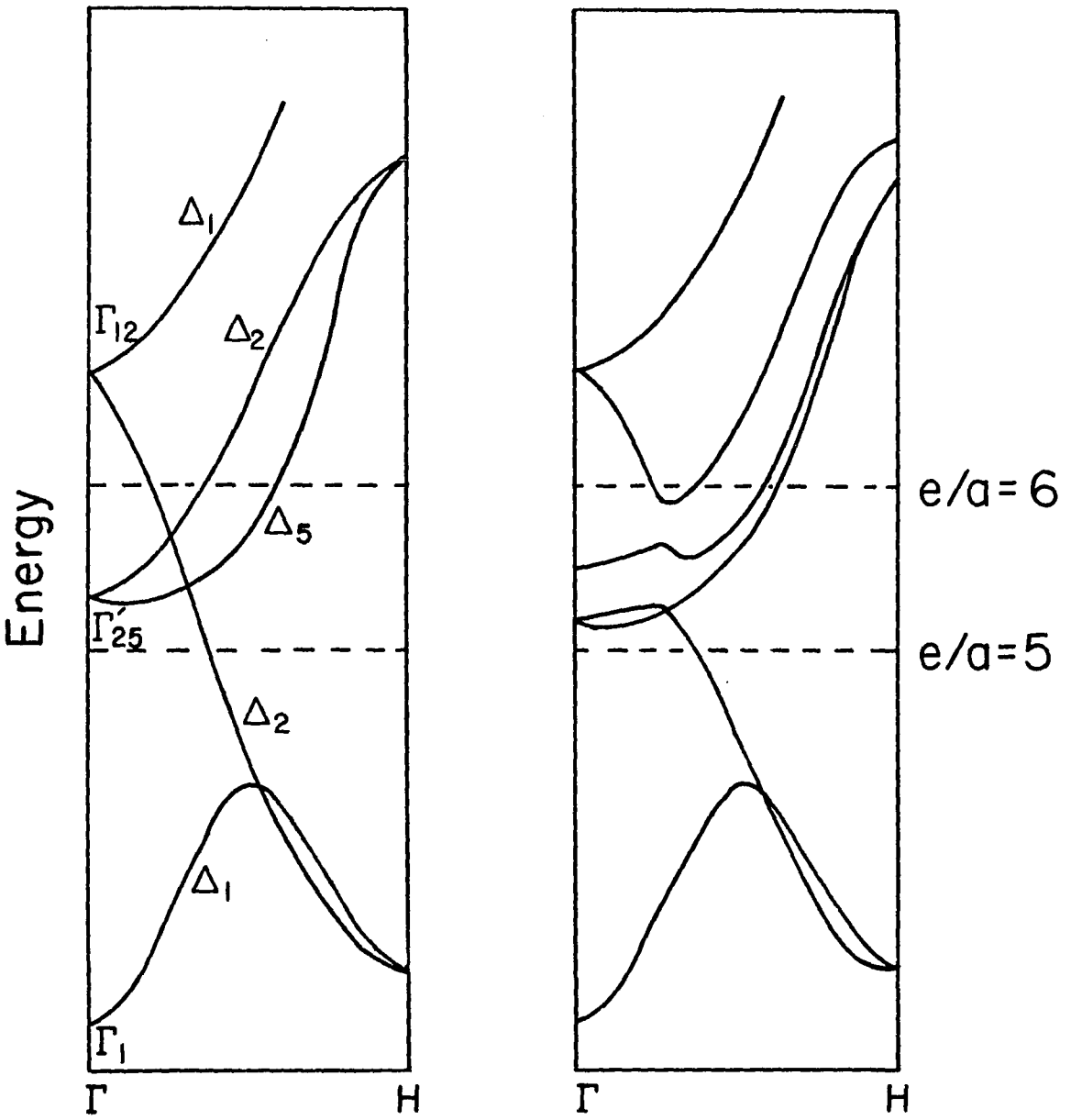

Figure 17. Band structure along [100] in reciprocal space for a bcc transition metal (after Mattheiss [1965]. Γ is the zone center and H is a corner. The dashed lines indicate the approximate positions of the Fermi energy at e/a = 5 and 6. The bands are shown without spin-orbit splitting on the left and with spin-orbit splitting on the right.

located elsewhere are positive [Anderson et al., 1973]. The second- and third-band states near the Brillouin zone center thus behave differently under stress compared to other states. It therefore seems reasonable to suppose that it is the occupation of these states that cause the large changes in the C_{ij} and, particularly, dC_{ij}/dP with e/a.

These states may also strongly influence the temperature derivatives of the moduli. It has already been noted that niobium-rich molybdenum alloys exhibit anomalous temperature derivatives of C_{44} [Hubbell et al., 1972; Hubbell and Brotzen, 1972]. There is a pronounced maximum in dC_{44}/dT at e/a = 5.3 - 5.4, i.e., at an electron population slightly less than that at which the second- and third-zone centers become completely occupied. Carpenter and Shannette [unpublished] also observed positive values of dC_{44}/dT in Ta-W alloys. In this case the maximum anomaly may be at e/a $\sim$ 5.4, but there is a gap in the data over the range 5.43 < e/a < 5.73, and the anomaly appears to persist up to e/a $\sim$ 5.7. This is consistent with the greater band widths and larger relativistic effects in the 5d metals as will be discussed later.

Now consider what happens when e/a is decreased below 5. In this case, the hole surfaces expand. From the vanadium band structure of Papaconstantopoulos et al. [1972] it is found that JG merges with ELL along Γ - N at an e/a value just slightly less than 5.0. This is again just where the extrema occur in Figures 13 and 15 for the 3d alloys. When

niobium band structures are used [Mattheiss, 1970; Anderson et al., 1973], the rigid-band model predicts that JG and ELL merge at e/a $\sim$ 4.9. Data on dC_{ij}/dP are not available for e/a < 5, but it has already been noted that there are bumps in the 4d C_{ij} curves at e/a $\sim$ 4.9 in Figure 11 which may be related to the topological change.

The dC_{ij}/dT of Zr-Nb alloys have been studied by Walker and Peter [unpublished]. Positive values of dC_{44}/dT were observed in the composition range 4.6 < e/a < 4.9. The maximum anomaly occurs at e/a = 4.8 which is again slightly less than the expected e/a value for the topological change in the 4d metals.

If e/a is decreased still further, ELL and JG merge more and more until they are completely joined in the (100) planes as e/a approaches 4. This topological change may be associated with the instability of the bcc structure in this composition region.

Another quantity whose composition dependence is relevant to this discussion is the electronic Grüneisen parameter, γ_e, which can be obtained from measurements of the electronic contributions to the specific heat and thermal expansion at low temperatures [Collins and White, 1964]. When mass enhancement effects are neglected, γ_e is given by [Collins and White, 1964, p. 457]:

$$\gamma_e = 1 + (\partial \ell n\, N(E_F)/\partial \ell n\, V)_T \ . \qquad (31)$$

Smith and Finlayson [1976] and White and Smith [unpublished] have evaluated γ_e for Zr-Nb-Mo-Re alloys and their results are shown in Figure 18. It can be seen from (29) and (31) that γ_e is related to the volume derivatives of the shear moduli. More precisely, if the total shear modulus is written as

$$G_T = G_0 + G_2 ,$$

then it follows from (29) and (31) that

$$\pi = \frac{d\ell nG_T}{d\ell nV} = \frac{G_2}{G_T}\left(\gamma_e - 2 + \frac{d\ell nD^2}{d\ell nV}\right) + \frac{G_0}{G_T}\frac{d\ell nG_0}{d\ell nV} \quad \ldots\ldots \quad (32)$$

Note from equation (20) that G_2 is negative. Comparisons of Figures 13 and 18 shows that there is a rough correlation between the extrema in π_{44} and $-\gamma_e$. This correlation is, of course, affected by a number of factors including the deformation potentials and their volume derivatives which are unknown as yet.

The predicted e/a values for the topological changes are reasonably consistent with the e/a values at which changes are seen in the elastic properties and related quantities. What is lacking is a clear physical picture of how the d-electrons respond to strain. A theoretical calculation along these lines would be helpful. Peter et al. [1974] have in fact carried out preliminary calculations of the electronic contributions to C_{44} and C' of Nb at 900^oK using a variant of equation (25) and a tight-binding model for the d-bands. Their results for the dC_{ij}/dT are in fair

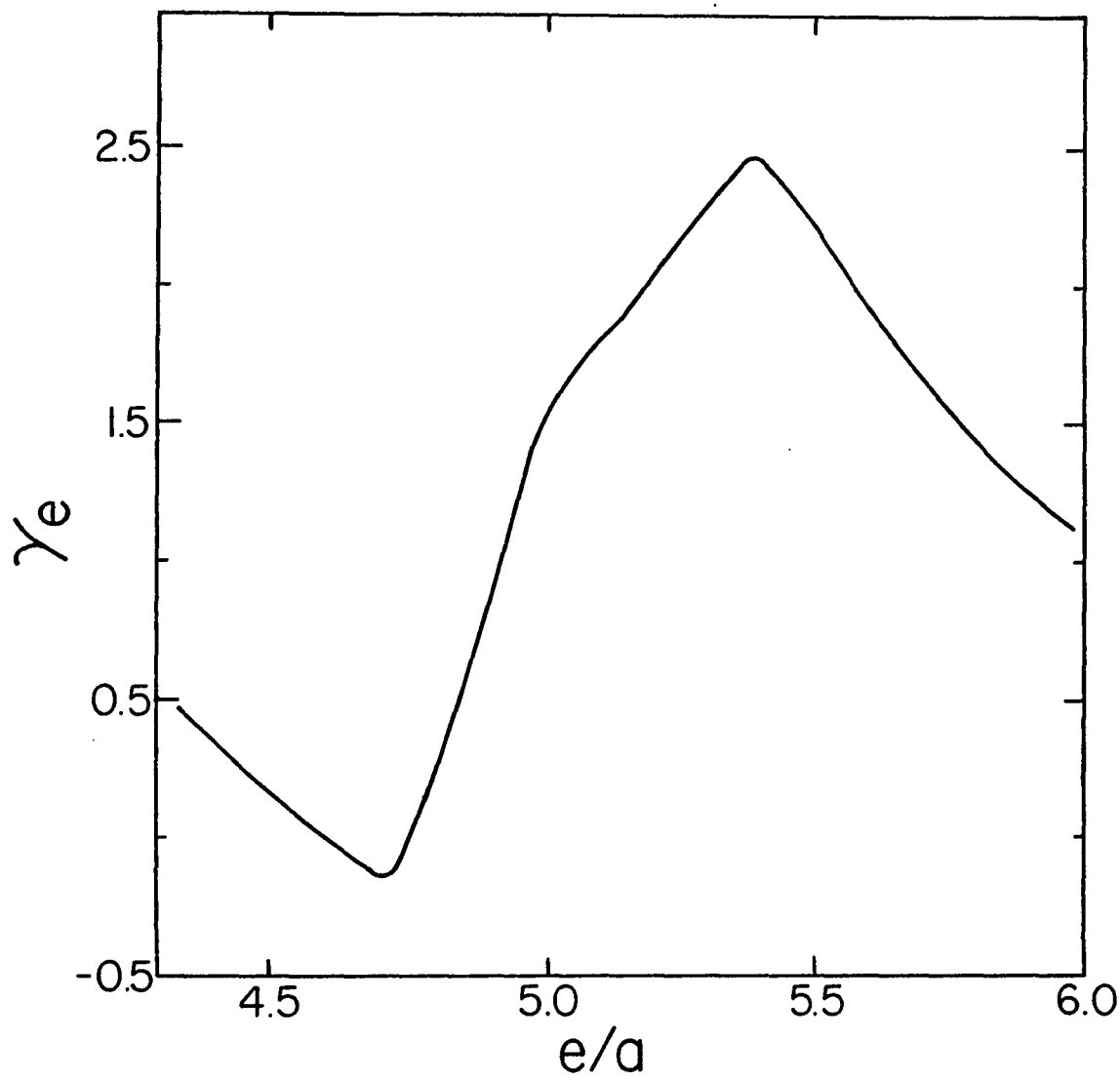

Figure 18. Electronic Grüneisen parameter, γ_e, vs. e/a for the 4*d* alloys [Smith and Finlayson, 1976; White and Smith, to be published].

qualitative agreement with the experiment. Their results for C_{44} and C' also indicated that d-electron contributions to the shear moduli are very substantial--on the order of a megabar. However they did not sort out contributions from different Fermi-surface sheets and they did not consider the effects of volume changes.

If it is accepted that the rigid-band model works, and that topological changes in the Fermi-surface are related to sharp changes in the elastic properties of the alloys, then it is possible to make predictions about composition regions which have not yet been studied. Using the vanadium band calculation of Papaconstantopoulos et al. [1972], it is expected that, in analogy to the 4d and 5d alloys, the 3d metals will exhibit minima in π_{44}, π' and $d\ell n\ A/d\ell n\ V$ near e/a = 5.7 corresponding to $E_F = \Gamma_{25}'$. Similarly, extrema, or sharp changes, should be seen in these quantities at e/a $\sim$ 4.9 and 4.7 for the 4d and 5d alloys respectively when ELL merges with JG.

Thus far only variations with e/a have been discussed. It is interesting to also look at interperiodic trends. Note first that, for a given e/a value, the 4d and 5d alloys have virtually identical atomic volumes while the 3d metals have smaller lattice parameters [Pearson, 1958, 1966]. This fact makes comparisons between the Nb-Mo and Ta-W systems relatively simple. The 5d-bands are broader and because of relativistic effects, fall higher in the nearly-free-electron bands than is the case for the 4d bands [Mattheiss, 1970,

1972]. The relatively large widths in the 5d bands imply less localization of the d-electrons and thus a generally smaller electronic contribution to the shear moduli. This is reflected in Figure 14 where the anisotropy is larger for the Ta-W alloys than for the Nb-Mo alloys. Similarly, Figures 13 and 15 display less pronounced minima for the 5d metals. The latter fact may also be due in part to increased spin-orbit splitting which reduces the degeneracies in the bands as shown schematically in Figure 17. The Γ_{25}' level is split and the topological changes are spread out over a wider e/a range. OCT(Γ) disappears and JG pinches off at lower e/a values, and the electron "jack" appears at higher e/a, than would be predicted without the splitting. This may also cause the anomaly in dC_{44}/dT to be spread out more with e/a as mentioned earlier.

The consequence of the 5d bands falling at higher energies relative to the nearly-free-electron band is that $E_F = \Gamma_{25}'$ at a higher e/a value than in the 4d metals. This accounts for the difference in the critical e/a values of 5.4 and 5.7 for the Nb-Mo and Ta-W alloys respectively.

Comparison with the 3d alloys is difficult because of the different atomic volumes and because the data do not cover the same e/a range. The major difference in the band structure is that the 3d bands are much narrower in V than the 4d and 5d bands in Nb and Ta [Mattheiss, 1972]. It might be expected therefore that the 3d alloys should exhibit even more pronounced changes than the 4d alloys in the

shear moduli and their pressure derivatives at e/a $\sim$ 5.7 corresponding to $E_F = \Gamma_{25}'$. But the narrower d bands would also tend to imply lower values of A. There is no evidence for this in Figure 14 although it is possible that the 3d curve passes under the 4d curve in the unexplored e/a region. It is also possible that the smaller atomic volumes in the 3d metals somehow offset the narrower band widths so that the 3d metals exhibit behavior intermediate between the 4d and 5d metals.

VI. SUMMARY AND CONCLUSIONS

A. Experimental Aspects

Sources of error in the ultrasonic measurements have been examined in some detail. It has been found both from experiment (Chapter IV) and theory (Appendices A and C) that compression of the pressure medium can cause appreciable errors by altering the boundary conditions on the surfaces of the transducer-bond-sample assembly. Wave-guide effects, reflection phase shifts and diffraction effects all contribute to errors in the dC_{ij}/dP (particularly for longitudinal modes) because of the variations in the properties of the pressure medium. Remedies for these problems have been suggested which include using the bond material as the pressure medium in the vicinity of the transducer, and choosing an appropriately high carrier frequency.

Values for the C_{ij} at zero-pressure were generally in fairly good agreement with those of other studies. Discrepancies could be explained for the most part by differences in the samples.

On the other hand, agreement with other studies was generally poor for the dC_{ij}/dP. In some of these cases possible errors have been identified in the previous work. Extrapolation of the ultrasonic data to high pressures via the Birch-Murnaghan equation resulted in satisfactory agreement in the low pressure region ($\sim 10^2$ kbar) with static X-ray and shock compression experiments. In the megabar

region the ultrasonic results predicted higher volumes than were found in the shock experiments. Although errors in the ultrasonic measurements could not be absolutely ruled out, it was suggested that neglect of higher-order derivatives of K_T was also a likely source for at least part of the disagreement.

B. Elasticity and Band Structure

The rigid-band model was used to deduce from existing band structure calculations the critical e/a values at which topological changes occur in the Fermi surface. These critical compositions were found to coincide very well with changes in the shear moduli and their pressure derivatives, and to a certain extent with their temperature derivatives as well. It was suggested that these correlations were due to the domination of the shear moduli by a term involving a Fermi surface integral. It was argued, qualitatively, that this integral could be sensitive to changes in E_F near a critical value because of changes in the Fermi surface area, changes in the strain dependence of energies near E_F, and singularities in the integral at critical points.

The crucial assumption is that the rigid-band model, as defined in Chapter V, works well for the bcc transition metals. The good consistency between the present results and the rigid-band model lends support to this assumption but further exploration of this question would be desirable.

APPENDIX A

TRANSDUCER-BOND PHASE SHIFTS

This appendix treats the problem of determining the phase shifts that occur when an ultrasonic wave train is reflected from the sample face to which the transducer is attached. It is assumed that the transducer diameter is much larger than the wavelength, and that the wave train is sufficiently long, and monochromatic, so that we need to consider only steady-state conditions. Our problem is thus the one-dimensional one of a continuous plane wave normally incident on the transducer-bond assembly as shown in Figure 19. We further assume that attenuation is negligible.

McSkimin [1957, 1961] and McSkimin and Andreatch [1962] have considered this problem using transmission line theory for cases in which the pressure medium has zero acoustical impedance. Their treatment is thus suitable for longitudinal waves at low pressure with a gaseous external medium or for shear waves when the pressure medium is a gas or a low viscosity liquid. Here we will consider explicitly the case of longitudinal waves when the pressure medium cannot be neglected. This problem does not appear to have been treated in the existing literature.

Following the usual procedure in elasticity theory (e.g., see Ewing, Jardetzky and Press [1957]), we define a scalar potential in each medium:

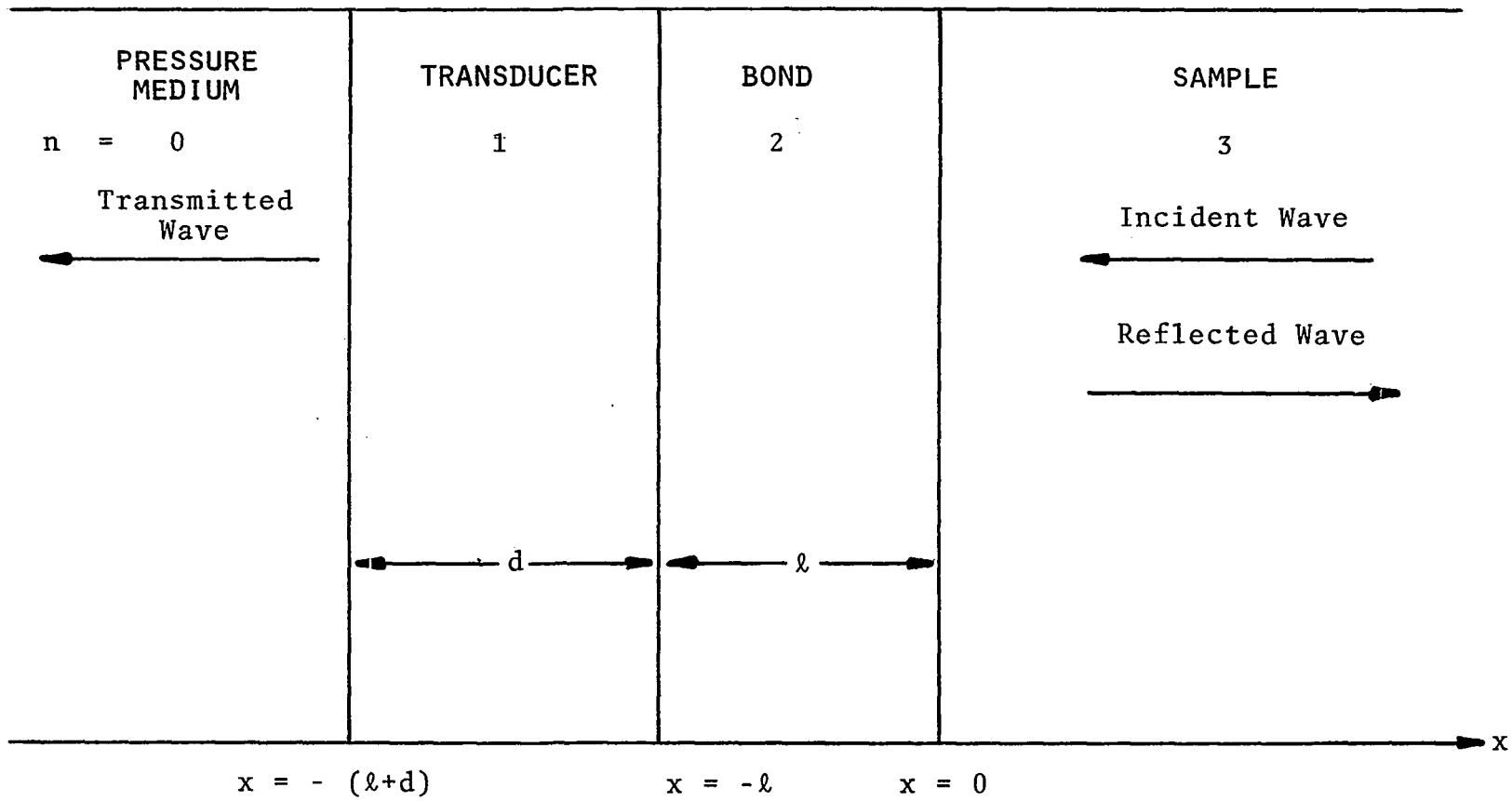

Figure 19. Schematic diagram of transducer-bond-sample assembly immersed in a pressure medium. The x-axis is normal to the boundaries and the boundary positions are shown at the bottom of the figure. The incident and transmitted waves propagate in the negative x direction, and the reflected wave in the positive x direction.

$$\psi_n = \left(a_n e^{i(k_n x - \alpha_n)} + b_n e^{-ik_n x} \right) e^{-iwt} , \qquad (A\text{-}1)$$

where n = 0,1,2,3 corresponds to the pressure medium, the transducer, the bond, and the sample respectively. The wave vectors are $k_n = w/v_n$. We require the ratio a_n/b_n to be real and positive, so the α_n are the phase differences between waves traveling in the positive and negative x-directions in each medium. Our objective is to solve for α_3 which gives the net phase shift of the ultrasonic wave upon reflection. Note that in normal experimental conditions, the bond is thin and the transducer thickness is an odd multiple of half the wavelength. Since the acoustical impedance of the pressure medium is, in all practical situations, much lower than that of the transducer or sample, it follows that $\alpha_3 \sim \pi$. In a round-trip through the specimen there is an additional phase shift of π at the other sample face which approximately cancels α_3. We are really interested only in the small residual phase shift defined by

$$\phi = \alpha_3 - \pi . \qquad (A\text{-}2)$$

In terms of ψ_n the particle displacement is

$$u_n = \frac{\partial \psi_n}{\partial x} ,$$

or, from (A-1),

$$u_n = ik_n \left[a_n e^{i(k_n x - \alpha_n)} - b_n e^{-ik_n x} \right] e^{-iwt} . \qquad (A\text{-}3)$$

The stress is given by

$$P_n = \rho_n \frac{\partial^2 \psi_n}{\partial t^2}$$

$$= - w^2 \rho_n \left[a_n e^{i(k_n x - \alpha_n)} + b_n e^{-ik_n x}\right] e^{iwt} , \qquad \text{(A-4)}$$

where ρ_n is the density of medium n.

Both the displacement and stress must be continuous at each boundary. We note that there is only a transmitted wave in the pressure medium so that $a_o = 0$. Thus at $x = -(\ell+d)$ (see Fig. 19) we have from (A-3) and (A-4):

$$-k_o b_o e^{ik_o(\ell+d)} = k_1 \left[a_1 e^{-i[k_1(\ell+d) + \alpha_1]} - b_1 e^{ik_1(\ell+d)}\right] \qquad \text{(A-5)}$$

and

$$\rho_o b_o e^{ik_o(\ell+d)} = \rho_1 \left[a_1 e^{-i[k_1(\ell+d) + \alpha_1]} + b_1 e^{ik_1(\ell+d)}\right] \qquad \text{(A-6)}$$

Manipulation of (A-5) and (A-6) yields

$$\frac{a_1}{b_1} e^{-2i(k_1\ell + \alpha_1/2)} = \frac{Z_o - Z_1}{Z_o + Z_1} e^{2ik_1 d} , \qquad \text{(A-7)}$$

where $Z_n = w\rho_n/k_n = \rho_n v_n$ is the impedance of medium n. Similarly, the boundary conditions at $x = -\ell$ and $x = o$ can be shown to lead, respectively, to

$$\frac{a_2}{b_2} e^{-i\alpha_2} = \frac{\frac{a_1}{b_1} e^{-2i(k_1 \ell + \alpha_1/2)} + \frac{Z_1 - Z_2}{Z_1 + Z_2}}{\frac{Z_1 - Z_2}{Z_1 + Z_2} \frac{a_1}{b_1} e^{-2i(k_1 \ell + \alpha_1/2)} + 1} \qquad \text{(A-8)}$$

and

$$\frac{a_3}{b_3} e^{-i\alpha_3} = \frac{\frac{a_2}{b_2} e^{-i\alpha_2} + \frac{Z_2 - Z_3}{Z_2 + Z_3}}{\frac{Z_2 - Z_3}{Z_2 + Z_3} \frac{a_2}{b_2} e^{-i\alpha_2} + 1} . \qquad \text{(A-9)}$$

Note that successive substitutions of (A-7) into (A-8) and of (A-8) into (A-9), and separation of the resulting expression into real and imaginary parts will yield a closed-form solution for α_3, or, equivalently, for ϕ (see equation (A-2)). The closed-form solution will not be given explicitly here since it is very cumbersome and because practical calculations of ϕ are probably more conveniently done in a stepwise fashion. Instead we will consider two special cases.

As a check on the present results, we first consider the problem solved by McSkimin [1957, 1961] in which there is a free surface at $x = -(\ell+d)$. We note that $Z_o = 0$ and $a_n/b_n = 1$ in equations (A-7), (A-8) and (A-9). These equations may be easily shown to reduce to

$$k_1 \ell + \frac{\alpha_1}{2} = k_1 d + \frac{\pi}{2} . \qquad \text{(A-10)}$$

$$\tan\left(k_2 \ell - \frac{\alpha_2}{2}\right) = \frac{Z_2}{Z_1} \tan\left(k_1 \ell - \frac{\alpha_1}{2}\right) , \qquad \text{(A-11)}$$

and

$$\tan \frac{\alpha_3}{2} = \frac{Z_3}{Z_2} \tan \left(\frac{\alpha_2}{2}\right) . \qquad \text{(A-12)}$$

These three equations, together with (A-2) and suitable trigonometric identities, yield

$$\tan \frac{\phi}{2} = - \frac{Z_2}{Z_3} \frac{\tan (K_2 \ell) + \frac{Z_1}{Z_2} \tan (k_1 d)}{1 - \frac{Z_1}{Z_2} \tan (k_1 d) \tan (k_2 \ell)} \qquad \text{(A-13)}$$

This is the same result as was obtained by McSkimin [1957, 1961]. Note that when the transducer is operated at its resonance or any harmonic, we have $k_1 d$ equal to a multiple of π, so (A-13) reduces to

$$\tan \frac{\phi}{2} = - \frac{Z_2}{Z_3} \tan (k_2 \ell) . \qquad \text{(A-14)}$$

Thus ϕ is negative. This causes the measured travel time at the in-phase condition of the pulse superposition method to be larger than the travel time through the sample alone. Note also that samples with large impedances will have small phase shifts. In the present study values of Z_2/Z_3 fell between 0.2 and 0.02, so ϕ was generally about an order of magnitude less than $k_2 \ell$.

As pointed out by McSkimin [1961], the phase shift ϕ can, in principle, be measured since the velocities and impedances are all known or can be determined. Measurement of travel times at different values of w then allows the determination of ℓ and ϕ using equations (A-13) and (2). This

was found to be rather difficult to do in practice, however. There are a number of possible reasons for this including inadequate flatness and parallelism of transducers and samples, inhomogeneities in the bond, wave-guide or "side-wall" effects, diffraction, lack of precision in measuring the travel times and the carrier frequencies, poor spectral purity of the wave train due to harmonic distortion and other causes, and attenuation in the transducer, bond and sample. The result is that the uncertainty in ϕ was generally as large as ϕ itself.

Consider now the case where $Z_o \neq 0$ and the transducer is operated at resonance or at harmonic so that $\tan(k_1 d) = 0$. Equation (A-7) becomes

$$\frac{a_1}{b_1} e^{-2i(k_1 \ell + \alpha_1/2)} = \frac{Z_o + Z_1}{Z_o + Z_1} . \qquad \text{(A-15)}$$

Inserting this into (A-8) yields

$$\frac{a_2}{b_2} e^{-i\alpha_2} = \frac{Z_o - Z_2}{Z_o + Z_2} e^{2ik_2\ell} . \qquad \text{(A-16)}$$

Combination of (A-2), (A-9) and (A-16) can be shown to lead to

$$\tan\phi = - \frac{\left(\frac{Z_o^2 - Z_2^2}{Z_o^2 + Z_2^2}\right)\left(\frac{2Z_2 Z_3}{Z_2^2 - Z_3^2}\right)\sin(2k_2\ell)}{1 + \left(\frac{Z_o^2 - Z_2^2}{Z_o^2 + Z_2^2}\right)\left(\frac{Z_2^2 + Z_3^2}{Z_2^2 - Z_3^2}\right)\cos(2k_2\ell)} \qquad \text{(A-17)}$$

This is the expression we have been seeking. Note that it

is equivalent to (A-14) when $Z_o = 0$.

Equation (A-17) shows that the phase shift ϕ is, in fact, a function of Z_o. This is a matter of practical importance in several respects. It has already been pointed out that accurate determination of ϕ is difficult in practice. From equation (A-17) it can be seen that $\phi = 0$ when $Z_o = Z_2$ regardless of the bond thickness. This might also have been seen intuitively since at its resonance frequency the transducer is 1/2 wavelength thick and is therefore "transparent" to the ultrasonic waves. There is thus in effect only a single medium with impedance $Z_o = Z_2$ bounding the sample. Thus, by immersing the sample-bond-transducer assembly in a medium whose impedance is equal to that of the bond, it is possible to eliminate the phase shift entirely. This would allow a higher degree of accuracy in velocity measurement--particularly for small samples with low acoustic impedances. Papadakis [1972] has recently discussed the absolute accuracy of ultrasonic velocity measurements. One point that emerges from his discussion is that the major sources of error are bond and diffraction effects. Bond errors tend to increase with carrier frequency while diffraction errors tend to decrease and there is thus normally a trade-off between these two effects when one chooses the rf. Elimination of the bond phase shifts as proposed here would allow use of higher frequencies to minimize the diffraction effects.

Equation (A-17) also indicates an alternative method

for determining ϕ. By measuring travel times with the sample immersed in different media it is in principle possible to obtain the bond thickness and the phase shift and thus to obtain corrected travel times.

For the purposes of this study, the most important implication of equation (A-17) is that the densification of the pressure medium can cause systematic errors in the measured values of the dC_{ij}/dP. In order to evaluate these, estimates of the effect of pressure on the phase shifts were made as follows. The sample impedance was chosen to be close to the longitudinal mode impedances in niobium. The sample and transducer properties were assumed to remain constant since they vary much more slowly than the properties of the bond and the pressure medium. The bond material was assumed to have the same properties as the "hypothetical" bond material of Davies and O'Connell [1977] except that the bond was assumed to compress uniaxially rather than isotropically --i.e., the bond cross section was taken to be constant. This is justified if the bond is assumed to be a viscous liquid with good adhesion to both the sample and the transducer. The surface tension at the edges of the bond, therefore, maintains an approximately constant cross section. The bond thickness is thus inversely proportional to its density, and since the wave vector is inversely proportional to the velocity, it follows that $k_2\ell$ is proportional to $1/Z_2$. The results are altered only slightly if the bond is assumed to compress isotropically as was done by Davies and O'Connell

[1977]. The pressure medium was assumed to be N_2 gas which has a negligible impedance at atmospheric pressure. The high pressure acoustic impedance of nitrogen was estimated from the compression data of Bridgman [1924], by neglecting the difference between isothermal and adiabatic compressibilities, and by assuming that Z_o is independent of frequency. These approximations are crude, but they are quite adequate for illustrative order-of-magnitude calculations.

The results are shown in Table 15 for two initial (P = 0) values of the bond thickness: $k_2\ell = 10^o$ and 30^o. The second row of ϕ values was calculated by using the bond properties estimated at 5 kbar, but the pressure medium was neglected as in the work of McSkimin and Andreatch [1963] and Davies and O'Connell [1977]. In accordance with their results, ϕ appears to be virtually independent of pressure. The third row of Table 15 shows ϕ values at 5 kbar with the pressure medium taken into account. The change in ϕ with compression in this case is much larger. If it is assumed that the $k_2\ell = 10^o$ and 30^o cases correspond to measurements on the present niobium sample at 20 and 60 MHz, then the observed uncorrected values of $d(\rho v^2)/dP$ will be too high by about 0.3 and 0.4% respectively. In general, the magnitude of the correction term will increase with (a) increasing carrier frequency, (b) decreasing sample impedance, (c) decreasing sample size, and (d) increasing bond thickness.

Similar calculations have also been carried out for a liquid pressure medium. The liquid chosen was n-pentane

Table 15. Values of the phase shift ϕ of equation (A-17) under different conditions. Impedances are in units of 10^5 g/cm^2-s.

P = 0 Z_o = 0.0 Z_2 = 1.82	$k_2\ell = 10^o$ $\phi = -0.919^o$	$k_2\ell = 30^o$ $\phi = -3.01^o$
P = 5 kbar Z_o = 0.0 Z_2 = 2.9	$k_2\ell = 6.3^o$ $\phi = -0.914^o$	$k_2\ell = 18.8^o$ $\phi = -2.83^o$
P = 5 kbar Z_o = 1.3 Z_2 = 2.9	$k_2\ell = 6.3^o$ $\phi = -0.73^o$	$k_2\ell = 18.8^o$ $\phi = -2.22^o$
P = 0 Z_o = 0.66 Z_2 = 1.82	$k_2\ell = 10^o$ $\phi = -0.80^o$	$k_2\ell = 30^o$ $\phi = -2.51^o$
P = 5 kbar Z_o = 1.9 Z_2 = 2.9	$k_2\ell = 6.3^o$ $\phi = -0.52^o$	$k_2\ell = 18.8^o$ $\phi = -1.55^o$

which is used occasionally in various laboratories. The density, compressibility and acoustic velocity of this material were taken from tables in the American Institute of Physics Handbook [Gray, 1972]. The results are given in the last two rows of Table 15. Note that the change in ϕ with pressure is greater than for the case where N_2 is the pressure medium. It should be kept in mind, however, that these results depend somewhat on the assumed bond properties. The hypothetical bond properties of Davies and O'Connell [1977] were used here because they were readily available, and because there appears to be no direct experimental data on this subject.

Since the bond properties are not well known, and since the initial bond thicknesses were difficult to determine, it is not at present feasible to apply corrections to the measured $d(\rho V^2)/dP$ reported here. In view of the calculations carried out above, it is tentatively concluded that the errors incurred by neglecting the corrections are probably acceptably small for the purpose of studying the composition dependence of the dC_{ij}/dP. For smaller samples with low impedance, or when more accurate results are desired, and especially when second-order derivatives need to be determined, the effect of the pressure medium must be taken into account. In this connection it is important to point out that the impedance of any gas increases very rapidly with pressure at low pressures and more slowly at higher pressures. Thus ϕ will not be a linear function of pressure, and uncorrected

values of d^2C_{ij}/dP^2 could be substantially affected. As was pointed out earlier, the difficulty can be circumvented by using the bond material as the pressure medium, at least in the vicinity of the transducer. Note that the phase shift can also be eliminated in this way for shear waves, since many bonding materials are in fact viscous liquids which transmit high frequency shear waves but which have no static shear strength (up to moderate pressures where they solidify or become glassy).

APPENDIX B

UNCERTAINTY IN THE DENSITY

In this appendix an expression is derived for the maximym error in the sample density due to inaccuracy of the balance and to errors in determining the water and air densities. In the notation of Chapter I, equation (1), the sample density is

$$\rho = \frac{W_A \rho_W - W_W \rho_A}{W_A - W_W} \tag{B-1}$$

The weight of the immersed sample W_W is obtained through two separate weighing operations. Measurements are made of the weight of the sample suspended from the balance, W_T, and of the weight of the suspension apparatus, W_o. Thus

$$W_W = W_T - W_o \tag{B-2}$$

Now let x be defined by

$$x = W_A - W_W = W_A - W_T + W_o \; . \tag{B-3}$$

Note that $\rho_A << \rho_W$ and that $\rho_W \simeq 1$ in units of g/cm^3. Hence

$$\rho \simeq \frac{W_A}{x} \tag{B-4}$$

Differentiation of equation (B-1) yields

$$\frac{d\rho}{\rho} \simeq \frac{dW_A}{W_A} - \frac{dx}{x} + d\rho_W - (1 - \frac{1}{\rho})\, d\rho_A \quad , \tag{B-5}$$

where (B-4) and the approximations leading to it have been used.

The maximum error in each of W_A, W_T and W_o is now taken to be ΔW. By the usual methods [Baird, 1962], the maximum relative error in the density is then given by:

$$\frac{\Delta\rho}{\rho} = (1 + 3\rho)\,\frac{\Delta W}{W_A} + (\Delta\rho_W + (1 - \frac{1}{\rho})\,\Delta\rho_A) \quad . \qquad \text{(B-6)}$$

This equation was used to compute the uncertainties in Table 2 with $\Delta W = 0.25$ mg taken from the specifications of the manufacturer of the balance. The second term in (B-6) is for the present measurements much smaller than the first. It was estimated to be 1×10^{-4}, most of which arises from uncertainty in the temperature of the water.

Since ρ is fairly large for transition metals, equation (B-6) can be approximated by

$$\frac{\Delta\rho}{\rho} \simeq 3\,\frac{\rho}{W_A}\,\Delta W \qquad \text{(B-7)}$$

which is convenient for quick estimates of uncertainty. Note that the uncertainty in the density is roughly inversely proportional to the sample volume through the factor ρ/W_A. This is, of course, what one would expect in measurements using buoyancy methods.

It is perhaps worth pointing out that when a more accurate balance is chosen, and when the sample volumes are larger, other types of errors become predominant [see Bowman and Schoonover, 1967].

APPENDIX C

VELOCITY ERRORS

This appendix describes the procedures used to obtain rough estimates of the bond and diffraction phase shifts and the resulting velocity errors.

Bond phase shifts were estimated by assuming the bond thickness to be 3 μm for all measurements. The longitudinal and shear velocities in the bond were taken to be 2.1 and 0.5 km/s, respectively, which are realistic values for Nonaq stopcock grease [Bateman, 1967]. The resulting phase shifts, ϕ_B, calculated from equation (A-14) in Appendix A, were of the proper magnitude as evidenced by rough measurements according to the method of McSkimin [1961].

Diffraction effects are more difficult to evaluate. Papadakis [1972] has pointed out that the phase shift due to diffraction in the PSP method is a complicated function not only of the sample and transducer geometry, but also of the attenuation. Furthermore, the phase shifts as functions of wavelength, transducer diameter and distance traveled have only been worked out for longitudinal waves propagating along axes of three, four, and sixfold rotation symmetry [Papadakis, 1966]. In other words, they can only be calculated for mode 1 in Table 1 and not for the other 4 modes. In the present case, very crude estimates were made by treating all the crystals as if they were elastically isotropic, and by assuming that the phase shifts for shear

waves were the same as for longitudinal waves.

Papadakis [1966] has calculated phase shifts as a function of $s = Z\lambda/a^2$ where Z is the distance traveled, λ is the wavelength, and a is the transducer radius. For isotropic materials, the phase shift in radians, ϕ_D, can be roughly approximated by

$$\phi_D = 0.18s \qquad \text{(C-1)}$$

up to $s \sim 5$, which includes about 5 to 10 echoes for the present samples. The phase difference between successive echoes is then obtained by taking $Z = 2\ell$.

Note from equations (3) and (4) that the velocity is given by

$$v = 2\ \ell\ pF'\ (1 - \frac{pF'}{f}\ \frac{\phi}{2\pi}) \qquad \text{(C-2)}$$

to first order in . The fractional corrections to v due to ϕ_B and ϕ_D are shown in Table 16 for niobium. Note that the two corrections are of opposite sign and of similar magnitude. Although the cancellation between the two terms was not always quite as good as for Nb, it serves as a partial justification for neglecting the phase shifts entirely. A more compelling reason for ignoring the corrections is that they cannot be accurately calculated for the crystals used in this study.

In fact, the uncertainty in ϕ_B is probably as large as ϕ_B itself, and the same can be said for ϕ_D. Because of this and because they tend to cancel, the corrections were assumed

Table 16. Fractional Velocity Corrections for Nb

Mode	f(MHz)	$\frac{pF'}{f}\frac{\phi_B}{2\pi}$	$\frac{pF'}{f}\frac{\phi_D}{2\pi}$
1	60	-0.00010	0.00009
2	60	-0.00011	0.00010
3	30	-0.00016	0.00004
4	20	-0.00010	0.00020
4	30	-0.00016	0.00009
5	60	-0.00010	0.00008

to contribute to the σ_n in equation (5) as if they were random errors. The length uncertainty was taken throughout to be 1 part in 10^4, and the three terms were added as standard errors to obtain the velocity uncertainties used in the fitting procedure for the moduli.

This appendix is probably the most appropriate place in which to comment upon still another source of error that has not yet been sufficiently studied. In connection with the foregoing discussion of diffraction effects, note that the apparent attenuation for longitudinal waves generally increases with pressure because of increasing transmission into the pressure medium. (The quantity s in equation (C-1) changes at a negligible rate under pressure.) $\phi_D(s)$ increases rapidly with s for small s and then levels off and asymptotically approaches π as s goes to infinity. When the

PSP method is used, an increase in the attenuation will give a greater weight to the early echoes. The average ϕ_D for PSP measurements will thus tend to increase with pressure. This effect is probably small for the present samples since they have relatively high impedances and therefore relatively low transmission losses. Such errors would be larger for low impedance samples, but they could be circumvented by using other ultrasonic methods such as the PEO technique.

APPENDIX D

ELECTRONIC CONTRIBUTIONS TO THE SHEAR MODULI

This appendix summarizes the perturbation formalism developed by Peter [1973, 1974] and Peter et al. [1974] for the electronic contributions to the shear moduli of metals.

The one-electron Schroedinger equation may be written as

$$H\ (\underline{k},\ \varepsilon)\ |\ \underline{k},\ n,\ \varepsilon) = E_n\ (\underline{k},\ \varepsilon)\ |\ \underline{k},\ n,\ \varepsilon)$$

where $\underline{k}$ is the electronic wavevector, n is the band index, ε is a parameter describing the strain, $H\ (\underline{k}, \varepsilon)$ is the Hamiltonian, and $E_n\ (\underline{k},\ \varepsilon)$ is the nth energy level corresponding to $\underline{k}$. The ket $|\ \underline{k},\ n,\ \varepsilon\ )$ denotes the Bloch state corresponding to $E_n\ (\underline{k},\ \varepsilon)$. Assume for the moment that the Hamiltonian and the zero-strain eigenstates and eigenvalues are known. The reciprocal space is defined such that for a given direct space vector $\underline{R}$,

$$\underline{k}\ (\varepsilon)\ \cdot\ \underline{R}\ (\varepsilon) = \text{constant}\ .$$

The Hamiltonian and its eigenvalues are expanded in a perturbation series to second order in the strain:

$$H\ (\underline{k},\varepsilon) = H\ (\underline{k},\ 0) + \varepsilon\ B(\underline{k}) + \frac{1}{2}\ \varepsilon^2\ C(\underline{k}) \qquad \text{(D-1)}$$

$$E_n(\underline{k},\varepsilon) = E_n(\underline{k},\ 0) + \varepsilon\ \frac{\partial E_n}{\partial \varepsilon} + \frac{1}{2}\ \varepsilon^2\ \frac{\partial^2 E_n}{\partial \varepsilon^2}$$

where the derivatives are evaluated at $\varepsilon = 0$. Because of

the definition of the reciprocal space, the strain derivatives of E_n may be thought of as "co-moving" derivatives in the sense that they give the variation of the energy for a $\underline{k}$ point which is displaced in reciprocal space as the strain is applied. It can be straightforwardly shown [see Peter et al., 1974] that

$$\frac{\partial E_n}{\partial \varepsilon} = B_{nn}(\underline{k}) \tag{D-2}$$

and

$$\frac{\partial^2 E_n}{\partial \varepsilon^2} = C_{nn}(\underline{k}) + 2 \sum_{m \neq n} \frac{|B_{nm}(\underline{k})|^2}{E_n(\underline{k}) - E_m(\underline{k})} \tag{D-3}$$

where

$$B_{nm}(\underline{k}) = (\underline{k}, n, \varepsilon = 0 \mid B(\underline{k}) \mid \underline{k}, m, \varepsilon = 0) \tag{D-4}$$

and

$$C_{nm}(\underline{k}) = (\underline{k}, n, \varepsilon = 0 \mid C(\underline{k}) \mid \underline{k}, m, \varepsilon = 0). \tag{D-5}$$

These are the results of conventional perturbation theory. Degeneracies require the usual special procedures.

The elastic moduli are strain derivatives of the free energy. The free energy of the electrons may now be written as

$$F(N,\varepsilon) = N\mu - 2\, k_B T \sum_{\underline{k},n} \ln(1+\exp((\mu - E_n(\underline{k}, \varepsilon))/k_B T)) \tag{D-6}$$

if exchange and correlation effects are ignored. Here N is the number of electrons, μ is the chemical potential and k_B

is Boltzmann's constant.

The volume-conserving shear strains used by Peter et al. are defined by

$$\varepsilon_{11} = -2\varepsilon_{22} = -2\varepsilon_{33} = \varepsilon$$

$$\varepsilon_{12} = \varepsilon_{13} = \varepsilon_{23} = 0$$

for the C' shear, and

$$\varepsilon_{11} = \varepsilon_{22} = \varepsilon_{33} = 0$$

$$\varepsilon_{12} = \varepsilon_{13} = \varepsilon_{23} = \varepsilon$$

for the C_{44} shear. In terms of these strains the appropriate shear modulus is

$$G = \frac{1}{3V} \frac{\partial^2 F}{\partial \varepsilon 2}$$

In order to obtain G, equation (D-6) is differentiated subject to the conditions of (a) equilibrium

$$\frac{\partial F}{\partial \varepsilon} = 0 \ ,$$

(b) particle conservation

$$\frac{\partial N}{\partial \varepsilon} = 0 \ ,$$

and (c) symmetry conservation

$$\frac{\partial}{\partial N} \left(\left(\frac{\partial F}{\partial \varepsilon} \right)_{N,\ \varepsilon = 0} \right) = 0 \ .$$

The last relation expresses the condition that $\varepsilon = 0$ remains

the equilibrium value for the strain when the number of electrons is varied (this does not hold for volume strains).

The final result may be written

$$G = \frac{2}{3V} \sum_{n,\underline{k}} \left(f(E_n) \frac{\partial^2 E_n}{\partial \varepsilon^2} + \frac{\partial f(E_n)}{\partial E_n} \left(\frac{\partial E_n}{\partial \varepsilon} \right)^2 \right). \qquad \text{(D-7)}$$

which is the expression quoted in equation (25) with a minor change in notation. f(E) is the Fermi-Dirac function.

The preceding formalism is fairly straightforward. The major problem in practical calculations lies in finding a suitable approximate strain-dependent Hamiltonian to use in equations (D-1) through (D-5) for the strain derivatives of the energy. The Hamiltonian must be good enough to accurately give second derivatives of the energy and at the same time it must be simple enough to keep the calculation tractable. Peter et al. [1974] computed G values for Nb using a tight-binding model which did not take accurate account of the s-d hybridization. Posternak et al. [1975, 1976] have since done calculations of stress derivatives of the Mo Fermi surface which indicate that the hybridization must be handled carefully. It would thus be of interest to refine the calculations of Peter et al. to see if their results can be improved to agree with the experimental results. It is worth noting that Papaconstantopoulos et al. [1972] and Anderson et al. [1973] have carried out self-consistent band structure calculations for V and Nb at normal and reduced

lattice spacing. Their results could be used to parameterize the model Hamiltonians used in the shear modulus computations in order to obtain pressure derivatives of these quantities for comparison with the results reported in this study.

REFERENCES

Alers, G. A., Elastic moduli of vanadium, Phys. Rev., 119, 1532-1535, 1960.

Anderson, O. L., The use of ultrasonic measurements under modest pressure to estimate compression at high pressure, J. Phys. Chem. Sol., 27, 547-565, 1966.

Anderson, J. R., D. A. Papaconstantopoulos, J. W. McCaffrey and J. E. Schirber, Self-consistent band structure of niobium at normal and reduced lattice spacings, Phys. Rev. B, 7, 5115-5121, 1973.

Ayres, R. A., G. W. Shannette and D. F. Stein, Elastic constants of tungsten-rhenium alloys from 77 to 298°K, J. Appl. Phys., 46, 1975.

Baird, D. C., Experimentation: An Introduction to Measurement Theory and Experiment Design, Prentice-Hall Englewood Cliffs, New Jersey, 1962.

Barsch, G. R. and Z. P. Chang, Ultrasonic and static equation of state for cesium halides, in Accurate Characterization of the High-Pressure Environment, edited by E. C. Lloyd, N.B.S. Special Publication No. 236, 173-187, U.S. GPO, Washington, D.C., 1971.

Bateman, T. B., Some materials for ultrasonic transducer bonding at cryogenic temperatures, J. Acoust. Soc. Am., 41, 1011-1014, 1967.

Bernstein, B. T., Electron contribution to the temperature dependence of the elastic constants of cubic metals. I. Normal metals, Phys. Rev., 132, 50-57, 1963.

Birch, F., The effect of pressure upon the elastic properties of isotropic solids, according to Murnaghan's theory of finite strain, J. Appl. Phys., 9, 279-288, 1938.

Birch, F., Finite elastic strain of cubic crystals, Phys. Rev., 71, 809-824, 1947.

Bolef, D. I., Elastic constants of single crystals of the bcc transition elements V, Nb, and Ta, J. Appl. Phys., 32, 100-105, 1961.

Bolef, D. I. and J. de Klerk, Elastic constants of single-crystal Mo and W between 77° and 500°K, J. Appl. Phys., 33, 2311-2314, 1962.

Bolef, D. I., R. E. Smith and J. G. Miller, Elastic properties of vanadium. I. Temperature dependence of the elastic constants and the thermal expansion, Phys. Rev. B, 3, 4100-4108, 1971.

Bowman, H. A. and R. M. Schoonover, Procedure for high precision density determinations by hydrostatic weighing, J. Rev. NBS, 71C, 179-198, 1967.

Bridgman, P. W., The compressibility of five gases to high pressures, Proc. Am. Acad. Arts Sci., 59, 173-211, 1924.

Brugger, K., Thermodynamic definition of higher order elastic coefficients, Phys. Rev., 133A, 1611-1612, 1964.

Chechille, R. A., Ultrasonic equation of state of tantalum, Office of Naval Research Technical Report No. 10, Contract Nonr-1141 (05), Project NR 017-309, Case Institute of Technology, 1967 (unpublished).

Chung, D. H., D. J. Silversmith and B. B. Chick, A modified ultrasonic pulse-echo-overlap method for determining sound velocities and attenuation of solids, Rev. Sci. Inst., 40, 718-720, 1969.

Cohen, M. L. and V. Heine, The fitting of pseudopotentials to experimental data and their subsequent application, Solid State Phys., 24, 38-248, 1970.

Collins, J. G. and G. K. White, Thermal expansion of solids, in Progress in Low Temperature Physics IV, edited by C. J. Gorter, pp. 450-479, North-Holland Publishing Co., Amsterdam, 1964.

Davidson, D. L. and F. R. Brotzen, Elastic constants of molybdenum-rich rhenium alloys in the temperature range -190°C to +100°C, J. Appl. Phys., 39, 5768-5775, 1968.

Davies, G. R., Quasi-harmonic finite strain equations of state of solids, J. Phys. Chem. Solids, 34, 1417-1429, 1973.

Davies, G. F. and A. M. Dziewonski, Homogeneity and constitution of the earth's lower mantle and outer core, Phys. Earth Planet, Inter., 8, 336-343, 1975.

Davies, G. F. and R. J. O'Connell, Transducer and bond phase shifts in ultrasonics, and their effect on measured pressure derivatives, in High-Pressure Research: Applications to Geophysics, edited by M. H. Manghnani and S. Akimoto, Academic Press, New York, 1977.

Dickinson, J. M. and P. E. Armstrong, Temperature dependence of the elastic constants of molybdenum, J. Appl. Phys., 38, 602-606, 1967.

Ehrenreich, H. and L. M. Schwartz, The electronic structure of alloys, Solid State Phys., 31, 149-286, 1976.

Evans, R., G. D. Gaspari and B. L. Gyorffy, A simple theory of the electron-phonon mass enhancement in transition metals, J. Phys. F: Metal Phys., 3, 39-54, 1973.

Ewing, W. M., W. S. Jardetzky and F. Press, Elastic Waves in Layered Media, McGraw-Hill, New York, 1957.

Featherston, F. H. and J. R. Neighbours, Elastic constants of tantalum, tungsten and molybdenum, Phys. Rev., 130, 1324-1333, 1963.

Fischer, O., M. Peter and S. Steinemann, Elasticité des métaux paramagnétiques, Helv. Phys. Acta, 42, 459-484, 1969.

Fisher, E. S., A review of solute effects on the elastic moduli of bcc transition metals, in The Physics of Solid Solution Strengthening, edited by E. W. Collins and H. G. Gegel, Plenum, New York, 1975.

Fisher, E. S., Effects of hydrogen and UHV annealling on the elastic moduli of tantalum, submitted for publication, 1977.

Fisher, E. S. and D. Dever, The single crystal elastic moduli of beta-titanium and titanium-chromium alloys, in The Science Technology and Application of Titanium, edited by R. Jaffee and N. Promisel, pp. 373-381, Pergamon Press, New York, 1970a.

Fisher, E. S. and D. Dever, Relation of the C' elastic modulus to stability of b.c.c. transition metals, Acta Met., 18, 265-269, 1970b.

Fisher, E. S., M. H. Manghnani and K. W. Katahara, Application of hydrostatic pressure and shock wave data to the theory of cohesion in metals, Rev. Phys. Chem. Japan, 373-397, 1975a.

Fisher, E. S., D. G. Westlake and S. T. Ockers, Effects of hydrogen and oxygen on the elastic moduli of vanadium, niobium and tantalum single crystals, phys. stat. sol. (a), 28, 591-602, 1975b.

Freeman, A. J., H. W. Myron, J. Rath and R. P. Gupta, Electronically driven instabilities in metals, Int. J. Quantum Chem. Symp. No. 9, 535-550, 1975.

Friedel, J., Transition metals. Electronic structure of the *d*-band. Its role in the crystalline and magnetic structures, in The Physics of Metals, edited by J. M. Ziman, pp. 340-408, Cambridge University Press, Cambridge, 1969.

Fuchs, K., A quantum mechanical investigation of the cohesive forces of metallic copper, Proc. Roy. Soc. (London) A, 151, 585-601, 1935.

Fuchs, K., A quantum mechanical calculation of the elastic constants of monovalent metals, Proc. Roy. Soc. (London) A, 153, 1936a.

Fuchs, K., The elastic constants and specific heats of the alkali metals, Proc. Roy. Soc. (London) A, 157, 444-450, 1936b.

Goodenough, J. B., Magnetism and Chemical Bond, Interscience, New York, 1963.

Graham, L. J., H. Nadler and R. Chang, Third-order elastic constants of single-crystal and polycrystalline columbium, J. Appl. Phys., 39, 3025-3033, 1968.

Gray, D. E., editor, American Institute of Physics Handbook, 3rd ed., McGraw-Hill, New York, 1972.

Halloran, M. H., J. H. Condon, J. E. Graebner, J. E. Kunzler and F. S. L. Hsu, Experimental study of the Fermi surfaces of niobium and tantalum, Phys. Rev. B., 1, 366-372, 1970.

Harrison, W. A., Pseudopotentials in the Theory of Metals, W. A. Benjamin, Inc., Reading, Massachusetts, 1966.

Hayes, D. J. and F. R. Brotzen, Elastic constants of niobium-rich zirconium alloys between 4.2K and room temperature, J. Appl. Phys., 45, 1721-1725, 1974.

Heine, V. and D. Weaire, Pseudopotential theory of cohesion and structure, Solid State Phys., 24, 249-463, 1970.

Hoekstra, J. A. and J. L. Stanford, Determination of the Fermi surface of molybdenum using the de Haas-van Alphen effect, Phys. Rev. B, 8, 1416-1432, 1973.

Hubbell, W. C., D. J. Hayes and F. R. Brotzen, Anomalous temperature dependence of elastic constants in Nb-Mo alloys, Phys. Letters, 39A, 261-262, 1972.

Hubbell, W. C. and F. R. Brotzen, Elastic constants of niobium-molybdenum alloys in the temperature range -190 to +100°C, J. Appl. Phys. 43, 3306-3312, 1972.

Isbell, W. M., D. R. Christman and S. G. Babcock, Measurements of Dynamic Properties of Materials, VI, Tantalum, Materials and Structures Laboratory Report No. MSL-70-23, General Motors Technical Center, Warren, Michigan, 1972 (unpublished).

Isenberg, I., Overlap forces and elastic constants of body-centered cubic metals, Phys. Rev., 83, 637-640, 1951.

Jones, D. W., N. Pessall and A. D. McQuillan, Correlation between magnetic susceptibility and hydrogen solubility in alloys of early transition elements, Phil. Mag. 6, 455-459, 1961.

Jones, D. W. and A. D. McQuillan, Magnetic susceptibility and hydrogen affinity of b.c.c. alloys of Nb-Mo Nb-Re and Mo-Re, J. Phys. Chem. Solids, 23, 1441-1447, 1962.

Jones, K. A., S. C. Moss and R. M. Rose, The effect of small oxygen additions on the elastic constants and low temperature ultrasonic attenuation of Nb single crystals, Acta Met., 17, 365-372, 1969.

Katahara, K. W., M. H. Manghnani and E. S. Fisher, Pressure derivatives of the elastic moduli of niobium and tantalum, J. Appl. Phys., 47, 434-439, 1976.

Kittel, C., Introduction to Solid State Physics, 4th ed., John Wiley & Sons, New York, 1971.

Koelling, D. D., F. M. Mueller, A. J. Arko and J. B. Ketterson, Fermi surface and electronic density of states of molybdenum, Phys. Rev. B, 10, 4889-4896, 1974.

Le Huy, H., Mesures de propriétés élastiques de quelques metaux de transition sous pression hydrostatique et a temperature variable, travail de diplome, Universite de Lausanne (Switzerland), 1972 (unpublished).

Le Huy, H., C. Weinmann and S. Steinemann, Elastic properties of some transition metals under hydrostatic pressure at different temperatures, Helv. Phys. Acta, 46, 390, 1973 (abstract).

Leigh, R. S., A calculation of the elastic constants of aluminum, Phil. Mag., 42, 139-155, 1951.

Leisure, R. G., D. K. Hsu and B. A. Seiber, Elastic properties of tantalum over the temperature range 4-300 K, J. Appl. Phys., 44, 3394-3397, 1973.

Lifshitz, I. M., Anomalies of electron characteristics of a metal in the high pressure region, Soviet Phys. JETP, 11, 1130-1135, 1960.

Lowrie, R. and A. M. Gonas, Single-crystal elastic properties of tungsten from 24° to 1800°C, J. Appl. Phys., 38, 4505-4509, 1967.

MacFarlane, R. E., J. A. Rayne and C. K. Jones, Anomalous temperature dependence of shear modulus C_{44} for platinum, Phys. Letters, 18, 91-92, 1965.

Magerl, A., B. Berre and G. Alefeld, Changes of the elastic constants of V, Nb, and Ta by hydrogen and deuterium, phys. stat. sol. (a), 36, 161-171, 1976.

Mathews, J. and R. L. Walker, Mathematical Methods of Physics, W. A. Benjamin, New York, 1965.

Mattaboni, P., Automatic frequency control system for the measurement of rapid changes of ultrasonic wave velocities in solids, Progress Report, Contract No. AF-44620-68-C-0079, Air Force Cambridge Research Laboratories, Office of Aerospace Research, USAF, 1970 (unpublished).

Mattheiss, L. F., Fermi surface in tungsten, Phys. Rev., 139, A1893-A1904, 1965.

Mattheiss, L. F., Electronic structure of niobium and tantalum, Phys. Rev. B, 1, 373-380, 1970.

Mattheiss, L. F., Energy bands for transition metals and compounds, in Superconductivity in *d*- and *f*-Band Metals, edited by D. H. Douglas, pp. 57-71, American Institute of Physics, New York, 1972.

May, J. E., Precise measurement of time delay, IRE Nat. Conv. Record, 6, 134-143, 1958.

McMillan, W. L., Transition temperature of strong-coupled superconductors, Phys. Rev., 167, 331-344, 1968.

McQueen, R. G., S. P. Marsh, J. W. Taylor, J. N. Fritz and W. J. Carter, The equation of state of solids from shock wave studies, in High Velocity Impact Phenomena, edited by R. Kinslow, pp. 293-417, Academic Press, New York, 1970.

McSkimin, H. J., Measurement of elastic constants at low temperatures by means of ultrasonic waves - data for silicon and germanium single crystals, and for fused silica, J. Appl. Phys., 24, 988-997, 1953.

McSkimin, H. J., Use of high frequency ultrasound for determining the elastic moduli of small specimens, IRE Trans. on U.E., PGUE-5, 25-43, 1957.

McSkimin, H. J., Pulse superposition method for measuring ultrasonic wave velocities in solids, J. Acoust. Soc. Am., 33, 12-16, 1961.

McSkimin, H. J., Variations of the ultrasonic pulse-superposition method for increasing the sensitivity of delay time measurements, J. Acoust. Soc. Am., 37, 864-871, 1965.

McSkimin, H. J. and P. Andreatch, Jr., Analysis of the pulse superposition method for measuring ultrasonic wave velocities as a function of temperature and pressure, J. Acoust. Soc. Am., 34, 609-615, 1962.

McSkimin, H. J. and P. Andreatch, Jr., Measurement of third-order moduli of silicon and germanium, J. Appl. Phys., 35, 3312-3319, 1964.

McSkimin, H. J., P. Andreatch, Jr., and R. N. Thurston, Elastic moduli of quartz versus hydrostatic pressure at 25° and -195.8°C, J. Appl. Phys., 36, 1624-1632, 1965.

Ming, L. C. and M. H. Manghnani, Isothermal compression of bcc transition metals to 100 kbar, submitted to J. Appl. Phys., 1977.

Murnaghan, F. D., Finite deformations of an elastic solid, Amer. J. Math., 59, 235-260, 1937.

Oli, B. A. and A. O. E Animalu, Lattice dynamics of transition metals in the resonance model, Phys. Rev. B. 13, 2390-2410, 1976.

Papaconstantopoulos, D. A., J. R. Anderson, and J. W. McCaffrey, Self-consistent energy bands in vanadium at normal and reduced lattice spacings, Phys. Rev. B, 5, 1214-1221, 1972.

Papadakis, E. P., Ultrasonic diffraction loss and phase change in anisotropic materials, J. Acoust. Soc. Am., 40, 863-876, 1966.

Papadakis, E. P., Ultrasonic phase velocity by the pulse-echo-overlap method incorporating diffraction phase corrections, J. Acoust. Soc. Am., 42, 1045-1051, 1967.

Papadakis, E. P., Absolute accuracy of the pulse-echo overlap method and the pulse-superposition method for ultrasonic velocity, J. Acoust. Soc. Am., 52, 843-846, 1972.

Pearson, W. B., Handbook of Lattice Spacings and Structures of Metals and Alloys, vol. 1, Pergamon Press, New York, 1958.

Pearson, W. B., Handbook of Lattice Spacings and Structures of Metals and Alloys, vol. 2, Pergamon Press, New York, 1966.

Peter, M., Electronic contribution to elastic constants in cubic transition metals, Phys. Letters, 44A, 337-338, 1973.

Peter, M., Electronic contributions to shear constants and susceptibility in cubic transition metals, Solid State Commun., 14, 271-273, 1974.

Peter, M., W. Klose, G. Adam, P. Entel, and E. Kudla, Tight-binding model for transition metal electrons - 1, Helv. Phys. Acta, 47, 807-832, 1974.

Pettifor, D. G., Theory of the crystal structures of transition metals, J. Phys. C, 3, 367-377, 1970.

Pickett, W. E., and P. B. Allen, Density of states of Nb and Mo using Slater-Koster interpolation, Phys. Letters, 43A , 91-92, 1974.

Posternak, M., and S. Steinemann, Corrélations entre modules élastiques et structure de bande dans le métaux de transition, Helv. Phys. Acta, 41, 1296-1299, 1968.

Posternak, M., W. B. Waeber, R. Griessen, W. Joss, W. van der Mark, and W. Wijgaard, The stress dependence of the Fermi surface of molybdenum: I. The electron lenses, J. Low Temp. Phys., 21, 47-74, 1975.

Posternak, M., W. B. Waeber, and W. Joss, Stress dependence of the Fermi surface of transition metals: molybdenum, Helv. Phys. Acta, 49, 709-716, 1976.

Powell, B. M., P. Martel, and A. D. B. Woods, Lattice dynamics of niobium-molybdenum alloys, Phys. Rev., 171, 1968.

Rayne, J. A., Elastic constants of palladium from 4.2-300^{o}K, Phys. Rev., 118, 1545-1549, 1960.

Redwood, M. and J. Lamb, On the propagation of high frequency compressional waves in isotropic cylinders, Proc. Phys. Soc. (London), B 70, 136-143, 1957.

Rice, M. H., R. G. McQueen and J. M. Walsh, Compression of solids by strong shock waves, Solid State Phys., 6, 1-63, 1958.

Smith, R. T., R. Stern, R. W. B. Stephens, Third-order elastic moduli of polycrystalline metals from ultrasonic velocity measurements, J. Acoust. Soc. Am., 40, 1002-1008, 1966.

Smith, T. F. and T. R. Finlayson, Thermal Expansion of bcc solid solution alloys in the system Zr-Nb-Mo-Re, J. Phys. F: Metal Phys., 6, 709-724, 1976.

Spetzler, H., E. Schreiber and R. O'Connell, Effect of stress-induced anisotropy and porosity on elastic properties of polycrystals, J. Geophys. Res., 77, 4938-4944, 1972.

Stewart, W. L., III, J. M. Roberts and N. G. Alexandropolous, Effect of hydrogen on the temperature dependence of the elastic constants of tantalum single crystals, J. Appl. Phys., 48, 75-81, 1977.

Suzuki, T., Second- and third-order elastic constants of aluminum and lead, Phys. Rev. B, 3, 4007-4014, 1971.

Thomsen, L. and O. L. Anderson, Consistency in the high-temperature equation of state of solids, in Accurate Characterization of the High-Pressure Environment, edited by E. C. Lloyd, N.B.S. Special Publication No. 326, 209-217, U.S. GPO, Washington, D.C., 1971.

Thurston, R. N., Ultrasonic data and the thermodynamics of solids, Proc. I.E.E.E., 53, 1320-1336, 1965.

Thurston, R. N. and K. Brugger, Third-order elastic constants and the velocity of small amplitude elastic waves in homogeneously stressed media, Phys. Rev., 133A, 1604-1610, 1964. Erratum 135, no. 7AB, p. AB3.

Truell, R., C. Elbaum and B. B. Chick, Ultrasonic Methods in Solid State Physics, Academic Press, New York, 1969.

Voronov, F. F. and L. F. Vereschchagin, Phys. Met. 4 Metallog., 11, 111-118, 1961 (quoted by Smith et al. [1966]).

Weinmann, C. and S. Steinemann, Lattice and electronic contributions to the elastic constants of palladium, Solid State Commun., 15, 281-285, 1974.

Westlake, D. G., On the densities of tantalum, niobium, and vanadium, submitted for publication, 1977.

Westlake, D. G., Anomalies in the physical properties of vanadium. The role of hydrogen, Phil. Mag., 16, 905-908, 1967.

Wigner, E. P. and F. Seitz, Qualitative analysis of the cohesion in metals, Solid State Phys., 1, 97-126, 1955.

Woods, A. D. B., Lattice dynamics of transition metals, in Superconductivity in *d*- and *f*-Band Metals, edited by D. H. Douglas, pp. 45-55, American Institute of Physics, New York, 1972.

Ziman, J. M., The calculation of Bloch functions, Solid State Phys. 26, 1-101, 1971.

Ziman, J. M., Principles of the Theory of Solids, 2nd edition, Cambridge University Press, Cambridge, 1972.